Gas exchange, carbon flows, and ecosystem metabolism over a temperate seagrass meadow

Kayleigh E. Granville

Charlottesville, VA

B.S. Environmental Science, University of Connecticut, 2019

A Dissertation presented to the Graduate Faculty of the University of Virginia in Candidacy for the Degree Doctor of Philosophy

Department of Environmental Sciences

University of Virginia

April 2024

Committee:

Peter Berg (advisor)

Karen McGlathery

Patricia Wiberg

Scott Doney

Lisa Colosi-Peterson

Table of Contents 2

Abstract

Blue carbon ecosystems such as seagrass meadows are widely regarded as carbon sinks that can partially mitigate the effects of anthropogenic climate change. However, the carbon sequestration potential of seagrass meadows is poorly constrained on local and regional scales due to methodological uncertainties and variability in biogeochemical processes such as air-water greenhouse gas exchange of carbon dioxide (CO_2), methane (CH_4), and nitrous oxide (N_2O). In this dissertation, I describe several projects that evaluate biogeochemical processes in a seagrass meadow in South Bay, a shallow coastal lagoon in the Virginia Coast Reserve (VCR), and educate the community about blue carbon ecosystems. 1) A new oxygen optode system for aquatic eddy covariance was rigorously evaluated over the full range of oxygen saturation states in the lab and in the field. The system was well-suited for aquatic eddy covariance and the protocols developed established a new standard for future systems. This work is increasingly relevant as aquatic eddy covariance can be used to derive seagrass metabolism estimates and estimates of air-water gas exchange. 2) The diurnal variability in the gas transfer velocity and CO_2 flux was evaluated using high-frequency data during peak seagrass density. South Bay was primarily a CO_2 sink during the day and a source overnight, following the diurnal pattern of seagrass photosynthesis and respiration. The gas transfer velocity was best predicted with empirical parameterizations based on wind speed. 3) Air-water CO_2 and CH_4 fluxes were derived throughout the seagrass growing season. South Bay was a moderate CO_2 sink and was a consistent source of CH_4 that increased throughout the growing season. CH_4 flux pathways were also assessed. Dissolved and ebullitive CH_4 fluxes were quantified, and CH_4 flux from plant-mediated transport was also identified. Finally, our knowledge of coastal processes in the VCR is leveraged to 4) develop a series of best practices for scientists co-developing authentic science learning experiences with teachers using evidence-based practices.

Acknowledgements

It has been an honor and a privilege to be a graduate student in the Department of Environmental Sciences, and there are many people who have helped and supported me over these last five years. First and foremost, my advisor, Peter Berg, for his wisdom and guidance, and for the many opportunities he has helped pursue throughout multiple projects and an entire pandemic. I would also like to thank the rest of my committee, Karen McGlathery, Scott Doney, Pat Wiberg, and Lisa Colosi-Peterson, for their invaluable feedback, ideas, and support that has helped shape this work. To my other collaborators, Markus Huettel, Bongkeun Song, Cora Baird, and Charles Carlson, and my Sea Grant mentor, Stef Simpson: I have learned so much from each of you. You have been inspiring to work with and this experience would not have been the same without you – thank you. To my undergraduate advisor, Ashley Helton, thank you for helping me get to the starting line, and for all of the advice since then. I have received so much help and support from so many other members of the department, especially Meg Miller, the members of the LTER lagoon group, and the Graduate Student Association. Thank you for everything.

Thank you to my labmates and my shoremates: Carly LaRoche, Ieva Juska, Kylor Kerns, Luke Groff, Carolyn Ewers Lewis, Amelie Berger, Martin Volaric, Kinsey Tedford, Libby Bieri, Elise Turrietta, Lauren Brideau, Paola Granados, and Emily Riffe. A million thank you's to Carly, my partner in crime in South Bay. And thank you to my wonderful friends and fellow scientists who I started this journey with, Marion McKenzie, Madeline Miles, and Zoe Bergman – I could not have done it without you.

I am eternally grateful to the staff at the UVA Coastal Research Center. To Sophia Hoffman, Tom Burkett, Jonah Morreale, and Buck Doughty, thank you for all the boat trips, feedback, and laughs. To Donna, thank you for all the hard work you do and for being a great neighbor in 2021. To Cora, thank you for being an incredible mentor in so many ways.

I am incredibly grateful for all of the unwavering love and support I have received on this journey from my family and friends, especially my partner, David Csordas, and of course, our cats, Adaira and Sidra. To David, thank you for being my rock, confidante, and biggest supporter.

Introduction

Atmospheric concentrations of greenhouse gases such as carbon dioxide (CO_2), methane (CH_4) and nitrous oxide (N_2O) have been rising since the start of the industrial era due to increases in anthropogenic emissions (IPCC 2023). The ocean is a significant global carbon reservoir and, in recent decades, has taken up ~25 % of anthropogenic CO_2 emissions annually (Wanninkhof et al. 2013; Devries 2022). In the coastal ocean and estuaries, physical processes such as mixing and biological processes such as photosynthesis facilitate carbon storage, sequestration, and export to the open ocean for burial (Dai et al. 2022; Resplandy et al. 2024). Coastal vegetated ecosystems, specifically salt marshes, mangroves, and seagrass meadows, are regarded as "blue carbon ecosystems" for their ability to sequester carbon for long periods of time, potentially increasing the amount of anthropogenic greenhouse gas emissions stored in the coastal ocean (Prentice et al. 2020; Macreadie et al. 2021). However, blue carbon ecosystems can also emit CO_2, CH_4, and N_2O, which can partially offset their uptake capacity (Banerjee et al. 2019; Al-Haj and Fulweiler 2020; Rosentreter et al. 2021b). CO_2, CH_4, and N_2O fluxes over seagrass meadows in particular are poorly constrained due to a lack of local and regional data and uncertainties in flux methodologies (Rosentreter et al. 2023).

Seagrasses are flowering marine angiosperms that form meadows off the coast of all continents except Antarctica, in both subtidal and intertidal areas (Dunic et al. 2021; Macreadie et al. 2021). Seagrass meadow ecosystems provide nursery habitat for marine species, increase water quality by trapping sediment and preventing resuspension, and store organic carbon (Corg) in their sediments and biomass (Lawson et al. 2007; Zhu and Wiberg 2022; do Amaral Camara Lima et al. 2023). Evidence suggests that seagrasses may be able to moderate water column pH and that they may be able to keep pace with sea level rise due to sediment deposition (Hendriks et al. 2014; Ricart et al. 2021a; b). In seagrass meadows, oxygen and carbon dioxide are biologically coupled through photosynthesis and respiration (Berg et al. 2019, 2022). Thus, the balance of gross primary production and respiration derived from high-frequency measurements of the benthic O_2 flux can serve as a proxy for carbon flows (Duarte et al. 2010; Rheuban et al. 2014a; Berger et al. 2020).

Aquatic eddy covariance is a groundbreaking flux technique that derives high-quality benthic O_2 fluxes from *in situ* velocity and O_2 concentration measurements. The technique, which is described in detail in Chapter 1, resolves fluxes at a high temporal resolution (15-60 minutes) and integrates fluxes over broad spatial scales (10-100 m^2) (Berg et al. 2003, 2022; Rheuban and Berg 2013). The quality and robustness of O_2 flux measurements has been improved over time by technological advances in the meters and sensors used to measure O_2 (Berg et al. 2016). Upside-down aquatic eddy covariance is an emerging technique that is modeled after aquatic eddy covariance. This approach, detailed in Chapter 2, directly measures O_2 fluxes across the air-water interface (Berg and Pace 2017; Long and Nicholson 2018; Berg et al. 2020).

The benefits of seagrass meadows and other blue carbon ecosystems are of particular importance to coastal communities, as these ecosystems can provide buffering from storm surges and floods, increased revenue through recreation and tourism, and can provide nursery ground for fishers and watermen (do Amaral Camara Lima et al. 2023). These ecosystem services can be especially valuable because coastal communities are more likely to be socially vulnerable, i.e., more susceptible to harm from environmental hazards, compared to non-coastal communities (Harris et al. 2022). Coastal communities are also likely to have higher populations of people from minoritized groups. Seagrass meadows are declining worldwide and are vulnerable to increased heating events as a result of increased atmospheric greenhouse gas concentrations (Aoki et al. 2021; Dunic et al. 2021). Educating coastal communities about coastal vegetated ecosystems in this context is an essential strategy to improve support for restoration and conservation practices.

The Eastern Shore of Virginia (ESVA) is located on the east coast of the United States on the Delmarva peninsula, which is located between the Chesapeake Bay and the Atlantic Ocean (see Ch.2, Fig. 1, Ch.3, Fig. 1). The ESVA is a socially vulnerable and historically-underserved area (U.S. Census, 2020). The research conducted in this dissertation occurred in the Virginia Coast Reserve (VCR), a system of shallow coastal lagoons and barrier islands located between the Delmarva peninsula and the Atlantic Ocean. The VCR is the longest stretch of coastal wilderness on the east coast of the United States and is a pristine coastal ecosystem with minimal anthropogenic influence. It is the location of a long-term ecological research site (VCR-LTER),

and many VCR-LTER scientists spend a significant amount of time living on the ESVA and interacting with the local community. It is also the site of a successful *Zostera marina*, or eelgrass, meadow. Large-scale restoration efforts were initiated in 2001, and after twenty years, the project has resulted in the restoration of 3,612 benthic ha of eelgrass (Orth et al. 2006, 2020; McGlathery et al. 2012). The VCR was also chosen as the site of the world's first eelgrass carbon crediting project (Needelman et al. 2018; Oreska et al. 2020). The carbon crediting project uses the verified carbon standard (VCS) to translate carbon stored in ecosystems into monetary credits, which are sold in the voluntary carbon market to fund further restoration and conservation initiatives (Needelman et al. 2018). When greenhouse gas fluxes are not measured, carbon crediting projects must take a conservative deduction in the number of credits that can be sold (Needelman et al. 2018).

The majority of the work reported in this dissertation was conducted in South Bay, one of the shallow coastal bays located in the VCR. South Bay is an ideal location to evaluate ecosystem metabolism, and the instruments used to measure it, because it is the site of over 12 years of high-quality seagrass metabolism measurements derived from benthic aquatic eddy covariance (Berger et al. 2020; Berg et al. 2022). It is also the central area of the seagrass restoration project, and the location of a significant body of work measuring carbon stocks and biogeochemical processes related to gas fluxes (Greiner et al. 2013; Oreska et al. 2018; Aoki and McGlathery 2018; Berg et al. 2019).

1 Dissertation outline

Chapter 1 details a thorough evaluation of a new O_2 measuring system for aquatic eddy covariance in the laboratory and field. The evaluation considered specific field conditions of environments where aquatic eddy covariance has been used. The results of our evaluation show that the system is well-suited for aquatic eddy covariance at the benthic interface, but not upside-down aquatic eddy covariance. Chapter 1 also outlines a set of guidelines, or best practices, for evaluating new systems that occur in the future.

Chapter 2 constrains air-water CO_2 fluxes over South Bay via a methodological evaluation and fine-scale CO_2 flux measurements. Wind speed, one of the primary drivers of the air-water CO_2 flux, was evaluated locally and regionally. The upside-down aquatic eddy covariance technique

was used to derive *in situ* measurements of gas transfer velocity (k), the primary source of uncertainty in CO_2 flux measurements. The *in situ* k values were used to determine the most appropriate wind-based empirical relationship to estimate k at our site. Finally, air-water CO_2 fluxes were derived for 5-7 days per year in July of 2021, 2022, and 2023 with the improved methods for measuring with speed and k.

Chapter 3 builds on the improved methodologies of Chapter 2 and provides estimates of air-water CO_2, CH_4, and N_2O fluxes over South Bay throughout the seagrass growing season of 2022 and 2023. For CH_4 and N_2O, fluxes were measured via the dissolved, ebullitive, and plant-mediated transport pathways.

Chapter 4 outlines a series of best practices for scientists and educators to use to translate research into authentic science learning experiences for students. The results of this work included implementing a lesson plan and field experience for high school students on the ESVA. The project followed a scholarly approach to teaching and learning.

2 Literature Cited

Al-Haj, A. N., and R. W. Fulweiler. 2020. A synthesis of methane emissions from shallow vegetated coastal ecosystems. Glob Chang Biol **26**: 2988–3005. doi:10.1111/gcb.15046

do Amaral Camara Lima, M., T. F. Bergamo, R. D. Ward, and C. B. Joyce. 2023. A review of seagrass ecosystem services: providing nature-based solutions for a changing world. Hydrobiologia **850**: 2655–2670. doi:10.1007/s10750-023-05244-0

Aoki, L. R., and K. J. McGlathery. 2018. Restoration enhances denitrification and DNRA in subsurface sediments of Zostera marina seagrass meadows. Mar Ecol Prog Ser **602**: 87–102. doi:10.3354/meps12678

Aoki, L. R., K. J. McGlathery, P. L. Wiberg, M. P. J. Oreska, A. C. Berger, P. Berg, and R. J. Orth. 2021. Seagrass Recovery Following Marine Heat Wave Influences Sediment Carbon Stocks. Front Mar Sci **7**. doi:10.3389/fmars.2020.576784

Banerjee, K., A. Paneerselvam, P. Ramachandran, D. Ganguly, G. Singh, and R. Ramesh. 2019. Seagrass and macrophyte mediated CO2 and CH4 dynamics in shallow coastal waters. PLoS One **13**. doi:10.1371/journal.pone.0203922

Berg, P., M. L. Delgard, P. Polsenaere, K. J. McGlathery, S. C. Doney, and A. C. Berger. 2019. Dynamics of benthic metabolism, O 2 , and pCO 2 in a temperate seagrass meadow . Limnol Oceanogr. doi:10.1002/lno.11236

Berg, P., M. Huettel, R. N. Glud, C. E. Reimers, and K. M. Attard. 2022. Aquatic Eddy Covariance: The Method and Its Contributions to Defining Oxygen and Carbon Fluxes in Marine Environments. Ann Rev Mar Sci **14**: 431–455. doi:10.1146/annurev-marine-042121-012329

Berg, P., D. J. Koopmans, M. Huettel, H. Li, K. Mori, and A. Wüest. 2016. A new robust oxygen-temperature sensor for aquatic eddy covariance measurements. Limnol Oceanogr Methods **14**: 151–167. doi:10.1002/lom3.10071

Berg, P., and M. L. Pace. 2017. Continuous measurement of air-water gas exchange by underwater eddy covariance. Biogeosciences **14**: 5595–5606. doi:10.5194/bg-14-5595-2017

Berg, P., M. L. Pace, and C. D. Buelo. 2020. Air–water gas exchange in lakes and reservoirs measured from a moving platform by underwater eddy covariance. Limnol Oceanogr Methods lom3.10373. doi:10.1002/lom3.10373

Berg, P., H. Roy, F. Janssen, V. Meyer, B. B. Jorgensen, M. Huettel, and D. de Beer. 2003. Oxygen uptake by aquatic sediments measured with a novel non-invasive eddy-correlation technique. Mar Ecol Prog Ser **261**: 75–83.

Berger, A. C., P. Berg, K. J. McGlathery, and M. L. Delgard. 2020. Long-term trends and resilience of seagrass metabolism: A decadal aquatic eddy covariance study. Limnol Oceanogr. doi:10.1002/lno.11397

Dai, M., J. Su, Y. Zhao, and others. 2022. Carbon Fluxes in the Coastal Ocean: Synthesis, Boundary Processes, and Future Trends.doi:10.1146/annurev-earth-032320

Devries, T. 2022. Annual Review of Environment and Resources The Ocean Carbon Cycle.doi:10.1146/annurev-environ-120920

Duarte, C. M., N. Marbà, E. Gacia, J. W. Fourqurean, J. Beggins, C. Barrón, and E. T. Apostolaki. 2010. Seagrass community metabolism: Assessing the carbon sink capacity of seagrass meadows. Global Biogeochem Cycles **24**. doi:10.1029/2010GB003793

Dunic, J. C., C. J. Brown, R. M. Connolly, M. P. Turschwell, and I. M. Côté. 2021. Long-term declines and recovery of meadow area across the world's seagrass bioregions. Glob Chang Biol **27**: 4096–4109. doi:10.1111/gcb.15684

Greiner, J. T., K. J. McGlathery, J. Gunnell, and B. A. McKee. 2013. Seagrass Restoration Enhances "Blue Carbon" Sequestration in Coastal Waters. PLoS One **8**. doi:10.1371/journal.pone.0072469

Harris, L. A., T. Grayson, H. A. Neckles, and others. 2022. A Socio-ecological Imperative for Broadening Participation in Coastal and Estuarine Research and Management. Estuaries and Coasts **45**: 38–48. doi:10.1007/s12237-021-00944-z/Published

Hendriks, I. E., Y. S. Olsen, L. Ramajo, L. Basso, A. Steckbauer, T. S. Moore, J. Howard, and C. M. Duarte. 2014. Photosynthetic activity buffers ocean acidification in seagrass meadows. Biogeosciences **11**: 333–346. doi:10.5194/bg-11-333-2014

IPCC. 2023. Climate Change 2023: Synthesis Report. Contribution of Working Groups I, II and III to the Sixth Assessment Report of the Intergovernmental Panel on Climate Change [Core Writing Team, H. Lee and J. Romero (eds.)].

Lawson, S. E., P. L. Wiberg, K. J. McGlathery, and D. C. Fugate. 2007. Wind-driven Sediment Suspension Controls Light Availability in a Shallow Coastal Lagoon. Estuaries and Coasts **30**: 102–112.

Long, M. H., and D. P. Nicholson. 2018. Surface gas exchange determined from an aquatic eddy covariance floating platform. Limnol Oceanogr Methods **16**: 145–159. doi:10.1002/lom3.10233

Macreadie, P. I., M. D. P. Costa, T. B. Atwood, and others. 2021. Blue carbon as a natural climate solution. Nat Rev Earth Environ. doi:10.1038/s43017-021-00224-1

McGlathery, K. J., L. K. Reynolds, L. W. Cole, R. J. Orth, S. R. Marion, and A. Schwarzschild. 2012. Recovery trajectories during state change from bare sediment to eelgrass dominance. Mar Ecol Prog Ser **448**: 209–221. doi:10.3354/meps09574

Needelman, B. A., I. M. Emmer, S. Emmett-Mattox, S. Crooks, J. P. Megonigal, D. Myers, M. P. J. Oreska, and K. McGlathery. 2018. The Science and Policy of the Verified Carbon Standard Methodology for Tidal Wetland and Seagrass Restoration. Estuaries and Coasts **41**: 2159–2171. doi:10.1007/s12237-018-0429-0

Oreska, M. P. J., K. J. McGlathery, L. R. Aoki, A. C. Berger, P. Berg, and L. Mullins. 2020. The greenhouse gas offset potential from seagrass restoration. Sci Rep **10**. doi:10.1038/s41598-020-64094-1

Oreska, M. P. J., G. M. Wilkinson, K. J. McGlathery, M. Bost, and B. A. McKee. 2018. Non-seagrass carbon contributions to seagrass sediment blue carbon. Limnol Oceanogr **63**: S3–S18. doi:10.1002/lno.10718

Orth, R. J., J. S. Lefcheck, K. S. Mcglathery, and others. 2020. Restoration of seagrass habitat leads to rapid recovery of coastal ecosystem services.

Orth, R. J., M. L. Luckenbach, S. R. Marion, K. A. Moore, and D. J. Wilcox. 2006. Seagrass recovery in the Delmarva Coastal Bays, USA. Aquat Bot **84**: 26–36. doi:10.1016/j.aquabot.2005.07.007

Prentice, C., K. L. Poppe, M. Lutz, and others. 2020. A Synthesis of Blue Carbon Stocks, Sources, and Accumulation Rates in Eelgrass (Zostera marina) Meadows in the Northeast Pacific. Global Biogeochem Cycles **34**. doi:10.1029/2019GB006345

Resplandy, L., A. Hogikyan, J. D. Müller, and others. 2024. A Synthesis of Global Coastal Ocean Greenhouse Gas Fluxes. Global Biogeochem Cycles **38**. doi:10.1029/2023GB007803

Rheuban, J. E., and P. Berg. 2013. The effects of spatial and temporal variability at the sediment surface on aquatic eddy correlation flux measurements. Limnol Oceanogr Methods **11**: 351–359. doi:10.4319/lom.2013.11.351

Rheuban, J. E., P. Berg, and K. J. McGlathery. 2014. Ecosystem metabolism along a colonization gradient of eelgrass (Zostera marina) measured by eddy correlation. Limnol Oceanogr **59**: 1376–1387. doi:10.4319/lo.2014.59.4.1376

Ricart, A. M., B. Gaylord, T. M. Hill, J. D. Sigwart, P. Shukla, M. Ward, A. Ninokawa, and E. Sanford. 2021a. Seagrass-driven changes in carbonate chemistry enhance oyster shell growth. Oecologia **196**: 565–576. doi:10.1007/s00442-021-04949-0

Ricart, A. M., M. Ward, T. M. Hill, and others. 2021b. Coast-wide evidence of low pH amelioration by seagrass ecosystems. Glob Chang Biol **27**: 2580–2591. doi:10.1111/gcb.15594

Rosentreter, J. A., A. V. Borges, B. R. Deemer, and others. 2021. Half of global methane emissions come from highly variable aquatic ecosystem sources. Nat Geosci **14**: 225–230. doi:10.1038/s41561-021-00715-2

Rosentreter, J. A., G. G. Laruelle, H. W. Bange, and others. 2023. Coastal vegetation and estuaries are collectively a greenhouse gas sink. Nat Clim Chang **13**: 579–587. doi:10.1038/s41558-023-01682-9

Wanninkhof, R., G.-H. Park, T. Takahashi, and others. 2013. Global ocean carbon uptake: magnitude, variability and trends. Biogeosciences **10**: 1983–2000. doi:10.5194/bg-10-1983-2013

Zhu, Q., and P. L. Wiberg. 2022. The Importance of Storm Surge for Sediment Delivery to Microtidal Marshes. J Geophys Res Earth Surf **127**. doi:10.1029/2022JF006612

Chapter 1: A high-resolution submersible oxygen optode system for aquatic eddy covariance

Adapted from: Granville, K.E., P. Berg, and M. Huettel. 2023. A high-resolution submersible oxygen optode system for aquatic eddy covariance. Limnology and Oceanography: Methods 21: 152-163

Abstract

The aquatic eddy covariance technique is increasingly used to determine oxygen (O_2) fluxes over benthic ecosystems. The technique uses O_2 measuring systems that have a high temporal and numerical resolution. In this study, we performed a series of lab and field tests to assess a new optical submersible O_2 meter designed for aquatic eddy covariance measurements and equipped with an existing ultrafast optical fiber sensor. The meter has a 16-bit digital-to-analog-signal conversion that produces a 0-5 V output at a rate up to 40 Hz. The device was paired with an acoustic Doppler velocimeter for velocity measurements. The combined meter and fiber-optic O_2 sensor's response time was significantly faster in O_2-undersaturated water compared to in O_2-supersaturated water (0.087 vs. 0.14 s), but still sufficiently fast for aquatic eddy covariance measurements. The O_2 concentration signal was not sensitive to variations in water flow or light exposure. However, the response time was affected by the direction of the flow. When the sensor tip was exposed to a flow from the back rather than the front, the response time increased by 37%. The meter's internal signal processing time was determined to be ~0.05 s, a delay that can be corrected for during post-processing. In order for the built-in temperature correction to be accurate, the meter should always be submerged in the same body of water as the fiber-optic sensor. In multiple 21 – 47 h field tests, the system recorded consistently high-quality, low-noise O_2 flux data. Overall, the new meter is a powerful option for collecting high-quality aquatic eddy covariance data.

1 Introduction

O_2 flux measurements at the sediment-water interface are typically used to quantify benthic ecosystem health and as a proxy for carbon cycling in aquatic environments such as

seagrass meadows, oyster reefs, and mudflats (Gazeau et al. 2005; Glud 2008; Eyre et al. 2011; Berg et al. 2022). However, representative *in situ* fluxes, determined under naturally varying environmental conditions, are difficult to obtain due to various limitations of standard flux methodologies (Cook et al. 2007; Glud 2008). Benthic flux chambers separate an enclosed area from the surrounding environment, which excludes *in situ* hydrodynamics and disturbs *in situ* light conditions (Tengberg et al. 2004; Polsenaere et al. 2021; Amo-Seco et al. 2021). *In situ* microelectrode profiling and subsequent profile interpretations exclude the effects of local macrofauna (Archer and Devol 1992; Glud 2008) and may produce artefacts in permeable sediments due to interactions with bottom flows (Huettel and Gust 1992). Laboratory sediment core incubations introduce additional artefacts by removing the sample from the natural environment (Khalil et al. 2013).

Over the last two decades, the aquatic eddy covariance (AEC) technique (Berg et al. 2003) has improved the quality of benthic O_2 flux measurements for many ecosystems, including seagrass meadows (Lee et al. 2017; Berger et al. 2020; Koopmans et al. 2020), oyster and mussel reefs (Attard et al. 2019b; Volaric et al. 2020), macroalgal and Maerl beds (Attard et al. 2019a; Polsenaere et al. 2021), permeable sands (Chipman et al. 2016; Merikhi et al. 2021), freshwater systems (McGinnis et al. 2008; Koopmans and Berg 2015), and coral reefs (Long et al. 2013; de Froe et al. 2019). It has also recently been used for upside-down measurements of gas exchange at the air-water interface (Berg and Pace 2017; Long and Nicholson 2018; Berg et al. 2020). The technique measures *in situ* O_2 fluxes without altering light and flow conditions or excluding the sampling area from the surrounding environment. It accounts for small-scale spatial variability and benthic heterogeneity by integrating the flux over an area of 10-100m^2 (Berg et al. 2007; Rheuban and Berg 2013). Deployments typically last for 24-72 hours, and fluxes are usually resolved over time intervals of 15 min to 1 h. The technique derives fluxes from simultaneously-measured *in-situ* water column velocities and associated water column O_2 concentrations. The velocities are measured at rates between 8-64 Hz by an acoustic Doppler velocimeter (ADV), while O_2 concentrations are recorded near the ADV measuring volume by a fast-responding O_2 measuring system (Berg et al. 2022).

Fast-responding O_2 measuring systems used for AEC include systems based on microelectrodes, fiber-optic optodes, or micro-planar optodes. Thin Clark-type glass

microelectrodes typically have short response times (< 0.3 s) but consume O_2, which makes their signal sensitive to current velocity changes (stirring sensitivity) (Reimers et al. 2016; Attard et al. 2016). Their fragile sensor tips (outer tip diameter 10-200 µm) break more easily than other sensors, resulting in a loss of data (Chipman et al. 2012; Attard et al. 2014). Fiber-optic optodes also typically have short response times (< 0.3 s), and use luminescence quenching by O_2 to quantify O_2 concentrations, a process that does not consume O_2 (Chipman et al. 2012; Koopmans et al. 2020). While some studies report no or negligible stirring sensitivity (Holtappels et al. 2015; Chipman et al. 2016), others have shown that fiber-optic sensors can exhibit stirring sensitivity (Berg et al. 2017). Although fiber-optic sensors are less susceptible to signal drift and typically have a more robust tip (e.g. outer tip diameter 430 µM) than microelectrodes (Chipman et al. 2016), they will experience a loss of signal strength over time due to bleaching of the fluorophore that coats the tip. Biofouling of both fiber-optodes and microelectrodes can cause erroneous signals (Huettel et al. 2020), and collisions with debris can lead to signal spikes, sensor defects and data loss (Koopmans et al. 2020, 2021). To increase robustness and thus, deployment success, some studies use multiple microelectrodes or fiber-optic optodes (Attard et al. 2014, 2019b; Merikhi et al. 2021). An alternative to these sensing systems is the micro-planar optode sensor, which is more robust because of its larger tip (8 mm diameter) that does not break and is rarely affected by floating debris (Berg et al. 2016; Amo-Seco et al. 2021). However, its relatively large tip can disturb the current flow, so recorded data may be compromised when the current flow comes from behind the sensor (Huettel et al. 2020). The micro-planar optode must be placed farther away from the ADV so that its tip does not disturb velocity measurements (Berg et al. 2016).

Due to their complexities, O_2 measuring systems used for AEC must undergo rigorous testing under well-defined lab and field conditions to assess performance, reliability, and potential limitations (McGinnis et al. 2011; Chipman et al. 2012; Berg et al. 2016). Typically, these O_2 measuring systems are tested in the lab in water that is close to atmospheric saturation or O_2-undersaturated. These conditions are indeed representative of some ecosystems where AEC has been used, such as unvegetated muddy sediments at depths below the photic zone (Berg et al. 2009; Attard et al. 2014; Amo-Seco et al. 2021). However, the water column of ecosystems dominated by photosynthesizing vegetation such as seagrass meadows (Rheuban et al. 2014b; Berger et al. 2020) or macroalgal canopies (Attard et al. 2019a; Volaric et al. 2019) can be highly

supersaturated with O_2 during the daytime. To best represent such field conditions, new O_2 measuring systems for AEC should be evaluated under both O_2-undersaturated and O_2-supersaturated conditions.

In this study, we assessed the suitability of a new fiber-optic O_2 measuring system for AEC. We provide a review of the system's characteristics and performance in the lab over a broad spectrum of conditions and in the field in a shallow, temperate seagrass meadow.

2 Materials and Procedures

2.1 New O_2 measuring system

The AquapHOx®-LX logger (hereafter termed "AquapHOx") is a new optical submersible meter designed and optimized for fast response times and high-resolution O_2 readings (PyroScience, GmbH; Aachen, Germany). The AquapHOx has a measuring frequency up to 40 Hz, a 16-bit digital-to-analog signal conversion, and a 0-5 V analog output. To measure O_2 concentrations, the AquapHOx is connected to a manufacturer-calibrated, ultra-fast-responding retractable fiber-optic minisensor (OXR430-UHS-SUB, PyroScience). The AquapHOx automatically compensates for O_2 signal drift due to the temperature dependency of the optode and changes in mean water temperature via a temperature sensor located on the meter's housing (response time = 0.5 s, accuracy = 0.05°C). The AquapHOx produces analog output signals of both the O_2 concentration and temperature at speeds up to 40 Hz.

For our AEC applications, the AquapHOx was also connected to a standard acoustic Doppler velocimeter (ADV) through a one-cable plug-and-play connection (Vector, Nortek, Norway). The ADV measured velocities (x, y, and z) at 64 Hz, powered the AquapHOx, and recorded the analog O_2 concentration and mean temperature output signals. It is advantageous to record all data on the same data logger to effectively identify and account for time offsets between signals (Berg et al. 2022).

We thoroughly tested the PyroScience system (AquapHOx and O_2 sensor) in the lab and the field (Table 1). In all tests, O_2 concentrations were measured by the PyroScience system at 40 Hz. The ADV recorded velocity data at 64 Hz in the lab experiments and at 16 Hz in the field experiments. For noise reduction, these high-frequency ADV and O_2 signals were reduced to 8

Hz through averaging before eddy fluxes were extracted (Berg et al. 2015, Lorrai et al. 2010, Berg et al. 2009).

Table 1. List of lab and field tests conducted with the PyroScience system.

Test	Description
Response time evaluation: O_2 saturation state	Fiber-optic sensor was dipped into a rotating water bath in O_2-undersaturated and O_2-supersaturated water
Response time evaluation: Effect of sensor angle	Sensor was dipped into a rotating water bath at three angles relative to the main current flow
System precision	O_2 signal readings from the new system and from reference optodes were compared in a rotating water bath with varying O_2 concentrations
Time delay	The time delay caused by internal signal processing was evaluated
Temperature correction bypass	The built-in temperature correction was bypassed, and the resulting temperature sensitivity was assessed
Sunlight sensitivity	The sensor was submerged in a rotating water bath that was exposed to periods of sunlight and darkness
Stirring sensitivity: water bath	The sensor was submerged in a rotating water bath with varying tangential velocities
Stirring sensitivity: wave tank	The AEC system was submerged in wave tank
Field test	The AEC system was deployed for 6 days in a seagrass meadow at the Virginia Coast Reserve Long-Term Ecological Research site

2.2 Response time evaluation

System response time was assessed by measuring the $t_{90\%}$ response time, which is the amount of time a system requires to register 90% of an abrupt change in O_2 concentration. To create this abrupt concentration change, the fiber-optic sensor tip was quickly dipped from the air into an O_2-undersaturated (<10% saturation) water bath at a perpendicular angle to the main current flow (90°). The water bath (diameter = 30 cm, depth = 20 cm) was continuously stirred with a stir bar to ensure no O_2 concentration gradients were present. The stable air and water O_2 concentrations, as well as 90% of the change between the two, were marked with dashed lines on a graph (Fig. 1a). The number of time intervals between data points for the signal to get from the

"air-line" to below the "$t_{90\%}$-line" were counted and divided by the ADV frequency (64 Hz). Because the AquapHOx updated its analog signal 40 times per second (40 Hz) while the ADV recorded data at 64 Hz, two data points sometimes occurred side-by-side (Fig. 1). Turbulent frequencies less than 8 Hz typically contribute little to the O_2 flux, so these side-by-side points would not compromise flux estimates. Three fiber-optic sensors were used, and each sensor was tested nine times. The entire test was repeated in O_2-supersaturated water (~200% saturation) (Fig. 1b).

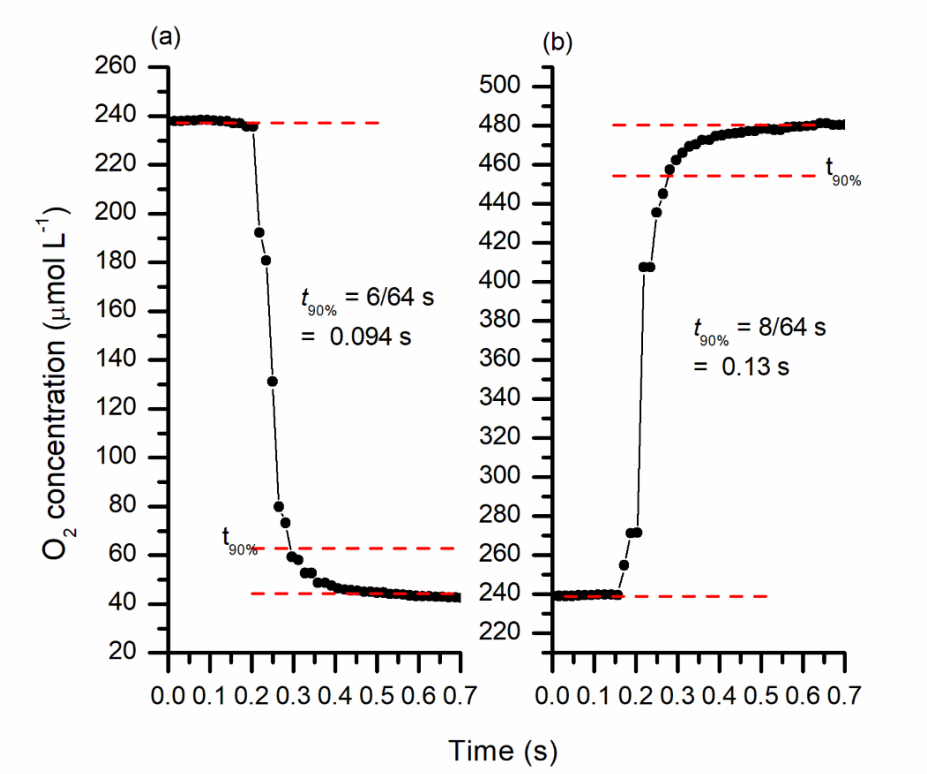

Fig. 1. Examples of the $t_{90\%}$ response time measured in **(a)** O_2-undersaturated water and **(b)** O_2-supersaturated water. Sensors were dipped vertically from the air (O_2 saturation ~240 µmol L^{-1}) into the water. The $t_{90\%}$ response time calculation is shown for each set of results.

The effect of sensor angle relative to the main current flow on the $t_{90\%}$ response time was also assessed. The response time test was repeated in O_2-undersaturated water while the sensor was dipped at two more angles: first, at a 45° angle pointing into the main flow direction (45°), and then at a 45° angle pointing away from the main flow direction (-45°). Response times were compared to the response times determined using perpendicular (90°) dips into O_2-

undersaturated water. Differences in $t_{90\%}$ response times were analyzed using a one-way ANOVA.

2.3 System precision

We evaluated system precision by comparing the PyroScience system's O_2 concentration readings to those of two reference planar optode systems ($t_{90\%}$ = ~30 s) (miniDOT, PME, USA) that are characterized by minimal drift. The fiber-optic sensor and the miniDOTs were submerged in an O_2-undersaturated, rotating water bath that was open to the atmosphere. The sensors remained in the water until the O_2 concentration in the water bath had re-equilibrated with the atmosphere. This test was repeated in an O_2-supersaturated water bath.

2.4 Time delay

Photon collection and subsequent signal processing within the AquapHOx can introduce a time lag between the ADV velocity data and the O_2 concentration data. Unless corrected for, such lag time can result in the systematic underestimation of fluxes. To assess this potential time lag, the fiber-optic sensor and the ADV transmitter were simultaneously dipped into an O_2-undersaturated water bath that was seeded with particles to ensure adequate backscatter for acoustic velocity measurements. The optical fiber tip was attached to the ADV a few millimeters away from and at the same height as the transmitter to ensure that they penetrated the water surface at the same time. We compared the times that the PyroScience system and the ADV recorded the transition from air into water by analyzing the ADV signal-to-noise ratio (SNR) and the PyroScience system's O_2 concentration reported by the ADV ("counts"). The internal time lag was found by averaging the time difference over 21 trials. To ensure that no time delay existed within the ADV itself, this experiment was repeated where the PyroScience system was replaced by an electric circuit. The circuit was comprised of a conducting wire with a non-insulated ending that was mounted similarly to the optical fiber sensor next to the ADV transmitter, and two 1.5 V batteries that were used as an electric switch that closed when the wire contacted the water surface.

2.5 Temperature correction bypass

Submersible O_2 measuring systems are sensitive to changes in water temperature (Gundersen et al. 1998; Berg et al. 2022). As a result, most newer systems have a built-in

temperature correction. The PyroScience system applies the correction using a temperature sensor fixed to the housing of the AquapHOx (Fig. 2b). We quantified the PyroScience system's sensitivity to temperature changes when the AquapHOx was not submerged in the same body of water as the fiber-optic sensor. The AquapHOx was placed on a lab bench in a room with a constant air temperature and the sensor was submerged in a water-filled flask along with a dual temperature-and-O_2 planar optode sensor (RINKO, JFE Advantech, Japan) (Fig. 2). The flask was capped to ensure a constant molar O_2 concentration and placed on a hot plate with a stir bar (Fig. 2). The RINKO sensor was chosen as a reference because its temperature and O_2 sensors are mounted next to one another (~3 mm apart). Both systems recorded O_2 concentrations and temperatures for 15 minutes at room temperature, and then for 45 minutes as the water was gradually heated. This test was performed in O_2-undersaturated water, O_2-saturated water, and O_2-supersaturated water.

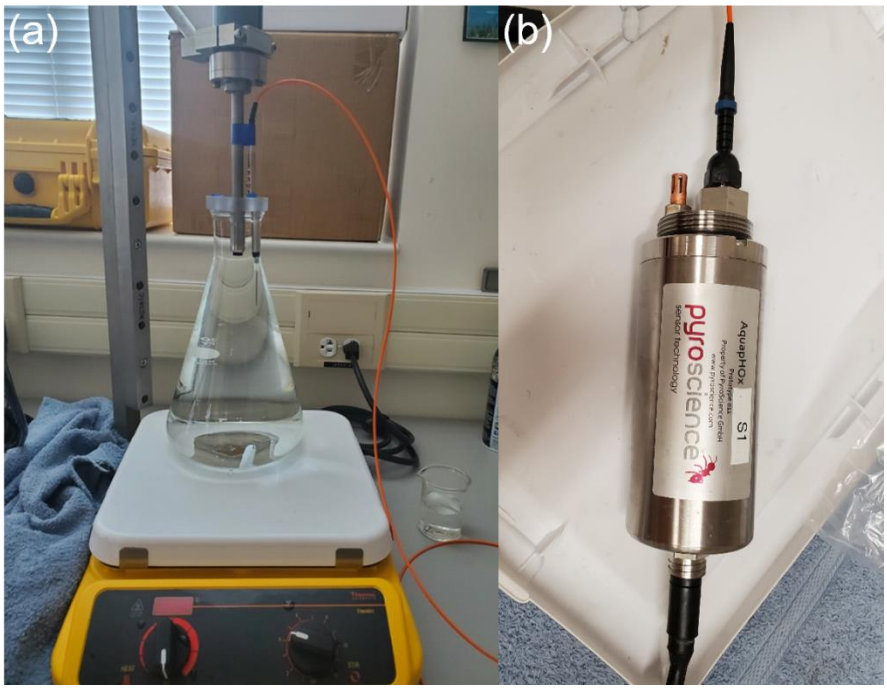

Fig. 2. To test the temperature sensitivity of the PyroScience system when the built-in temperature correction was bypassed, **(a)** the PyroScience sensor and the RINKO sensor were submerged in a water-filled, capped flask while **(b)** the AquapHOx was placed on the lab bench. The temperature sensor mounted on the AquapHOx is contained in the copper-colored small cylinder located next to the fiber connector.

2.6 Sunlight sensitivity

Some fiber-optic sensors are sensitive to changes in light, which can affect the precision of O_2 concentration measurements during the diurnal cycle. We submerged the fiber-optic sensor in an O_2-saturated, rotating water bath that was positioned in direct sunlight. O_2 concentrations were recorded as the water bath was exposed to alternating 5-minute periods of direct sunlight and complete darkness by placing a black box over the entire setup.

2.7 Stirring sensitivity

To assess stirring sensitivity, the fiber-optic sensing tip was exposed to varying tangential velocities in an O_2-saturated, rotating water bath. No O_2 concentration gradients were present due to the mixing applied to the bath, so any observed changes in the O_2 concentration could be attributed to changes in velocity. The water was rotated at tangential velocities of 0 cm s^{-1}, 4 cm s^{-1}, and 15 cm s^{-1}.

The PyroScience system was similarly evaluated for stirring sensitivity in the presence of wave motion using the setup and data analysis described by Berg et al. (2016). In short, the PyroScience system and the ADV were mounted on a frame used for AEC field measurements (see below) and submerged in a wave tank with seeding particles added to facilitate acoustic flow measurements. Velocities and O_2 concentrations were measured by the AEC system.

2.9 Field test

An AEC system comprised of an ADV and the PyroScience system was deployed in a restored eelgrass (*Zostera marina*) meadow in South Bay, a shallow subtidal lagoon located within the Virginia Coast Reserve Long-Term Ecological Research site (VCR-LTER). The lagoon has a mean water depth of 1.2 m and a tidal range of 1 m (Safak et al. 2015). South Bay is an ideal location to evaluate the PyroScience system because it is the site of 15 years of AEC measurements (Hume et al. 2011; Rheuban et al. 2014b; Berger et al. 2020; Juska and Berg 2022).

Four continuous deployments occurred between June 1st, 2021, and June 18th, 2021. Deployments ranged from 21 – 47 h in length, resulting in approximately 6 full days of data. In all deployments, the ADV and the AquapHOx were mounted on a thin, light, stainless-steel frame (Fig. 3) (Berg and Huettel 2008). The ADV measured velocity (x, y, z) continuously at 16 Hz in a ~2 cm^3 measuring volume located 30 cm above the benthic surface, which is the average

eelgrass canopy height at slack tide. The fiber-optic sensor tip was positioned ~0.7 cm away from the edge of the ADV measuring volume to avoid interfering with the velocity measurements (Fig. 3c). To calibrate O_2 concentrations, two reference miniDOTs were positioned at 2 and 30 cm above the sediment surface. No significant vertical stratification was detected. Photosynthetically-active radiation (PAR) was measured at 5-minute intervals by two planar Odyssey PAR loggers mounted 30 cm above the sediment surface. All instruments were deployed and retrieved during low tide.

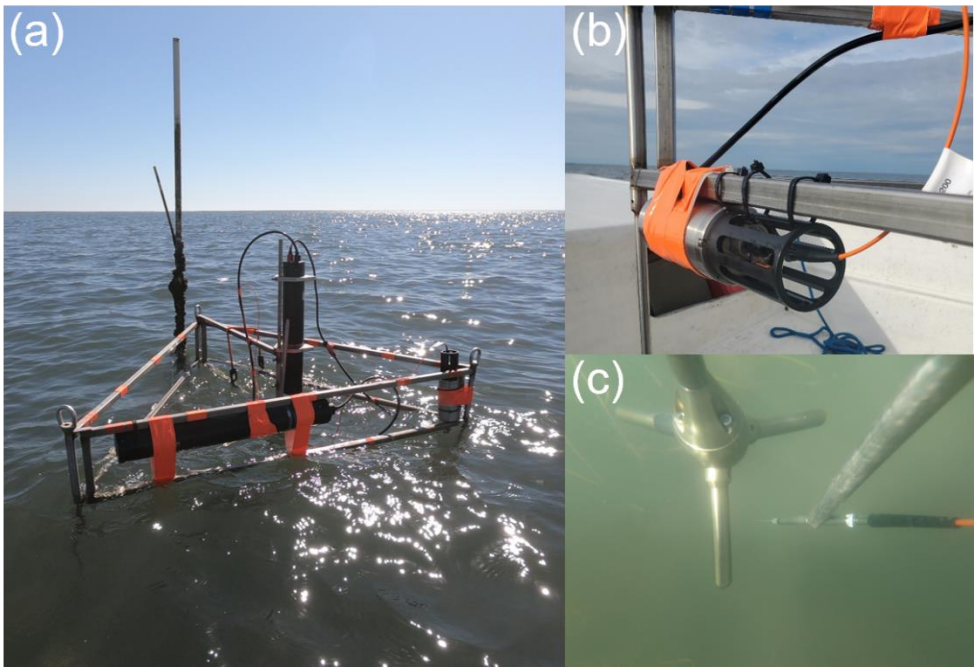

Fig. 3. (a) The ADV, AquapHOx, and fiber-optic sensor were deployed on a light stainless steel frame over a seagrass meadow in South Bay, VA, USA. **(b)** A close-up of the AquapHOx. **(c)** The submerged ADV head and optical O_2 sensor.

Eddy fluxes were extracted following protocols that have been described in detail by Berg et al. (2022) and others. Briefly, 15-minute O_2 fluxes were extracted from the data using EddyFlux3.2 software (Peter Berg, unpublished). In this process, a standard time shift correction (Fan et al. 1990; McGinnis et al. 2008; Lorrai et al. 2010) and storage correction (Rheuban et al. 2014b) were applied. Flux data with signal spikes, which indicate collisions with or temporary attachment of debris in the flow, were removed. The remaining 15-minute fluxes were binned into hourly fluxes.

3 Assessment

3.1 Response time evaluation

The O_2 saturation state of the water had a significant effect on the $t_{90\%}$ response time of the PyroScience system (Fig. 4). The $t_{90\%}$ response time was significantly longer in O_2-supersaturated water than in O_2-undersaturated water ($p = 0.0015$). Specifically, the mean $t_{90\%}$ response time was 0.088 ± 0.0034 s ($n = 27$, mean ± SE) in O_2-undersaturated water and 0.12 ± 0.0067 s ($n = 27$, mean ± SE) in O_2-supersaturated water (Fig. 4).

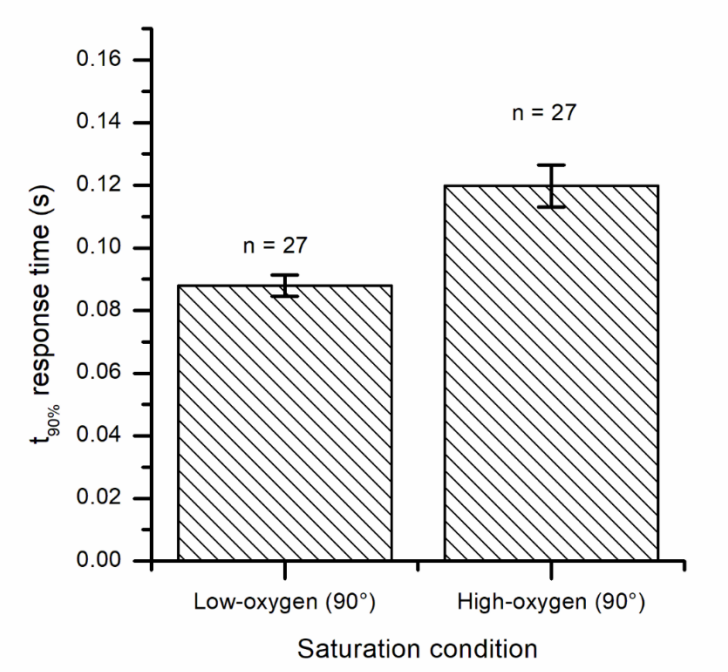

Fig. 4. Mean $t_{90\%}$ response times in low-O_2 (~10% saturation) and high-O_2 (~200% saturation) water when sensors were dipped perpendicularly (90°) into the main current flow. Error bars depict standard error.

The $t_{90\%}$ response time was not significantly different when the sensor was dipped at a 90° angle ($t_{90\%}$ = 0.088 ± 0.0034 s, $n = 27$, mean ± SE) and at a 45° angle ($t_{90\%}$ = 0.087 ± 0.0038 s, $n = 27$, mean ± SE) ($p = 0.91$) in O_2-undersaturated water (Fig. 5). However, the $t_{90\%}$ response time was significantly longer when the sensor was dipped at a -45° angle ($t_{90\%}$ = 0.14 ± 0.010 s, $n = 27$) ($p = 0.00001$) (Fig. 5). Thus, the PyroScience system $t_{90\%}$ response time is shortest when the sensor is positioned at a 90° angle or 45° angle facing into the main current flow.

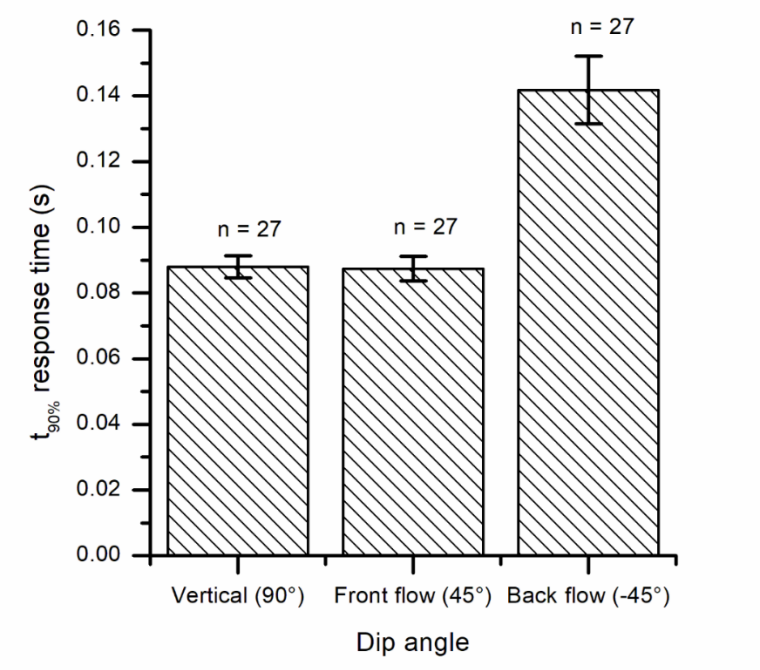

Fig. 5. Mean $t_{90\%}$ response times in O_2-undersaturated water for sensors dipped at three different angles: perpendicular to the main current flow (90°), at a 45° angle facing into the flow ("front flow"), and at a -45° angle facing away from the flow direction ("back flow"). Error bars depict standard error.

3.2 System precision

There was a good overall agreement between O_2 concentrations measured by the PyroScience system and by the two miniDOTs used as references (Fig. 6). There were no noticeable discrepancies between the sensor readings in O_2-undersaturated water or in O_2-saturated water (Fig. 6a). In O_2-supersaturated water, the PyroScience system reported lower O_2 concentrations than the miniDOTs (Fig. 6b). This relatively small concentration difference occurred largely outside of the manufacturer-specified calibration range of the miniDOTs (0-150% O_2 saturation, +/- 10 µM accuracy), and thus, is difficult to address.

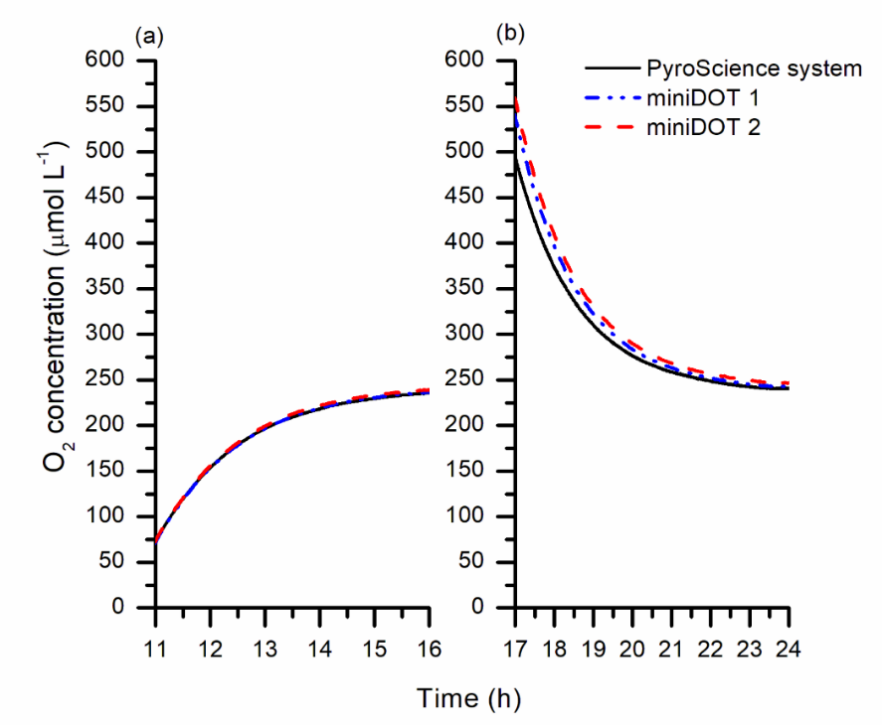

Fig. 6. The fiber-optic sensor and two reference optodes (miniDOT, PME) were submerged in **(a)** an O_2-undersaturated and **(b)** an O_2-supersaturated water bath. During both tests, O_2 concentrations in the water bath re-equilibrated with the atmosphere.

3.3 Time delay

The ADV and electric circuit recorded the dip into water at the same time (Fig. 7a, 7b). Thus, no time delay was detected within the ADV. On the contrary, a distinct time delay was identified between the input and the output sides of the AquapHOx (Fig. 7c, 7d). The average time delay was 0.046 ± 0.0023 s (n = 21, mean ± SE). This time delay can be corrected in post-processing by applying a standard time shift correction.

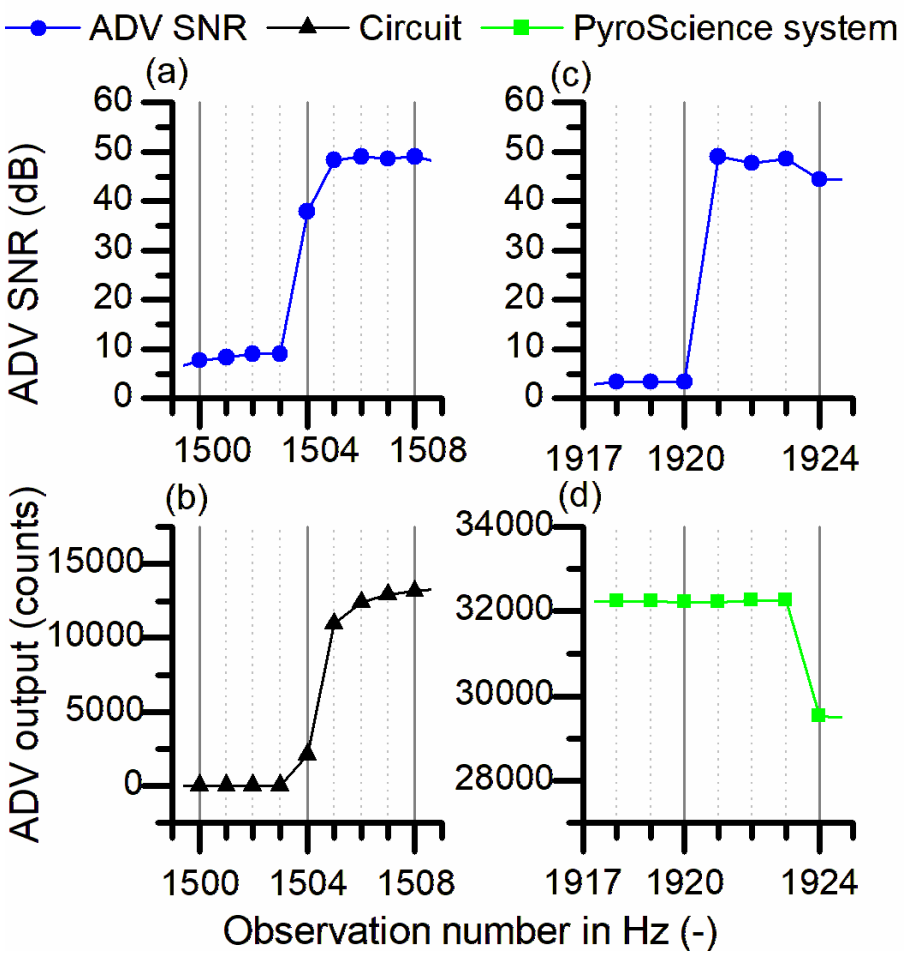

Fig. 7. Potential time delays associated with the ADV **(a, b)** and the PyroScience system **(c, d).** No time delay was observed between **(a)** the ADV signal-to-noise ratio (SNR) and **(b)** the ADV output of the electric circuit. An average time delay of 0.046 ± 0.0023 s (n = 21, mean ± SE) was observed in the PyroScience system when **(c)** the ADV SNR was compared to **(d)** the PyroScience system.

3.4 Temperature correction bypass

When the temperature correction of the O_2 signal was bypassed in the lab, the PyroScience system showed temperature sensitivities comparable to other O_2 measuring systems used for AEC (Berg and Pace 2017; Berg et al. 2022) (Fig. 8). Specifically, when the water temperature was increased, the PyroScience system had a temperature sensitivity of 2.5% per °C in O_2-saturated water, 1.7% per °C in O_2-undersaturated water, and 2.4% per °C in O_2-supersaturated water (Fig. 8).

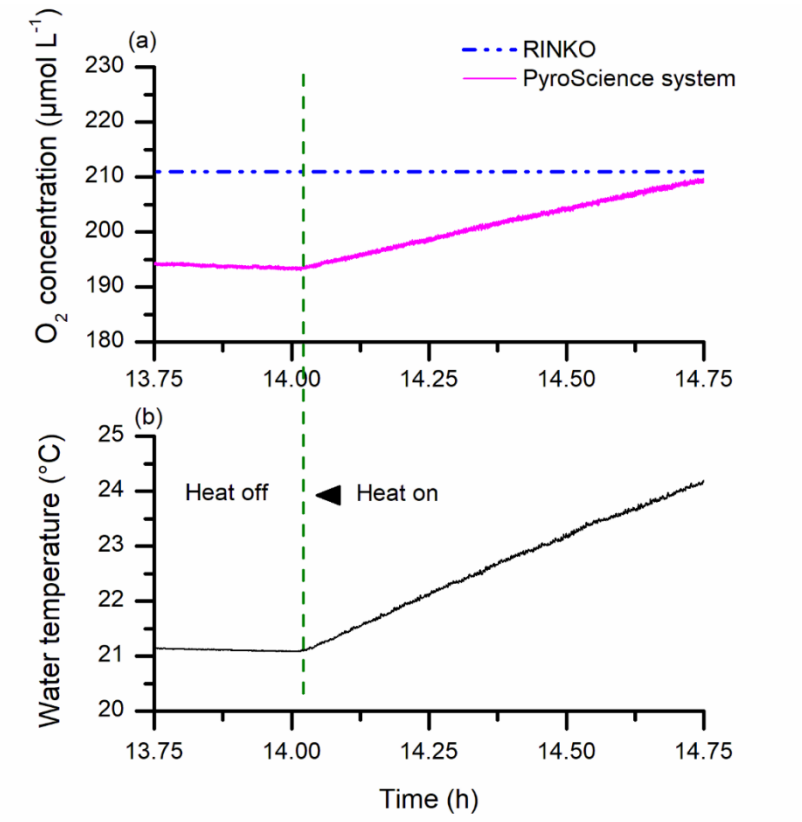

Fig. 8. A fiber-optic sensor and a RINKO planar optode sensor were submerged in a capped flask filled with O_2-saturated water (see Fig. 2). The AquapHOx was placed on a lab bench at room temperature. The PyroScience system and the RINKO recorded **(a)** O_2 concentrations and **(b)** water temperatures. The water was at room temperature for 15 minutes and then was gradually heated for 45 minutes.

3.5 Sunlight sensitivity

The fiber-optic sensor's O_2 concentration readings were not affected by exposure to strong sunlight. The PyroScience system correctly reported consistent O_2 concentrations when the sensor was exposed to periods of strong sunlight and periods of complete darkness (Fig. 9).

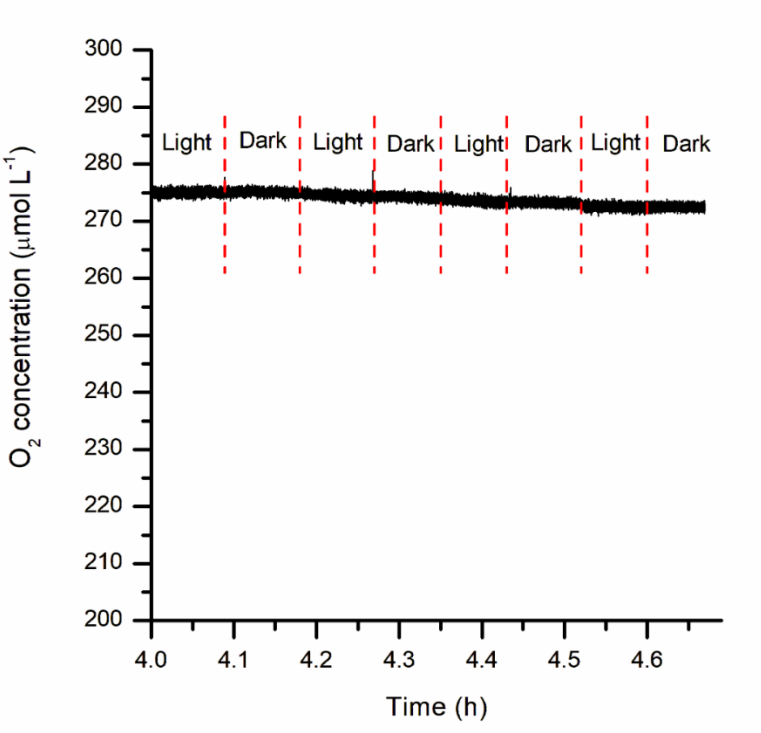

Fig. 9. The PyroScience system was evaluated for sensitivities to strong sunlight. There was no significant change in O_2 concentration readings when the sensor was exposed to periods of strong sunlight and periods of complete darkness.

3.6 Stirring sensitivity

We detected no measurable stirring sensitivity. When the fiber-optic sensor was submerged in the rotating water bath, concentration readings were not significantly different at different tangential velocities (Fig. 10). The minimal upward drift likely occurs because the water bath was slightly O_2-undersaturated with respect to the air at the onset of the test. Similarly, O_2 concentration readings recorded by the AEC system in the wave tank were not affected by wave motion.

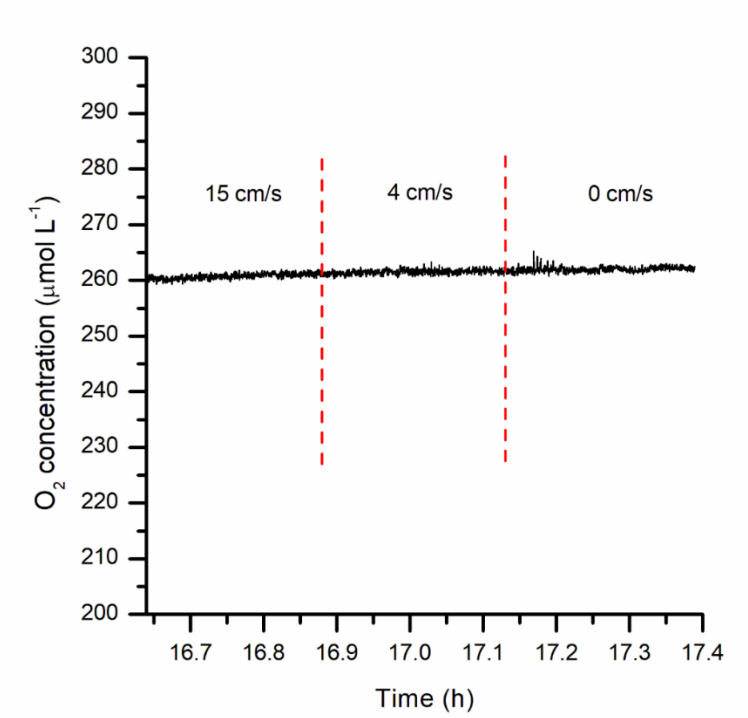

Fig. 10. The fiber-optic O_2 sensor was evaluated for sensitivities to changes in tangential flow velocity. No stirring sensitivity was detected.

3.7 Field test

All field deployments produced high-quality AEC data from which benthic O_2 fluxes were extracted. In the 43-hour sample deployment, O_2 concentrations recorded by the PyroScience system and the two miniDOTs agreed well (Fig 11b). The hourly O_2 fluxes derived from these data were well-correlated with PAR (Fig 11c, 11d). The maximum positive O_2 flux was 599 mmol O_2 m^{-2} d^{-1} and the maximum negative O_2 flux was -284 mmol O_2 m^{-2} d^{-1} (Fig. 11d). These values are within the range of O_2 fluxes previously recorded in South Bay with Clark-type microelectrodes (Berg et al. 2019; Berger et al. 2020). A smaller flux was observed in the middle of day 2 (hour 37), likely due to the effect of a decrease in flow velocity on benthic flux (Fig. 11a, 11d), a relationship that has been documented for seagrass meadows before (Hume et al. 2011; Long et al. 2015).

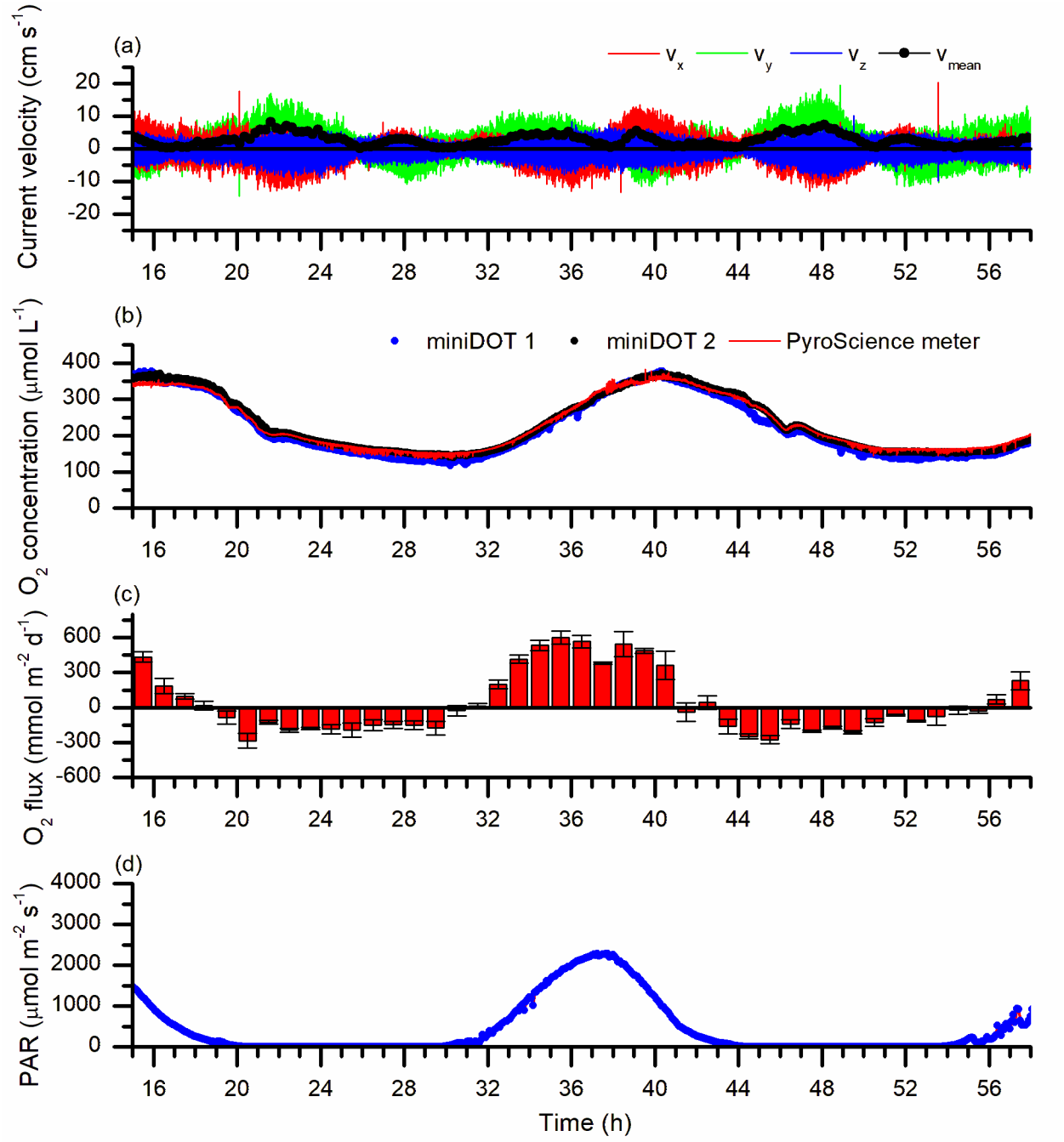

Fig. 11. An example 43-hour-long AEC deployment over a dense seagrass meadow in South Bay (VCR-LTER). **(a)** Velocity measured in three directions (x, y, and z) and the mean current velocity. **(b)** O_2 concentrations measured with two miniDOTs and the PyroScience system. **(c)** Photosynthetically-active radiation (PAR) measured at the average seagrass canopy height. **(d)** Hourly O_2 fluxes extracted from the data in Panel (a) and (b). Positive fluxes represent an O_2 flux into the water column. Error bars depict standard error.

4 Discussion

Aquatic eddy covariance (AEC) is a cutting-edge technique that is increasingly used to quantify *in situ* benthic O_2 fluxes under naturally varying environmental conditions (Berg et al. 2003, 2022; Long 2021). While the principle of the technique is simple – it relies on rapid measurements of the vertical water velocities and O_2 concentrations above the benthic surface – there are challenges associated with the technologies applied to secure such data. In this study, we tested a new optical submersible meter (the AquapHOx®-LX, PyroScience), which was designed and optimized by the manufacturer to fit the criteria for high-quality AEC measurements of O_2 fluxes. We present a series of rigorous lab and field tests to evaluate the performance of the AquapHOx. In all tests, the AquapHOx was connected to an ultra-fast-responding fiber-optic O_2 sensor (OXR430-UHS-SUB, PyroScience) to measure O_2 concentrations and to an acoustic Doppler velocimeter (Vector, Nortek) to provide power to and record the output from the AquapHOx.

The $t_{90\%}$ response time of the PyroScience system was 27% slower when the sensor was dipped into O_2-supersaturated water (~200%) compared to into O_2-undersaturated water (<10%). Typically, sensor response times are not assessed in O_2-supersaturated water, even though O_2-supersaturated conditions have been reported in shallow-water environments (Attard et al. 2014, 2019a; Long et al. 2020). For example, Berger et al. (2020) reported frequent O_2 saturation levels of over 200% in a temperate seagrass meadow. The substantial difference in response times found here may be caused by the diminishing phosphorescence decay of fiber-optic measuring systems associated with increasing O_2 concentrations or the low luminescence at high O_2 concentrations which reduces system sensitivity.

Similarly, the dipping angle between the sensor and the water surface affected response time. The sensor response times were, on average, 37% slower when the sensor was dipped at a -45° angle (flow approaching the back of the sensor) compared to a 45° angle (flow approaching the front of the sensor). Dip angles of 45° or 90° (vertical) gave statistically identical response times. The identified difference is presumably due to a thicker diffusive boundary layer between the bulk flow and the O_2 sensing coating on the tip at the -45° angle. Regardless of these differences, all identified response times ($t_{90\%}$ = 0.087-0.14 s) are well within the range of those reported for other O_2 sensors successfully used for AEC ($t_{90\%}$ = 0.25 – 0.5 s) (Berg et al. 2016;

Attard et al. 2019b; Long et al. 2019; Koopmans et al. 2020). It should also be noted that such differences will be corrected for if a standard time shift correction (Fan et al. 1990; McGinnis et al. 2008) is applied to the flux calculation. This data processing step is increasingly used in AEC work (Lorrai et al. 2010; Koopmans et al. 2020; Berg et al. 2022). An added advantage of using this correction is that it will also automatically correct for the internal time delay (0.046 s) associated with signal processing in the AquapHOx found in this study.

A fundamental principle of AEC measurements is that recorded variations in O_2 concentrations are not attributed to changes in other environmental variables. This condition can be challenging to achieve. For example, some O_2 sensors are subject to stirring sensitivity, a phenomenon where changes in velocity alone affect the recorded O_2 concentration. Microelectrode sensors are inherently subject to stirring sensitivity due to their internal consumption of O_2 (Gust et al. 1987; Holtappels et al. 2015). For unknown reasons, optical sensors are sometimes affected by stirring sensitivity as well (Berg et al. 2017), but not always (Holtappels et al. 2015). These conflicting results still need to be investigated. In this study, which included sensor exposure to both varying currents and wave action in separate tests, the O_2 sensors showed no sign of stirring sensitivity. In an independent test, we similarly documented that the O_2 sensors did not show any sensitivity to varying light exposure, which is another dynamic environmental variable that can potentially bias the concentration reading.

All electrochemical and optical O_2 sensors are sensitive to changes in temperature (Gundersen et al. 1998; Berg and Pace 2017). Typically, when exposed to a constant molar O_2 concentration, O_2 sensor readings will change 2-3% per °C of temperature change. For that reason, newer O_2 measuring systems, including the PyroScience system, have a built-in temperature correction of the O_2 signal. We documented that the PyroScience system has a temperature sensitivity that ranges from 1.7–2.5% when this correction is bypassed (Fig. 8). As a result, care must be taken to ensure that the AquapHOx and sensor are submerged in the same body of water at all times during deployments. Even then, the distance between the AquapHOx and the sensor can present a challenge in environments with substantial vertical heat fluxes, such as at the air-water interface or in benthic systems where tides or currents drive pronounced temperature changes (Berg and Pace 2017). In such settings, rapid turbulent fluctuations in temperature associated with the heat flux can be falsely recorded as turbulent fluctuations in O_2

concentration and can bias the O_2 flux. The only means to avoid this is to measure the temperature with a fast-responding temperature sensor located right next to the O_2 sensor (Berg et al. 2016).

The AEC technique requires that data segments corrupted by particle interference or sensor breakage are excluded to reduce the error margin of derived fluxes (Berg et al. 2013; Rheuban and Berg 2013; Attard et al. 2016). The amount of data that is excluded varies with site conditions and the sensor used. Ecosystems with turbid water, floating debris, and frequent high flow rates and wave action such as seagrass meadows sometimes require high percentages of data to be excluded (Rheuban and Berg 2013). For example, no full 24-h data record was collected in South Bay in June 2018 due to breakage of the Clark-type microelectrodes used (Berger et al. 2020). Similarly, and despite using the more robust optical fiber sensors used in this study, 42% of recorded data were excluded from measurements in a eutrophic freshwater embayment (Koopmans et al. 2021). Also, sometimes 50% of the data are excluded when planar optode sensors are used in tidal systems as the larger sensor tip may disrupt velocity measurements (Berg et al. 2016; Amo-Seco et al. 2021). In comparison with these studies, 17% of the recorded data were excluded in our four deployments. Overall, the data were characterized by low noise and less disturbances, and no sensors broke or were compromised by fouling.

The extracted O_2 fluxes from our deployments were fully in line with previous flux measurements recorded at our site using microelectrodes (Rheuban et al. 2014a; Berg et al. 2019; Berger et al. 2020). In our example deployment, hourly O_2 fluxes ranged from -295 to 590 mmol m^{-2} d^{-1}. In comparison, hourly O_2 fluxes from the same site ranged from -267 to 359 mmol m^{-2} d^{-1} in June 2015 (Berg et al. 2019) and from -500 to 550 mmol m^{-2} d^{-1} in June 2014 (Berger et al. 2020). Overall, our lab and field tests demonstrate that the PyroScience system resolves high quality O_2 fluxes, and is an excellent choice for future AEC measurements.

5 Comments and Recommendations

We recommend that future studies of O_2 measuring systems for AEC include an evaluation of $t_{90\%}$ response times at different O_2 saturation states, perhaps tailored using site-specific knowledge of where the sensors will be used. Because such tests, to our knowledge, have not been done before, it is unknown if other sensors may show an even stronger O_2 concentration level dependency. Although it can be a challenge in shallow water systems, the

AquapHOx and O_2 sensor must be submerged in the same body of water at all times during deployments to ensure an accurate temperature correction of the O_2 signal. Finally, we propose that the test protocols developed during this study should be used as guidelines or as a starting point for future evaluations of new O_2 systems that are going to be used for AEC measurements.

6 Literature cited

Amo-Seco, M., C. G. Castro, N. Villacieros-Robineau, F. Alonso-Pérez, R. Graña, G. Rosón, and P. Berg. 2021. Benthic oxygen fluxes in a coastal upwelling system (Ria de Vigo, NW Iberia) measured by aquatic eddy covariance. Mar. Ecol. Prog. Ser. **670**: 15–31. doi:10.3354/meps13770

Archer, D., and A. Devol. 1992. Benthic oxygen fluxes on the Washington shelf and slope: A comparison of in situ microelectrode and chamber flux measurements.

Attard, K. M., R. N. Glud, D. F. McGinnis, and S. Rysgaard. 2014. Seasonal rates of benthic primary production in a Greenland fjord measured by aquatic eddy correlation. Limnol. Oceanogr. **59**: 1555–1569. doi:10.4319/lo.2014.59.5.1555

Attard, K. M., K. Hancke, M. K. Sejr, and R. N. Glud. 2016. Benthic primary production and mineralization in a High Arctic Fjord: In situ assessments by aquatic eddy covariance. Mar. Ecol. Prog. Ser. **554**: 35–50. doi:10.3354/meps11780

Attard, K. M., I. F. Rodil, P. Berg, J. Norkko, A. Norkko, and R. N. Glud. 2019a. Seasonal metabolism and carbon export potential of a key coastal habitat: The perennial canopy-forming macroalga Fucus vesiculosus. Limnol. Oceanogr. **64**: 149–164. doi:10.1002/lno.11026

Attard, K. M., I. F. Rodil, R. N. Glud, P. Berg, J. Norkko, and A. Norkko. 2019b. Seasonal ecosystem metabolism across shallow benthic habitats measured by aquatic eddy covariance. Limnol. Oceanogr. Lett. **4**: 79–86. doi:10.1002/lol2.10107

Berg, P., M. L. Delgard, R. N. Glud, M. Huettel, C. E. Reimers, and M. L. Pace. 2017. Non-invasive Flux Measurements at the Benthic Interface: The Aquatic Eddy Covariance Technique. Limnol. Oceanogr. e-Lectures. doi:10.1002/loe2.10005

Berg, P., M. L. Delgard, P. Polsenaere, K. J. McGlathery, S. C. Doney, and A. C. Berger. 2019. Dynamics of benthic metabolism, O 2 , and pCO 2 in a temperate seagrass meadow . Limnol. Oceanogr. doi:10.1002/lno.11236

Berg, P., R. N. Glud, A. Hume, H. Stahl, K. Oguri, V. Meyer, and H. Kitazato. 2009. Eddy correlation measurements of oxygen uptake in deep ocean sediments. Limnol. Oceanogr. Methods **7**: 576–584.

Berg, P., and M. Huettel. 2008. Monitoring the Seafloor Using the Noninvasive Eddy Correlation Technique:: Integrated Benthic Exchange Dynamics. Spec. ISSUE Coast. Ocean Process. **21**: 164–167. doi:10.2307/24860020

Berg, P., M. Huettel, R. N. Glud, C. E. Reimers, and K. M. Attard. 2022. Aquatic Eddy Covariance: The Method and Its Contributions to Defining Oxygen and Carbon Fluxes in

Marine Environments. Ann. Rev. Mar. Sci. **14**: 431–455. doi:10.1146/annurev-marine-042121-012329

Berg, P., D. J. Koopmans, M. Huettel, H. Li, K. Mori, and A. Wüest. 2016. A new robust oxygen-temperature sensor for aquatic eddy covariance measurements. Limnol. Oceanogr. Methods **14**: 151–167. doi:10.1002/lom3.10071

Berg, P., M. H. Long, M. Huettel, and others. 2013. Eddy correlation measurements of oxygen fluxes in permeable sediments exposed to varying current flow and light. Limnol. Oceanogr. **58**: 1329–1343. doi:10.4319/lo.2013.58.4.1329

Berg, P., and M. L. Pace. 2017. Continuous measurement of air-water gas exchange by underwater eddy covariance. Biogeosciences **14**: 5595–5606. doi:10.5194/bg-14-5595-2017

Berg, P., M. L. Pace, and C. D. Buelo. 2020. Air–water gas exchange in lakes and reservoirs measured from a moving platform by underwater eddy covariance. Limnol. Oceanogr. Methods lom3.10373. doi:10.1002/lom3.10373

Berg, P., H. Roy, F. Janssen, V. Meyer, B. B. Jorgensen, M. Huettel, and D. de Beer. 2003. Oxygen uptake by aquatic sediments measured with a novel non-invasive eddy-correlation technique. Mar. Ecol. Prog. Ser. **261**: 75–83.

Berg, P., H. Røy, and P. L. Wiberg. 2007. Berg, Peter, Hans Røy, and Patricia L. Wiberg. Eddy correlation flux measurements: The sediment surface area that contributes to the flux. Limnol. Oceanogr., 52(4), 2007, 1672–1684.

Berger, A. C., P. Berg, K. J. McGlathery, and M. L. Delgard. 2020. Long-term trends and resilience of seagrass metabolism: A decadal aquatic eddy covariance study. Limnol. Oceanogr. doi:10.1002/lno.11397

Chipman, L., P. Berg, and M. Huettel. 2016. Benthic Oxygen Fluxes Measured by Eddy Covariance in Permeable Gulf of Mexico Shallow-Water Sands. Aquat. Geochemistry **22**: 529–554. doi:10.1007/s10498-016-9305-3

Chipman, L., M. Huettel, P. Berg, V. Meyer, I. Klimant, R. Glud, and F. Wenzhoefer. 2012. Oxygen optodes as fast sensors for eddy correlation measurements in aquatic systems. Limnol. Oceanogr. Methods **10**: 304–316. doi:10.4319/lom.2012.10.304

Cook, P. L. M., F. Wenzhöfer, R. N. Glud, F. Janssen, and M. Huettel. 2007. Benthic solute exchange and carbon mineralization in two shallow subtidal sandy sediments: Effect of advective pore-water exchange. Limnol. Oceanogr. **52**: 1943–1963.

Eyre, B. D., D. Maher, J. M. Oakes, D. V. Erler, and T. M. Glasby. 2011. Differences in benthic metabolism, nutrient fluxes, and denitrification in Caulerpa taxifolia communities compared to uninvaded bare sediment and seagrass (Zostera capricorni) habitats. Limnol. Oceanogr. **56**: 1737–1750. doi:10.4319/lo.2011.56.5.1737

Fan, O., S. C. Wofsy, D. J. Jacob, and D. R. F. 1990. Atmosphere-Biosphere Exchange of CO2 and 03 in the Central Amazon Forest.

de Froe, E., L. Rovelli, R. N. Glud, S. R. Maier, G. Duineveld, F. Mienis, M. Lavaleye, and D. van Oevelen. 2019. Benthic Oxygen and Nitrogen Exchange on a Cold-Water Coral Reef in

the North-East Atlantic Ocean. Front. Mar. Sci. **6**. doi:10.3389/fmars.2019.00665

Gazeau, F., C. M. Duarte, J.-P. Gattuso, and others. 2005. Whole-system metabolism and CO 2 fluxes in a Mediterranean Bay dominated by seagrass beds (Palma Bay, NW Mediterranean).

Glud, R. N. 2008. Oxygen dynamics of marine sediments. Mar. Biol. Res. **4**: 243–289. doi:10.1080/17451000801888726

Gundersen, J. K., N. B. Ramsing, and R. N. Glud. 1998. Predicting the signal of 02 microsensors from physical dimensions, temperature,salinity, and 02 concentration. Limnol. Oceanogr. **43**: 1932–1937.

Gust, G., K. Booij, W. Helder, and B. Sundby. 1987. ON THE VELOCITY SENSITIVITY (STIRRING EFFECT) OF POLAROGRAPHIC OXYGEN MICROELECTRODES.

Holtappels, M., C. Noss, K. Hancke, C. Cathalot, D. F. McGinnis, A. Lorke, and R. N. Glud. 2015. Aquatic eddy correlation: Quantifying the artificial flux caused by stirring-sensitive O2 sensors. PLoS One **10**. doi:10.1371/journal.pone.0116564

Huettel, M., P. Berg, and A. Merikhi. 2020. Technical note: Measurements and data analysis of sediment-water oxygen flux using a new dual-optode eddy covariance instrument. Biogeosciences **17**: 4459–4476. doi:10.5194/bg-17-4459-2020

Huettel, M., and G. Gust. 1992. Impact of bioroughness on interfacial solute exchange in permeable sediments.

Hume, A. C., P. Berg, and K. J. McGlathery. 2011. Dissolved oxygen fluxes and ecosystem metabolism in an eelgrass (Zostera marina) meadow measured with the eddy correlation technique. Limnol. Oceanogr. **56**: 86–96. doi:10.4319/lo.2011.56.1.0086

Juska, I., and P. Berg. 2022. Variation in seagrass meadow respiration measured by aquatic eddy covariance. Limnol. Oceanogr. Lett. **7**: 410–418. doi:10.1002/lol2.10276

Khalil, K., M. Raimonet, A. M. Laverman, and others. 2013. Spatial and Temporal Variability of Sediment Organic Matter Recycling in Two Temperate Eutrophicated Estuaries. Aquat. Geochemistry **19**: 517–542. doi:10.1007/s10498-013-9213-8

Koopmans, D., P. Berg, S. Brunner, and J. V. Klump. 2021. Seiche- and storm-driven benthic oxygen uptake in a eutrophic freshwater bay determined with aquatic eddy covariance. Freshw. Sci. **40**: 259–273. doi:10.1086/714542

Koopmans, D., M. Holtappels, A. Chennu, M. Weber, and D. de Beer. 2020. High Net Primary Production of Mediterranean Seagrass (Posidonia oceanica) Meadows Determined With Aquatic Eddy Covariance. Front. Mar. Sci. **7**. doi:10.3389/fmars.2020.00118

Koopmans, D. J., and P. Berg. 2015. Stream oxygen flux and metabolism determined with the open water and aquatic eddy covariance techniques. Limnol. Oceanogr. **60**: 1344–1355. doi:10.1002/lno.10103

Lee, J. S., D. J. Kang, E. Hineva, V. Slabakova, V. Todorova, J. Park, and J. H. Cho. 2017. Estimation of net ecosystem metabolism of seagrass meadows in the coastal waters of the

East Sea and Black Sea using the noninvasive eddy covariance technique. Ocean Sci. J. **52**: 243–256. doi:10.1007/s12601-017-0032-5

Long, M. H. 2021. Aquatic Biogeochemical Eddy Covariance Fluxes in the Presence of Waves. J. Geophys. Res. Ocean. **126**. doi:10.1029/2020JC016637

Long, M. H., P. Berg, D. de Beer, and J. C. Zieman. 2013. In Situ Coral Reef Oxygen Metabolism: An Eddy Correlation Study. PLoS One **8**. doi:10.1371/journal.pone.0058581

Long, M. H., P. Berg, K. J. McGlathery, and J. C. Zieman. 2015. Sub-tropical seagrass ecosystem metabolism measured by eddy covariance. Mar. Ecol. Prog. Ser. **529**: 75–90. doi:10.3354/meps11314

Long, M. H., and D. P. Nicholson. 2018. Surface gas exchange determined from an aquatic eddy covariance floating platform. Limnol. Oceanogr. Methods **16**: 145–159. doi:10.1002/lom3.10233

Long, M. H., J. E. Rheuban, D. C. McCorkle, D. J. Burdige, and R. C. Zimmerman. 2019. Closing the oxygen mass balance in shallow coastal ecosystems. Limnol. Oceanogr. **64**: 2694–2708. doi:10.1002/lno.11248

Long, M. H., K. Sutherland, S. D. Wankel, D. J. Burdige, and R. C. Zimmerman. 2020. Ebullition of oxygen from seagrasses under supersaturated conditions. Limnol. Oceanogr. **65**: 314–324. doi:10.1002/lno.11299

Lorrai, C., D. F. McGinnis, P. Berg, A. Brand, and A. Wüest. 2010. Application of oxygen eddy correlation in aquatic systems. J. Atmos. Ocean. Technol. **27**: 1533–1546. doi:10.1175/2010JTECHO723.1

McGinnis, D. F., P. Berg, A. Brand, C. Lorrai, T. J. Edmonds, and A. Wüest. 2008. Measurements of eddy correlation oxygen fluxes in shallow freshwaters: Towards routine applications and analysis. Geophys. Res. Lett. **35**. doi:10.1029/2007GL032747

McGinnis, D. F., S. Cherednichenko, S. Sommer, P. Berg, L. Rovelli, R. Schwarz, R. N. Glud, and P. Linke. 2011. Simple, robust eddy correlation amplifier for aquatic dissolved oxygen and hydrogen sulfide flux measurements. Limnol. Oceanogr. Methods **9**: 340–347. doi:10.4319/lom.2011.9.340

Merikhi, A., P. Berg, and M. Huettel. 2021. Technical note: Novel triple O2sensor aquatic eddy covariance instrument with improved time shift correction reveals central role of microphytobenthos for carbon cycling in coral reef sands. Biogeosciences **18**: 5381–5395. doi:10.5194/bg-18-5381-2021

Polsenaere, P., B. Deflandre, G. Thouzeau, and others. 2021. Comparison of benthic oxygen exchange measured by aquatic Eddy Covariance and Benthic Chambers in two contrasting coastal biotopes (Bay of Brest, France). Reg. Stud. Mar. Sci. **43**. doi:10.1016/j.rsma.2021.101668

Reimers, C. E., H. T. Özkan-Haller, A. T. Albright, and P. Berg. 2016. Microelectrode velocity effects and aquatic eddy covariance measurements under waves. J. Atmos. Ocean. Technol. **33**: 263–282. doi:10.1175/JTECH-D-15-0041.1

Rheuban, J. E., and P. Berg. 2013. The effects of spatial and temporal variability at the sediment surface on aquatic eddy correlation flux measurements. Limnol. Oceanogr. Methods **11**: 351–359. doi:10.4319/lom.2013.11.351

Rheuban, J. E., P. Berg, and K. J. McGlathery. 2014a. Ecosystem metabolism along a colonization gradient of eelgrass (Zostera marina) measured by eddy correlation. Limnol. Oceanogr. **59**: 1376–1387. doi:10.4319/lo.2014.59.4.1376

Rheuban, J. E., P. Berg, and K. J. McGlathery. 2014b. Multiple timescale processes drive ecosystem metabolism in eelgrass (Zostera marina) meadows. Mar. Ecol. Prog. Ser. **507**: 1–13. doi:10.3354/meps10843

Safak, I., P. L. Wiberg, D. L. Richardson, and M. O. Kurum. 2015. Controls on residence time and exchange in a system of shallow coastal bays. Cont. Shelf Res. **97**: 7–20. doi:10.1016/j.csr.2015.01.009

Tengberg, A., H. Stahl, G. Gust, V. Müller, U. Arning, H. Andersson, and P. O. J. Hall. 2004. Intercalibration of benthic flux chambers I. Accuracy of flux measurements and influence of chamber hydrodynamics. Prog. Oceanogr. **60**: 1–28. doi:10.1016/j.pocean.2003.12.001

Volaric, M. P., P. Berg, and M. A. Reidenbach. 2019. An invasive macroalga alters ecosystem metabolism and hydrodynamics on a tidal flat. Mar. Ecol. Prog. Ser. **628**: 1–16. doi:10.3354/meps13143

Volaric, M. P., P. Berg, and M. A. Reidenbach. 2020. Drivers of Oyster Reef Ecosystem Metabolism Measured Across Multiple Timescales. Estuaries and Coasts **43**: 2034–2045. doi:10.1007/s12237-020-00745-w/Published

7 Acknowledgements

KEG was supported by a graduate research fellowship from Virginia Sea Grant and by the National Science Foundation (NSF) through grants from the Virginia Coast Reserve Long-Term Ecological Research Program (DEB-1832221). PB was supported by the NSF through grants from the Chemical Oceanography Program (OCE-1851424) and the Ocean Technology and Interdisciplinary Coordination Program (OCE-1824144 and OCE-2223204). MH was supported by the NSF through grants from the Chemical Oceanography Program (OCE-1851290). We thank two anonymous reviewers for their insightful feedback to improve the manuscript. We thank PyroScience GmbH for providing the new prototype AquapHOx and fiber-optic sensors for all our tests. Finally, we thank Ieva Juska and Davis Coffey for their help in the field and the lab. The authors report no known conflicts of interest.

Chapter 2: Gas transfer velocities and CO_2 fluxes vary diurnally over a temperate seagrass meadow

Conducted with support from: Peter Berg, Carly LaRoche, Scott Doney, and Patricia Wiberg.

Abstract

Seagrass meadows sequester carbon for long periods of time. They can also emit or take up greenhouse gases such as carbon dioxide (CO_2). Air-water greenhouse gas fluxes over seagrass meadows are poorly understood primarily due to methodological limitations and lack of local data on fine temporal scales. In this study, we evaluated methodological uncertainties and derived *in situ* air-water CO_2 fluxes over South Bay, a shallow coastal bay located in the Virginia Coast Reserve, USA, that has a benthic environment dominated by a temperate seagrass meadow. To address methodological uncertainties, we evaluated the gas transfer velocity, which is the primary source of uncertainty in the CO_2 flux estimates. Gas transfer velocities over estuaries and oceans are typically derived from empirical relationships with wind speed as the main driver. We compared wind speeds measured *in situ* and at nearby regional wind stations. All wind stations located in proximity to land features significantly underestimated wind speeds over South Bay, while a wind station located in a nearby estuary (Chesapeake Bay) matched the in situ wind speed measurements well. We then derived *in situ* gas transfer velocities using upside-down aquatic eddy covariance and compared them to multiple wind-based gas transfer velocity models. The best-fitting models for South Bay were originally derived over the ocean and had an intercept of zero. Lastly, we derived hourly air-water CO_2 fluxes over South Bay during the peak seagrass density period (early July) for three years. CO_2 fluxes exhibited a distinct diurnal pattern that correlated well with photosynthetically active radiation, suggesting that fluxes are driven by photosynthesis and respiration from photosynthetic organisms such as seagrasses and water column microalgae. Overall, South Bay was a small sink of CO_2 (-0.60 mmol CO_2 m^{-2} d^{-1}) during July. During a storm period captured in our measurements, South Bay was a source of CO_2. When the storm period was removed, South Bay was a larger sink of CO_2 (-4.20 mmol CO_2

m^{-2} d^{-1}). Our results underline the importance of evaluating air-water greenhouse gas fluxes over multiple day-night cycles and during multiple weather conditions.

1 Introduction

Coastal vegetated ecosystems such as seagrass meadows contribute to the global carbon cycle by transporting terrestrial carbon to the ocean and by storing and sequestering organic carbon (C_{org}) (Bianchi et al. 2018; Fennel et al. 2019; Macreadie et al. 2021). The global carbon sequestration capacity of seagrass meadows is uncertain, with global seagrass extent estimates ranging from 16-165 million ha and C_{org} stock estimates ranging from 1,700 to 21,000 Tg C (Prentice et al. 2020; Macreadie et al. 2021). Local- and regional-scale C_{org} stock variability is partially attributed to uncertainties in the carbon dioxide (CO_2), methane (CH_4), and nitrous oxide (N_2O) fluxes over seagrass meadows, which either contribute to or partially offset the carbon sequestration potential of the ecosystem, depending on the direction of the flux (Oreska et al. 2020; Ricart et al. 2020; Kim et al. 2022).

Air-water greenhouse gas flux estimates are highly variable over seagrass meadows because common methodologies often do not capture the rapid internal cycling of flux drivers such as wind speed, gas concentrations, and temperatures that have previously been documented in seagrass meadows (Yang et al. 2019; Berg et al. 2019; Van Dam et al. 2021; Rosentreter et al. 2021c). Additionally, variations in ecosystem metabolism due to changes in photosynthetically active radiation (PAR) and oxygen (O_2) availability, and these changes can significantly influence CO_2 fluxes hourly, daily, and seasonal scales (Ho et al. 2018; Berger et al. 2020; Oreska et al. 2020). CO_2 uptake can also be partially offset by CO_2 emissions from inorganic carbon burial (C_{inorg}) that are facilitated by calcification and carbonate dissolution, especially in meadows that have active bivalve communities or that are located near coral reefs (Saderne et al. 2019; Prentice et al. 2020).

Variability in air-water greenhouse gas flux estimates over estuaries is also partially attributed to uncertainties in existing flux methodologies. Common techniques used to directly measure the *in situ* air-water gas flux, including cavity ring-down spectrometry (Ollivier et al. 2022) and floating chambers (Rosentreter et al. 2017; Jeffrey et al. 2018), usually only provide several hours of flux estimates on fair-weather days. These measurements are often not representative of fluxes over full tidal, diurnal, and annual cycles, or during poor-weather

periods. Eddy covariance towers deployed over estuaries measure fluxes at fine temporal scales for longer periods but have high start-up and maintenance costs (Van Dam et al. 2021). Upside-down aquatic eddy covariance systems can measure fluxes across the air-water interface as well, but this technique has not yet been applied in a tidal estuary for CO_2 flux measurements (Berg et al. 2017, 2020; Long and Nicholson 2018).

As a result of these shortcomings, air-water gas exchange is frequently estimated by a mass transfer equation such as:

$$F = k * (C_w - C_0) \quad \text{(Eqn. 1)}$$

where F is the air-water gas flux (mass area^{-1} time^{-1}), k is the gas transfer velocity (length time^{-1}), C_w is the bulk concentration of the gas in the water column (mass volume^{-1}), and C_0 is the air-equilibrium concentration of the gas at the air-water interface (mass volume^{-1}) (Garcia and Gordon 1992; Cole et al. 2010; Wanninkhof 2014). The gas transfer velocity is the primary source of uncertainty in this calculation because it describes the effect of air-water boundary layer processes on the flux, which is difficult to measure and is often parameterized as a function of an environmental variable (Wanninkhof 1992; Vieira Borges et al. 2004; Ho et al. 2006; Wanninkhof et al. 2009). These empirical parameterizations are usually presented as k_{600} or k_{660} models, where 600 and 660 are the Schmidt numbers for CO_2 at 20°C in freshwater and seawater, respectively (Ho et al. 2011; Wanninkhof 2014). The majority of models used over seagrass meadows or other fetch-limited systems are typically derived from parameterizations of wind speed scaled to 10 m above the ground (U_{10}) (Frankignoulle and Borges 2001; Borges et al. 2018; Ollivier et al. 2022). A number of well-tested wind-based empirical parameterizations were derived over the open ocean, where wind is the major driver of gas exchange for slightly soluble gases (Nightingale et al. 2000; McGillis et al. 2004; Ho et al. 2006; Wanninkhof et al. 2009). Parameterizations based on current velocity and water depth instead of or in addition wind speeds are also used in estuaries, but these variables are often difficult to constrain, whereas wind speed estimates are generally available from regional wind stations or global models (Wanninkhof 2014; Ho et al. 2016; Rosentreter et al. 2017). There is an implicit assumption that the most appropriate wind data over estuaries are those collected closest to the study area, but this assumption has been challenged because bed stress over the land is greater than over the water due to increased roughness from vegetation (Lawson et al. 2007; Mariotti et al. 2018).

Here, we thoroughly assess air-water CO_2 flux dynamics over a shallow, temperate seagrass meadow (South Bay, Virginia, USA) by evaluating major sources of variability in the flux calculation and by deriving hourly CO_2 fluxes over multiple years. Through a comparison of *in situ* and regional wind speed measurements, we determine the ability of regional wind stations on land to predict *in situ* wind speeds. We conduct an analysis of *in situ* and modelled k_{600} values at wind speeds ≤ 4.5 m s^{-1} using upside-down aquatic eddy covariance. Finally, we used the wind speed comparison and k_{600} model analysis to report three years of diurnal CO_2 fluxes on during the peak seagrass density period at our site.

2 Methods

Fig. 1. Map of the Virginia Coast Reserve (VCR), located between the Atlantic Ocean and the Delmarva peninsula. The study site, SB-152, is located in central South Bay. The regional wind speed stations are located on a channel north of the VCR (Wachapreague, NOAA NDBC WAHV2), at the land-water interface of the Chesapeake Bay (Kiptopeke, NOAA NDBC KPTV2), offshore in the Chesapeake Bay (Rappahannock, NOAA NDBC RPLV2), and on one of the VCR barrier islands (Hog, VCR-LTER).

2.1 Study site

This study was conducted in South Bay (SB-152, 37.261881 N, 75.815125 W), a shallow coastal lagoon in the Virginia Coast Reserve (VCR), located offshore of the Delmarva peninsula in the Mid-Atlantic region of the United States (Fig. 1). South Bay has a tidal range of 1.2 m and an average water depth of 1.0 m below mean sea level, is bordered by a barrier island with a

back-barrier marsh (Wreck Island) to the east, and is connected to the Atlantic Ocean by two inlets at the north and south (Fig. 1) (Reidenbach and Thomas 2018). The meadow has minimal anthropogenic influence and no significant freshwater inputs. Wind is the dominant forcing on circulation and has a strong seasonality, with southerly winds typically occurring in the summer and northerly winds typically occurring in the winter (Fagherazzi and Wiberg 2009; Wiberg et al. 2015). The benthos is dominated by a *Zostera marina* meadow that is the result of a successful seagrass restoration project (McGlathery et al. 2012; Orth et al. 2020). The seagrass meadows exhibit a typical growth pattern for temperate seagrasses and seagrass densities peak around 400 – 550 shoots m^{-2} in early July (Rheuban et al. 2014b; Berger et al. 2021; Aoki et al. 2021). The average C_{org} sequestration rate of the meadow is 1070 t CO_2 yr^{-1} from 2013-2016 (Oreska et al., 2020). Significant C_{inorg} burial has not been observed (Saderne et al. 2019; Oreska et al. 2020). Our primary site is in the central area of the seagrass meadow (SB-152, Fig. 1), which is also the site of over a decade of ecosystem metabolism measurements conducted with the aquatic eddy covariance technique (Berg et al. 2003; Berger et al. 2020).

2.2 Regional wind analysis

Regional and *in situ* wind speeds were compared for 5-7 days per month in June, July, August, and October of 2022. *In situ* wind speeds and directions over South Bay were measured at a 1-minute resolution with a compact anemometer (WindLog data logger, RainWise). The compact anemometer was mounted at SB-152 on a 5 m PVC pole that was driven into the sediment. Wind speeds were rescaled to a 10 m height (U_{10}) following (Mariotti et al. 2018):

$$U_{10} = \frac{U_z * \log\left(\frac{10}{z_0}\right)}{\log\left(\frac{z}{z_0}\right)} \quad \text{(Eqn. 2)}$$

where z is the height of the wind sensor above the water (m) and z_0 is the roughness coefficient (0.002 m). Changes in z were accounted for with water depth measurements that were taken at 1-minute intervals with a water level data logger (HOBO U20-04, Onset). *In situ* U_{10} measurements were averaged to 1-hour intervals to reduce noise.

Wind speed and direction measurements were collected from four geographically distinct regional wind stations that have previously been used to estimate wind over the VCR. 6-minute resolution measurements were collected over a channel ("Wachapreague", NOAA NDBC

WAHV2; 37.608 N, 75.686 W), at the land-water interface of the Chesapeake Bay ("Kiptopeke", NOAA NDBC KPTV2; 37.165 N, 75.988 W), and at an open-water site in the Chesapeake Bay ("Rappahannock", NOAA NDBC RPLV2; 37.538 N, 76.014 W) (Fig. 1). 1-hour resolution measurements were collected over a barrier island in the VCR ("Hog" Island, VCR-LTER, 37.45052 N, 75.6668 W) (Fig. 1) (Porter and Williams, 2024). All wind speed measurements were rescaled to U_{10} (Eqn. 2) and averaged to a 1-hour resolution for comparison with our *in situ* wind speed measurements.

Hourly wind speed and direction estimates were also collected from a global climate and weather reanalysis product (ERA5). The data occur in a latitude-longitude grid of 0.25 degrees. The wind field site was located offshore of the Chesapeake Bay.

2.3 Upside-down aquatic eddy covariance

High-frequency air-water O_2 fluxes were derived using the upside-down aquatic eddy covariance technique (UAEC) (Berg and Pace 2017; Long and Nicholson 2018; Berg et al. 2020). Briefly, the technique measures the three-dimensional current velocity field using an acoustic Doppler velocimeter (ADV) equipped with a cabled sensor head positioned upward (Vector, Nortek AS), and water column O_2 concentrations using a fast-responding O_2 sensor that is standard for aquatic eddy covariance at 16 Hz ~10 cm below the air-water interface (Berg et al. 2003, 2022; Berg and Pace 2017). An important consideration for UAEC is that turbulent heat fluxes at the air-water interface, unlike those typically found in the benthic environment, can be substantial (Berg et al. 2020). Fast-responding O_2 sensors are inherently sensitive to temperature changes, so O_2 sensor readings must be corrected with parallel high-speed temperature measurements to prevent temperature bias in the O_2 eddy flux calculation (Berg et al. 2020; Granville et al. 2023). Thus, we used a fast-responding dual O_2-temperature planar optode sensor that measured O_2 and temperature at the same point in the water column for this study (RINKO, JFE Advantech). We also independently measured water column O_2 concentrations and temperatures with stable oxygen optodes with a 1-minute resolution (miniDOT, PME). The UAEC system was mounted to a stainless steel pole with a custom mounting device that allowed the system to slide up and down the pole with tidal height. Two buoys and a rudder held the system at a fixed point beneath the water surface, oriented into the main current. O_2 fluxes were extracted from the eddy covariance data, cleaned, and binned into 15-minute intervals following

protocols described in detail in Berg and Pace (2017) and Berg et al. (2022). The UAEC system measured high-quality O_2 fluxes when wind speeds were ≤ 4.5 m s^{-1}. For the purpose of this analysis, we selected a 4-hour deployment period when wind speeds consistently met this condition (August 26th, 2021, 02:45 – 06:45 AM EDT).

We then used Equation 1 to calculate *in situ* k values for O_2 (k_{O_2}), where F was the O_2 flux measured by the UAEC system, C_w was the water column O_2 concentration measured with the stable optode, and C_0 was the air-equilibrium concentration of O_2 derived within the UAEC analysis software (Peter Berg, unpublished). The k_{O_2} values were converted to k_{CO_2}:

$$\frac{k_{O_2}}{k_{CO_2}} = \left(\frac{Sc_{O_2}}{Sc_{CO_2}}\right)^n \quad \text{(Eqn. 3)}$$

where the value of -0.5 was used for n in low-wind systems, and Sc_{O_2} and Sc_{CO_2} are the Schmidt numbers for O_2 and CO_2, respectively (Cole et al. 2010). Sc_{O_2} and Sc_{CO_2} were derived from *in situ* water temperature measurements collected with the miniDOTs, a standard salinity estimate for South Bay (31 ppt), and well-established solubility coefficients for O_2 and CO_2 (Weiss 1974; Jähne et al. 1987; Garcia and Gordon 1992; Wanninkhof 2014).

k_{CO_2} values were also normalized to k_{600} for comparison with the k_{600} models:

$$k_{600} = k_{CO_2} * \left(\frac{600}{Sc_{CO_2}}\right)^n \quad \text{(Eqn. 4)}$$

2.4 k_{600} model analysis

The *in situ* k_{600} values from the August 2021 deployment were compared to values derived from several empirical relationships to determine the best-fitting model for our site (Table 1). We selected k_{600} and k_{660} relationships that had been designed for seagrass meadows or previously been established for use over shallow fetch-limited estuaries comparable to our site. All k_{660} models were normalized to k_{600} assuming the Schmidt numbers were scaled to n = -0.5 for low wind systems (Eqn. 4). A k_{600} model used to derive air-water CO_2 fluxes was chosen through this analysis and scaled to kCO_2.

2.5 Diurnal CO_2 flux estimates

Air-water CO_2 fluxes were derived for 3 days in 2021 (10:00 EDT on July 14th – 10:00 EDT on July 17th), 5 days in 2022 (08:30 EDT on July 6th – 12:30 EDT on July 11th), and 6.5 days in 2023 (16:00 EDT on July 4th – 09:00 EDT on July 11th). These deployments coincided with peak seagrass density. We measured photosynthetically active radiation (PAR) with a LI-192 underwater quantum sensor (miniPAR, PME) and water column temperature and O_2 concentrations with a stable O_2 optode (miniDOT, PME) once per minute at mid-canopy height (30 cm above the seafloor). Salinity was measured with a salt water conductivity logger (HOBO U24-002-C, Onset) in 2023 and a pH sensor in 2022 (SeapHOx V2, SeaBird Scientific). Salinity measurements were unavailable in 2021 and for three days in 2022, so a standard value for South Bay was used (31 ppt). In 2022 and 2023, *in situ* wind speeds were measured with the compact anemometer as described above. *In situ* wind speed data were not available for 2021, so wind data were collected from Rappahannock (NOAA NDBC RPLV2), the best-fitting regional wind station (see below). We counted seagrass shoot densities by hand during each deployment.

The air-water CO_2 flux was calculated every minute following:

$$FCO_2 = K_0 * kCO_2 * (pCO_{2w} - pCO_{2a}) \quad \text{(Eqn. 5)}$$

where FCO_2 is the air-water CO_2 flux (mmol m^{-2} h^{-1}), K_0 is the gas solubility based on temperature and salinity (mmol m^{-3} atm^{-1}), kCO_2 is the gas transfer velocity at the air-water interface (m h^{-1}), and pCO_{2w} and pCO_{2a} are the partial pressures of CO_2 in the water column and overlying air, respectively (atm) (Wanninkhof 1992; Mu et al. 2014). pCO_{2w} was measured continuously (every 2 seconds) with an autonomous, submersible infrared sensor (miniCO_2, Pro Oceanus Systems Inc.). Atmospheric CO_2 mole fractions were retrieved from the NOAA Carbon Tracker Near-Real Time (CT-NRT.v2023-5, Jacobson et al. 2023) and converted to pCO_{2a} using barometric pressure measured over the VCR (Porter and Williams, 2024) and water vapor pressure, which was derived from the *in situ* temperature and salinity measurements using the RStudio "seacarb" package (Weiss and Price 1980; Mu et al. 2014). K_0 was derived from the 1-minute *in situ* temperature and salinity data and a modified form of Henry's law (Weiss 1974; Wanninkhof 2014). kCO_2 was derived using a best fitting k_{600} model determined by the k600 model analysis (see below), The k_{600} equation was converted to kCO_2 by using *in situ* temperature and salinity data to derive Sc_{CO_2} throughout the deployment (Eqn. 4). The 1-minute fluxes were summed to hourly values for analysis. All analyses were conducted in RStudio,

primarily with the "tidyverse" package (v3.3.3, R Core Team). All mean values are reported as mean ± standard deviation.

3 Results

3.1 Regional wind analysis

Throughout the 2022 deployments, *in situ* wind speeds over South Bay were not significantly different than wind speeds measured at the open water station (Rappahannock) or reported by the ERA5 reanalysis (Table 1). The *in situ* wind speeds were under-estimated by an average of 33% by the land-water interface station (Kiptopeke), 43% by the channel station (Wachapreague) and 68% by the barrier island station (Hog) (Table 1). Time series of the July 2022 data are shown to demonstrate the variability across stations (Fig. 2, Table 1). The empirical relationship between U_{10} and k_{600} is often represented by a quadratic or power function, so using these stations to estimate *in situ* wind speeds over South Bay would significantly under-estimate k_{600} and the flux calculation (Ho et al. 2011).

Table 1. The number of observations (n), mean, and standard deviation (sd) of hourly wind speeds scaled to a height of 10 m (U_{10}, m s^{-1}) reported for the *in situ* station, regional stations, and the ERA5 reanalysis for the 2022 study period (June, July, August, and October, 2022). For each regional station and the ERA5 reanalysis, the mean percent deviation from the *in situ* wind station (%) was provided, as well as the p value resulting from the pairwise Wilcoxon rank-sum tests with the *in situ* wind station (significance level $p > 0.05$).

Site	*n*	*Mean*	*Sd*	*Percent difference*	*p value*
South Bay (in situ)	485	4.99	2.36	-	-
Rappahannock	485	4.79	2.48	3.8	0.19
Kiptopeke	485	3.34	1.71	33	$3.7 * 10^{-29}$
Wachapreague	485	2.84	2.16	43	$2.3 * 10^{-47}$
Hog	485	1.60	0.88	68	$5.6 * 10^{-116}$
ERA5 Reanalysis	485	4.85	2.42	2.7	0.42

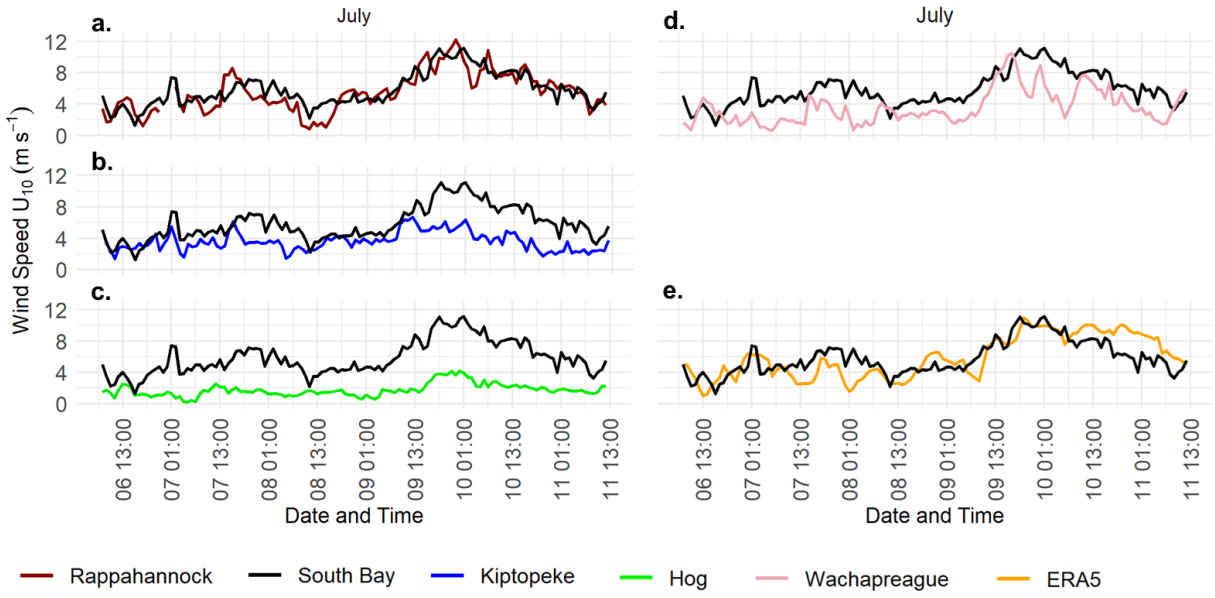

Fig. 2. The July 2022 time series of *in situ* wind speeds (South Bay) was compared to wind speeds reported at the following wind stations: **(a)** Rappahannock, **(b)** Kiptopeke, **(c)** Hog, and **(d)** Wachapreague, as well as by the **(e)** ERA5 reanalysis product. All wind speeds were converted to U_{10}. See Fig. 1 for wind station locations.

3.2 k_{600} model analysis

3.2.1 Peak seagrass density deployments

During the peak seagrass density deployments that occurred in 2021, 2022, and 2023, the mean wind speed was U_{10} = 4.95 ± 2.01 m s^{-1} (mean ± standard deviation). The relationship between k_{600} and wind speed during these deployments was derived for each wind-based empirical relationship (Fig 3a, Table 2). The relative standard deviation of the mean k_{600} across all wind speeds revealed that k_{600} model variability was greatest at low wind speeds, ranging from 123 % when U_{10} = 0.33 m s^{-1} to 50.9 % when U_{10} = 3.50 m s-^{1} (Fig. 3b). k_{600} model variability was lowest when U_{10} ranged from 7.0 – 11.1 m s^{-1}, and the minimum relative standard deviation (18.3 %) occurred when U_{10} = 9.36 m s^{-1} (Fig. 3b). The relative standard deviation increased again at the highest wind speed 43.6 % at U_{10} = 13.70 m s^{-1} (Fig. 3b).

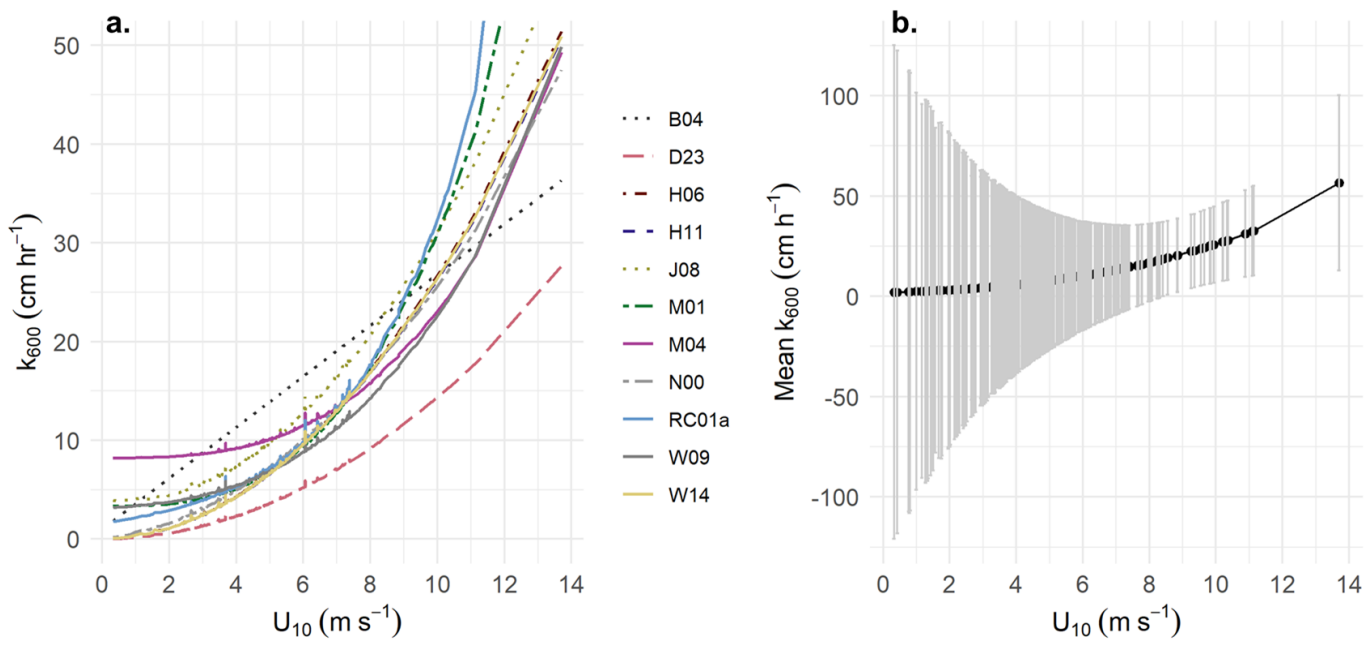

Fig. 3. (a) The k_{600} models in Table 1 and *in situ* U_{10} measurements were used to derive *in situ* k_{600} values during peak seagrass density. **(b)** The relative standard deviation of the mean k_{600} value across measured U_{10}.

3.2.2 Ground-truthed *in situ* k_{600}

The upside-down aquatic eddy covariance technique produced high-quality O_2 fluxes for four hours (August 26th, 2021, 02:45 – 06:45 EDT) when wind speeds were low. The mean wind speed at the Rappahannock station was U_{10} = 3.03 ± 0.63 m s^{-1}. Current velocity decreased throughout the deployment and had a mean value of 4.90 ± 2.22 cm s^{-1} (Fig. 4a). The deployment occurred during low tide and the mean water depth was 0.87 ± 0.0082 m. The O_2 flux was negative throughout the deployment, showing that the water column was a net sink of O_2 (Fig. 4c). The gas transfer velocity of O_2 (k_{O_2}) was positively correlated with both current velocity and wind speed (Fig. 4, Fig. 3). Similarly, a positive correlation between wind speed and current velocity (r = .64, p = .0055, n = 17) was identified with a Spearman's rank-order correlation test using the Hmisc R package (v5.1-1, Harrell, 2023). When k_{O_2} was converted to k_{600}, simple linear regressions showed that wind speed explained 58.84% of the variation in k_{600} and velocity explained 80.63% of the variation.

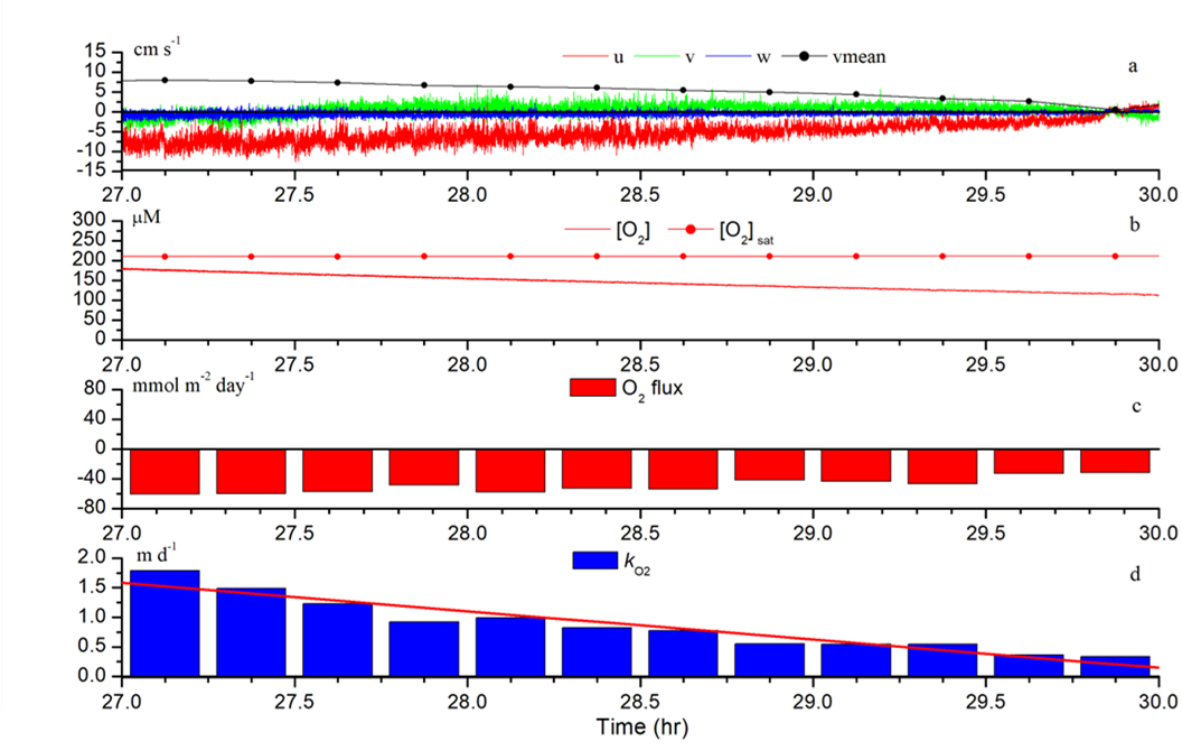

Fig. 4. (a) Current velocity measured in three directions (u, v, and w) and the mean current velocity (vmean), as well as **(b)** water column O_2 concentrations ($[O_2]$) and percent O_2 saturations ($[O_2]_{sat}$) were measured with the upside-down aquatic eddy covariance technique and used to derive **(c)** 15-minute air-water O_2 fluxes. Negative values represent uptake by the water column. **(d)** The gas transfer velocity of O_2 (k_{O_2}) was derived from the O_2 fluxes.

The *in situ* k_{600} values derived from UAEC ranged from 1.08 cm h^{-1} to 5.71 cm h^{-1} and had a mean value of 2.64 ± 1.46 cm h^{-1} during the August 2021 deployment (Fig. 5a). A Kruskal-Wallis rank-sum test identified significant differences between the k_{600} models (chi-squared = 203.97, p = 2.2 * 10^{-16}) using the R stats package (v4.3.2, R Core Team, 2023). Pairwise Wilcoxon rank-sum tests conducted with the stats R package revealed that the k_{600} values derived from *in situ* data were not significantly different from those calculated by the following models: Nightingale et al. (2000) (N00, p = 0.14), Ho et al. (2006) (H06, p = 0.88), Ho et al. (2011) (H11, p = 0.92), and Wanninkhof (2014) (W14, p = 0.92) (n = 17) (v4.3.2, R Core Team, 2023). The relative root-mean-square-error (rRMSE) between the *in situ* k_{600} values and each k_{600} model was derived using the Metrics R package (v0.1.4, Hamner and Frasco, 2018), where a lower rRMSE represents a better goodness-of-fit of the model (Table 2) (Ho et al. 2011, 2016). The rRMSE results are in agreement with the results of the rank-sum tests.

The positive correlation between k_{O_2} and current velocity indicates that current velocity partially drove the variability in gas transfer velocity at our site (Fig. 4a, 4d). However, while the models that included current velocity and water depth (B04c, B04a, and H16) replicated the variability in our *in situ* data, they consistently over-estimated the magnitude (Fig. 5a, Table 2).

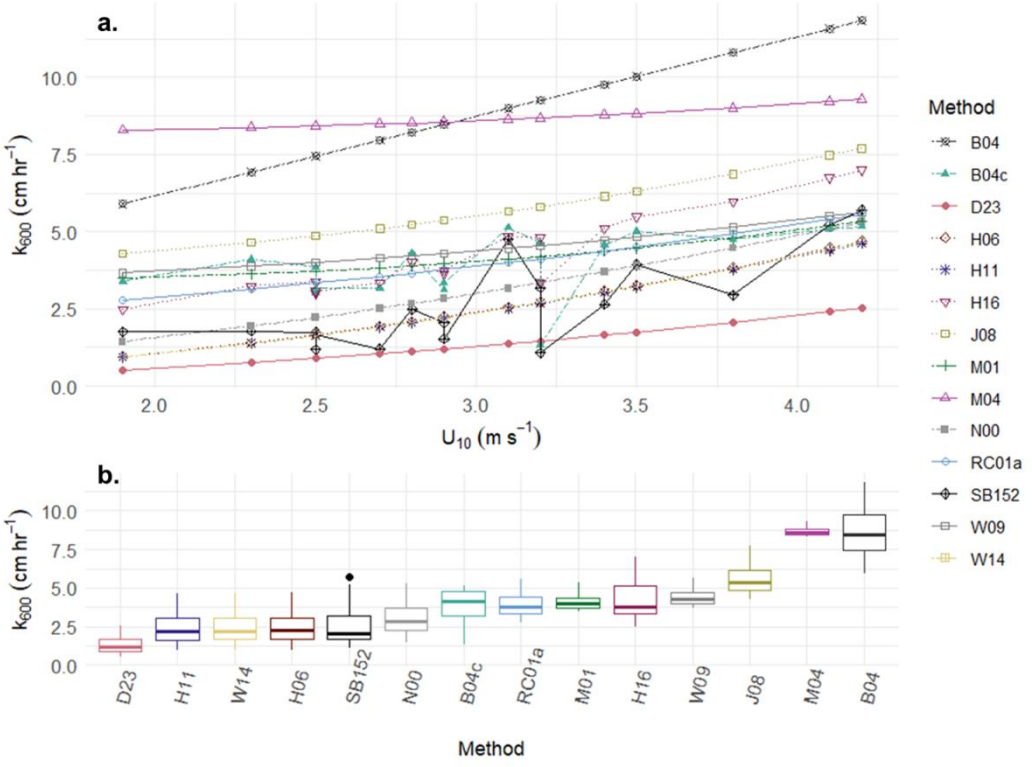

Fig. 5. (a) k_{600} values derived from Rappahannock wind speed measurements and wind-based empirical parameterizations were compared to *in situ* k_{600} values from upside-down aquatic eddy covariance measurements. **(b)** The mean and relative standard deviation of the k_{600} models across deployment wind speeds. The method described by each code is given in Table 2. The *in situ* measurements are denoted by the code "SB152".

Table 2. For each empirical parameterization, the analysis code, the reference, and the original k_{600} or k_{660} model equation is provided. All equations were standardized to k_{600} for our analysis. U_{10} is wind speed scaled to a height of 10 m above the water surface (m s^{-1}), v is current velocity (cm s^{-1}), and h is water depth (m). The mean k_{600} (m s^{-1}) during the August 2021 upside-down aquatic eddy covariance deployment, as well as the relative root-mean-square-error (rRMSE, %) of the *in situ* and modeled data, is shown for each parameterization.

Parameterization		Parameterization	Mean k_{600}	rRMSE
Wind speed parameterizations				
N00	Nightingale et al. 2000	$k_{600} = 0.333U_{10} + 0.222{U_{10}}^2$	3.13 ± 0.264	0.685

M01	McGillis et al. 2001	$k_{660} = 3.3 + 0.026{U_{10}}^3$	4.15 ± 0.128	1.26
RC01	Raymond and Cole 2001	$k_{600} = 1.58e^{0.3U_{10}}$	3.99 ± 0.188	1.12
M04	McGillis et al. 2004	$k_{660} = 8.2 + 0.014{U_{10}}^3$	8.66 ± 0.0691	4.20
B04	Vieira Borges et al. 2004	$k_{600wind} = 1.0 + 2.58U_{10}$	8.82 ± 0.395	4.28
H06	Ho et al. 2006	$k_{600} = (0.266 \pm 0.019){U_{10}}^2$	2.54 ±0.256	0.598
J08	Jiang et al. 2008	$k_{600} = 0.314{U_{10}}^2 - 0.436U_{10} + 3.990$	5.67 ± 0.235	2.16
W09	Wanninkhof et al. 2009	$k_{660} = 3 + 0.1U_{10} + 0.064{U_{10}}^2 + 0.011{U_{10}}^3$	4.47 ± 0.135	1.44
H11	Ho et al. 2011	$k_{600} = (0.262 \pm 0.022){U_{10}}^2$	2.50 ± 0.252	0.603
W14	Wanninkhof 2014	$k_{660} = 0.251{U_{10}}^2$	2.51 ± 0.253	0.601
D23	Dobashi and Ho 2023	$k_{600} = 0.143{U_{10}}^2$	1.37 ± 0.137	1.12
Multi-variable parameterizations				
B04c	Vieira Borges et al. 2004	$k_{600current} = 1.719v^{0.5}h^{-0.5}$	3.95 ± 0.252	1.05
B04a	Vieira Borges et al. 2004	$k_{600all} = 1.0 + 1.719v^{0.5}h^{-0.5} + 2.58U_{10}$	9.77 ± 0.378	4.95
H16	Ho et al. 2016	$k_{600} = 0.77w^{0.5}h^{-0.5} + 0.266{U_{10}}^2$	4.31 ± 0.332	1.22

3.3 Diurnal CO_2 fluxes

Hourly CO_2 fluxes ranged from -2.00 mmol m^{-2} h^{-1} to 5.51 mmol m^{-2} h^{-1} and had a mean value of -0.01 ± 0.842 (Fig. 6a). Here, negative fluxes represent uptake by the water column and positive fluxes represent emission by the water column. The mean k_{CO_2} value was 11.1 ± 7.36 cm h^{-1}. Mean wind speeds were U_{10} = 4.95 ± 2.01 m s^{-1}. Water column p_{CO_2} concentrations and temperatures, components of the CO_2 flux equation, exhibited a negative relationship across all years. Changes in the flux magnitude generally followed the sinusoidal pattern of water column pCO_2 and the inverse of the sinusoidal patterns of water column temperature and dissolved O_2 (Fig. 6).

A storm occurred in 2022 from July 9th at 17:00 to July 10th at 08:00 (Fig. 6a). Flux magnitudes were approximately 2-5 times greater than the average flux during the storm period and reached the maximum positive CO_2 flux value (CO_{2max} = 5.51 mmol m^{-2} h^{-1}) (Fig. 6a). During the storm period, the water column temperature oscillations were disrupted, and

temperatures decreased from 26.70 °C to 21.7 °C, which was the minimum value recorded (Fig. 6a). pCO_2 concentrations increased and reached the maximum value (pCO_{2max} = 1032 µatm) that was well above the average pCO_2 value of 342 ± 176 µatm (Fig. 6b). Wind speeds also increased during the storm period (Fig. 2) and reached the maximum value for the 2022 deployment (U_{10max} = 11.1 m s^{-1}). The maximum negative CO_2 flux (CO_{2min} = -2.00 mmol m^{-2} h^{-1}) occurred on July 14th, 2021, at 20:00 EDT due to a high wind event that occurred within one hour (U_{10} = 13.70 ± 2.40 m s^{-1}, mean ± standard deviation). The increased negative flux likely did not persist like the 2022 storm flux increase because there were no noticeable changes to other variables that were used to derive the flux, such as water column pCO_2 concentrations and temperature (Eqn. 5, Fig. 6).

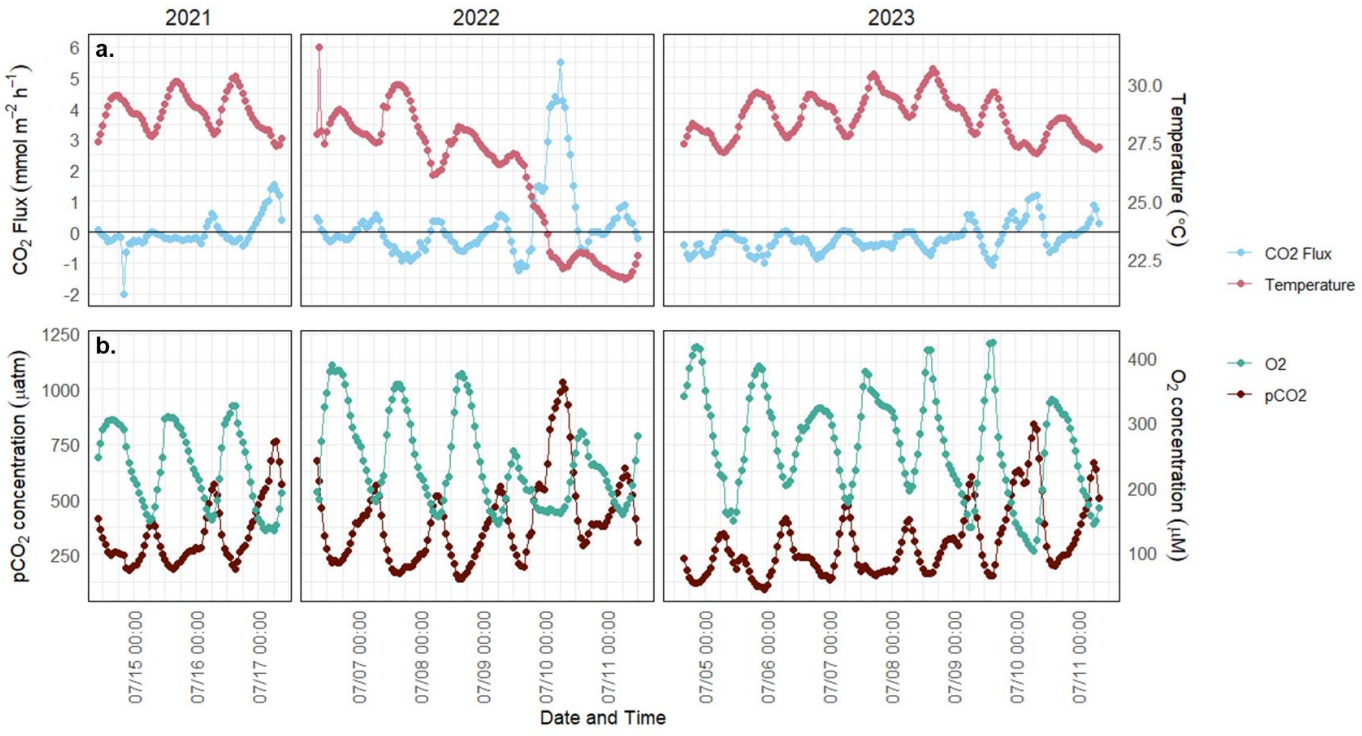

Fig. 6. Hourly time series data of **(a)** CO_2 fluxes, water column temperatures, **(b)** water column pCO_2 concentrations, and water column O_2 concentrations during the peak seagrass density deployments that occurred in July of 2021, 2022, and 2023. The time of "00:00" on the x axis denotes midnight of each day. Negative CO_2 fluxes represent an uptake of CO_2 by the water column.

3.4 Fair-weather CO_2 fluxes

All hourly CO_2 fluxes were binned by the hour of the day (Fig. 7). Fluxes followed a diurnal sink-source cycle where South Bay was a source of CO_2 from 01:00 – 11:00 EDT and a sink of CO_2 from 11:00 – 24:00 EDT (Fig. 7). The cumulative daily sum was -0.60 mmol CO_2 m^{-2} d^{-1}. To illustrate the potential bias in flux measurements that would occur from only measuring fluxes during fair-weather periods, we compared the full dataset of hourly average CO_2 fluxes to the non-storm period (referred to as the "fair-weather dataset"), in which the 2022 storm period was removed (Fig. 7). The fair-weather dataset followed a similar diurnal source-sink cycle as the full dataset, but the magnitude and duration of the negative CO_2 flux was greater (Fig. 7). The magnitudes of the positive CO_2 fluxes were significantly smaller (Fig. 7). The cumulative daily sum of the fair-weather dataset was -4.20 mmol CO_2 m^{-2} d^{-1}, significantly overestimating the CO_2 sink capacity. The significant decrease in the negative flux magnitude one hour after last light (21:00) is partially attributed to the high negative flux (-0.66 mmol CO_2 m^{-2} d^{-1}) that occurred for one hour in 2021 and to the 2022 storm, which primarily occurred overnight (Fig. 6). South Bay was a greater CO_2 source during the storm period compared to the fair-weather period. The decrease is also partially attributed to the length of the datasets, which consistently ended in daytime, resulting in more measurements during the day than the night (Fig. 7).

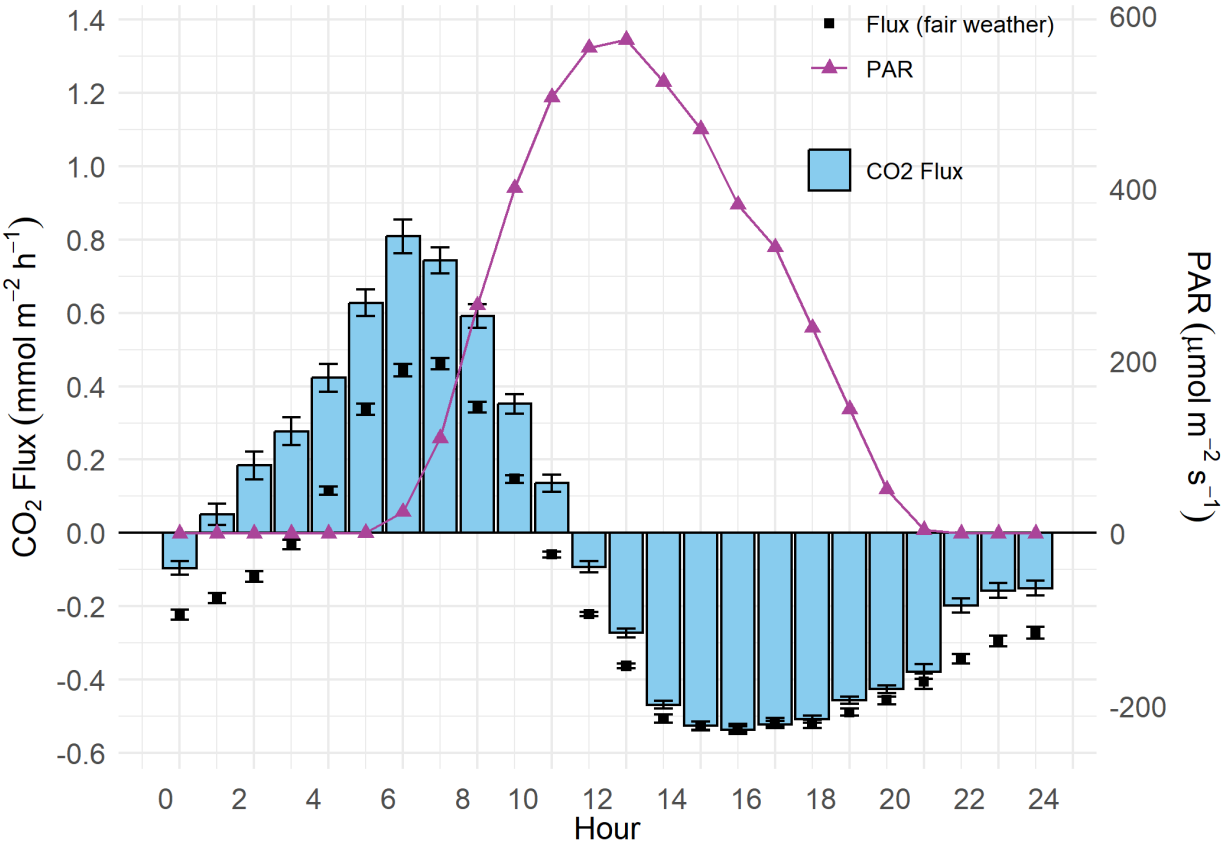

Fig. 7. CO_2 fluxes and PAR values across all three deployments binned into hourly averages (mean ± SE). To determine the difference between fair-weather and all-weather fluxes, the 2022 storm was removed and the fair-weather CO_2 fluxes were plotted in addition to the full dataset. Negative CO_2 fluxes represent an uptake of CO_2 by the water column.

4 Discussion

4.1 Regional wind speed analysis

Wind speeds measured at stations located at or near a land-water interface are assumed to be representative of estuarine waters, even though the surface roughness over land is greater than over water due to shear stress from land and vegetation (Lawson et al. 2007; Mariotti et al. 2018). In this study, wind speeds measured over a barrier island, a channel, and at the land-water interface were surprisingly not representative of wind speeds measured over South Bay (Fig. 2, Table 1). These stations consistently underestimated wind speeds. Similar results were reported in the Mississippi Delta estuary, where the underestimation of bay wind speeds by land stations was greatest when the winds were oriented from the direction of the land (Mariotti et al. 2018). To appropriately represent wind speeds over bays such as South Bay with land stations, a

boundary layer correction is needed when the wind blows from the direction of land (Schwing and Blanton 1984; Hsu 1986). This is particularly important for gas exchange estimates because the relationship between wind speed and gas transfer velocity (k) is generally reported with a quadratic or power function, so an underestimation in wind speeds would result in a significant underestimation of k. In turn, this would then result in an underestimation of the derived gas flux (Eqn. 5). Ultimately, a bias in the wind speed of ≥ 1 m s^{-1} can bias the CO_2 flux by 43% or greater (Wanninkhof et al. 2002, 2009).

Our study suggests that the absence of land is more important than site proximity when selecting a regional wind station to represent an estuary (Mariotti et al. 2018). Wind speeds measured at Rappahannock, the wind station located in the Chesapeake Bay, were not significantly different to those measured over South Bay (Fig. 2a, Table 1). Wind speed estimates derived offshore of the Chesapeake Bay with the ERA5 analysis were also not significantly different from the *in situ* station or from Rappahannock (Fig. 2e, Zhu et al. *in prep*). Overall, regional wind stations located over water or fine-scale models such as the ERA5 reanalysis likely provide the most appropriate estimates of wind speeds over estuaries.

4.2 *k* value analysis

4.2.1 *In situ* trends in wind speed

Recently, there has been an enhanced effort to constrain gas transfer velocities (k) in estuaries (Van Dam et al. 2019; Rosentreter et al. 2021c; Dobashi and Ho 2023). Different empirical wind speed parameterizations can produce highly variable k_{600} values in estuaries, partially because of the lack of observational data over the ocean when U_{10} < 4 m s^{-1}, a value that estuarine wind speeds are often at or below (Wanninkhof et al. 2009; Ho et al. 2018; Dobashi and Ho 2023). During the peak seagrass density deployments in 2021, 2022, and 2023, we observed the most variability in the wind speed k_{600} models when U_{10} ≤ 5 m s^{-1} (Fig. 3b). This is particularly relevant for selecting a k_{600} model for our site because U_{10} ≤ 5 m s^{-1} for 60 % of the total period of our CO_2 flux estimates (Fig. 6, Fig. 7). During our k_{600} model analysis period in August 2021, wind speeds ranged from 0.3 – 4.5 m s^{-1} (U_{10}), capturing the majority of this variability (Fig. 5).

4.2.2 k_{600} model analysis

The *in situ* k_{600} values derived from upside-down aquatic eddy covariance varied with wind speed (Fig. 3, Fig. 5). In other vegetated estuaries, variability in k_{600} values indicated that gas transfer velocity is driven by multiple processes, such as wind speed, current velocity, and water depth (Ho et al. 2016; Rosentreter et al. 2017). Thus, we evaluated parameterizations that included current velocity and water depth (B04c, B04a, H16) in addition to the wind speed parameterizations during the k_{600} model analysis (Table 2). The current velocity and water depth parameterizations were representative of variability the *in situ* k_{600} values, but consistently over-estimated the magnitude (Fig. 5). This may be because wind-driven waves and currents are recognized as a dominant forcing in South Bay, which indicates that wind speed and current velocity are correlated (Lawson et al. 2007; Fagherazzi and Wiberg 2009). In this study, we also observed a correlation between wind speed and velocity. Due to this correlation, including both wind speed and velocity in parameterizations may overestimate the gas transfer velocity at our site.

Ultimately, the best fitting models in our study (N00, H06, H11, and W14) were wind speed parameterizations that were derived over the ocean and had an intercept of zero (Fig. 5, Table 2). These findings are at odds with the established concept that gas transfer velocity does not approach zero at low wind speeds and rather asymptotes at a finite value due to environmental forcings such as buoyancy, chemical enhancement, and physical mixing (Mcgillis et al. 2001; McGillis et al. 2004; Wanninkhof et al. 2009). However, our results are in agreement with a study conducted in a tidal river estuary that found that parameterizations derived from the open ocean with an intercept of zero were better predictors of k_{600} compared to parameterizations derived over estuaries or over the ocean with a nonzero intercept (Ho et al. 2016). In contrast, the parameterizations with nonzero intercepts derived over either the open ocean (M01, M04, J08, and W09) or estuaries (R01 and B04) overestimated k_{600} at the low wind speeds in our study, although the curves of M01 and W09 suggest that they may better predict k_{600} over South Bay when $U_{10} \geq 5$ m s^{-1} (Fig. 5). This phenomenon may be explained by the aforementioned lack of k_{600} measurements over the ocean at low wind speeds, or by the influence of current velocity on gas transfer velocity at our site (Wanninkhof et al. 2009; Ho et al. 2016).

Surprisingly, k_{600} was consistently underestimated by an empirical wind speed parameterization derived over a different seagrass meadow (D23) (Dobashi and Ho 2023). The Dobashi and Ho (2023) parameterization was determined in the early growing season, whereas our k_{600} analysis occurred in August after seagrass senescence. High seagrass densities are known to attenuate flow, and it is possible that their parameterization may fit our site better during the early or peak growing season periods (Reidenbach and Thomas 2018; Zhu et al. 2021). Potential seasonality in the drivers of gas transfer velocity in shallow vegetated ecosystems have not been evaluated, to our knowledge.

Differences in k_{600} within ecosystems have been reported in mangrove forests, where a uniform k_{600} value derived at one site (Ho et al. 2016) underestimated CO_2 fluxes at a different site 60-70 %. The presence of submerged, floating, and emergent vegetation can similarly affect gas exchange by reducing flows, facilitating direct gas exchange across the sediment-water or plant-water interface, and disrupting the air-water boundary layer (Ho et al. 2018; Zhu et al. 2021).

We determined that there were four models that fit our site best because they produced k_{600} values that were not significantly different from the *in situ* values: Nightingale et al. (2000), Ho et al. (2006), Ho et al. (2011), and Wanninkhof et al. (2014) (Table 2, Fig. 5). We chose Nightingale et al. (2000) (N00) as the empirical parameterization for our CO_2 flux estimates because this parameterization considered local measurements in fetch-limited environments. Wanninkhof (2014) (W14), a widely used model, was also one of our best fitting models. We selected N00 over W14 because W14 was recommended for regional to global wind speed estimates of k. Our analysis was limited to low and low-intermediate wind speeds. In the future, it would be informative to assess gas transfer velocities over consecutive full tidal cycles and during stormy periods.

4.3 Diurnal variability in CO_2 fluxes

Hourly CO_2 fluxes varied in magnitude and direction, demonstrating the rapid internal cycling of C_{inorg} that occurs in seagrass meadows (Fig. 6a). The inverse sinusoidal relationship of water column p_{CO_2} and O_2 concentrations shown here and in previous work (Berg et al. 2019) suggests that the hourly-scale variability in the CO_2 fluxes is driven by patterns in photosynthesis

and respiration (Fig. 6b). The differences between the water column concentration patterns and the variability in the CO_2 flux suggests that a significant amount of this metabolism is occurring in the water column, which is in agreement with the findings of Berg et al. (2019). The time periods in which South Bay was a CO_2 sink primarily occurred during the day, and the time periods in which South Bay was a CO_2 source primarily occurred overnight (Fig. 6, Fig. 7). This suggests that daytime measurements will overestimate the total CO_2 sink capacity of seagrass meadow ecosystems. We find that these patterns are interannually persistent, except for the storm period. Averaged over all deployments, the hourly CO_2 fluxes followed a diurnal source-sink pattern with PAR and the cumulative daily sum was -0.60 mmol CO_2 m^{-2} d-1, indicating that South Bay is in metabolic balance during peak seagrass density (Fig. 7). Our results are in line with an analysis of decadal ecosystem metabolism in South Bay determined from benthic O_2 fluxes that found similarly that the seagrass meadow was in metabolic balance (Berger et al. 2020).

4.4 Effect of storms on CO_2 fluxes

The maximum positive CO_2 flux recorded in this study occurred during the storm period in 2022 (Fig. 6a). During this period, there was a corresponding increase in wind speed that was documented *in situ* over South Bay, as well as at the Chesapeake Bay station, the channel station, and the barrier island station (Fig. 2). A decrease in water temperature and an increase in water column pCO_2 concentrations also occurred during the storm period. Using water level data collected at the NOAA Wachapreague station (NOAA NDBC WAHV2), we also identified a storm surge during the 2022 storm period where the difference between the predicted astronomical tide and the measured water levels was > 0.2 m (NOAA NDBC WAHV2) (Zhu and Wiberg, 2022; Castagno et al., 2018). By measuring all components of the flux equation (Eq. 5) on temporal scales ≤ 1 min, we captured the effect of rapid changes in k_{CO_2} from wind speed, K_0 from temperature, and ΔpCO_2 from water column pCO_2 on the CO_2 flux (Fig. 6). The maximum negative CO_2 flux recorded in this study occurred in 2021 when the mean wind speed was U_{10} = 13.70 ± 2.40 m s^{-1}, but this flux did not persist for more than an hour and no significant change in temperature was identified. We also did not identify a storm surge during this period, so this flux was not included as a storm period.

During storm periods, there is increased resuspension of suspended sediments that may facilitate increased gas exchange from the sediment to the water column and then to the atmosphere (Zhu and Wiberg, 2024; Zhu et al., 2021). Increased wind speeds, whitecapping, and rainfall may also contribute to a thinning of the air-water boundary layers, further facilitating gas exchange (Wanninkhof et al., 2009; Ho et al., 2000). The relationship between wind speed and gas exchange should be studied further during storm periods to better constrain the effect of rain on gas fluxes.

Storms in particular are not well-documented in existing greenhouse gas flux measurements over estuaries. When the 2022 storm was removed to demonstrate the difference between determining fluxes during fair-weather and all-weather conditions, we observed an overestimation of the daily CO_2 sink capacity of South Bay (Fig. 7). Storm events over the VCR occurred for 5 % of the total time between August 2008 to December 2020, but storm events may increase in the future due to sea level rise and potential changes to the intensity and frequency of storms from climate change (Lin et al. 2019; Kulp and Strauss 2019; Zhu and Wiberg 2022). The frequency, intensity, and duration of storms should be taken into consideration when fluxes are scaled temporally and spatially.

5 Conclusions

Measuring air-water CO_2 fluxes on fine temporal scales is essential for disentangling diurnal and inter-annual patterns. In this study, we performed a regional wind speed analysis, an analysis of *in situ* and modelled k_{600} values, and diurnal CO_2 flux patterns over South Bay, a shallow coastal bay with a temperate seagrass meadow dominating the benthos. The regional wind speed station that gave measurements closest to those recorded at our site was located in the Chesapeake Bay. All stations located in proximity to land underestimated wind speeds over South Bay, which would ultimately underestimate both the k value, and thus, the CO_2 flux. The results of the analysis of *in situ* and modeled k_{600} values determined that the best fitting k_{600} models were wind speed parameterizations that were derived over the ocean and had a zero intercept. In estuaries, the most appropriate k_{600} model is likely site-specific and should be determined using *in situ* k_{600} data when possible, or alternatively, by thoroughly evaluating site

characteristics such as water depth, current velocity, and wind speed. We applied the regional wind speed analysis and the k_{600} model analysis and derived air-water hourly CO_2 fluxes during the peak seagrass density period (early July) for three years. The magnitude and direction of the CO_2 flux varied on hourly and diurnal time scales, but the daily average showed that South Bay was in metabolic balance and was a minor CO_2 sink. We compared the fair-weather CO_2 fluxes to the full CO_2 flux dataset, which included the storm period, and found that the meadow was a significantly larger CO_2 sink during the fair-weather period. During the fair-weather period, multiple components of the flux equation (water column pCO_2 and temperature) followed predictable patterns. During the storm period, these components deviated from their predictable patterns and largely drove the increase in CO_2 flux.

6 References

Aoki, L. R., McGlathery, K. J., Wiberg, P. L., Oreska, M. P. J., Berger, A. C., Berg, P., and Orth, R. J.: Seagrass Recovery Following Marine Heat Wave Influences Sediment Carbon Stocks, Front Mar Sci, 7, https://doi.org/10.3389/fmars.2020.576784, 2021.

Berg, P. and Pace, M. L.: Continuous measurement of air-water gas exchange by underwater eddy covariance, Biogeosciences, 14, 5595–5606, https://doi.org/10.5194/bg-14-5595-2017, 2017.

Berg, P., Roy, H., Janssen, F., Meyer, V., Jorgensen, B. B., Huettel, M., and de Beer, D.: Oxygen uptake by aquatic sediments measured with a novel non-invasive eddy-correlation technique, Mar Ecol Prog Ser, 261, 75–83, 2003.

Berg, P., Delgard, M. L., Glud, R. N., Huettel, M., Reimers, C. E., and Pace, M. L.: Non-invasive Flux Measurements at the Benthic Interface: The Aquatic Eddy Covariance Technique, Limnology and Oceanography e-Lectures, https://doi.org/10.1002/loe2.10005, 2017.

Berg, P., Delgard, M. L., Polsenaere, P., McGlathery, K. J., Doney, S. C., and Berger, A. C.: Dynamics of benthic metabolism, O 2 , and pCO 2 in a temperate seagrass meadow , Limnol Oceanogr, https://doi.org/10.1002/lno.11236, 2019.

Berg, P., Pace, M. L., and Buelo, C. D.: Air–water gas exchange in lakes and reservoirs measured from a moving platform by underwater eddy covariance, Limnol Oceanogr Methods, lom3.10373, https://doi.org/10.1002/lom3.10373, 2020.

Berg, P., Huettel, M., Glud, R. N., Reimers, C. E., and Attard, K. M.: Aquatic Eddy Covariance: The Method and Its Contributions to Defining Oxygen and Carbon Fluxes in Marine Environments, Ann Rev Mar Sci, 14, 431–455, https://doi.org/10.1146/annurev-marine-042121-012329, 2022.

Berger, A. C., Berg, P., McGlathery, K. J., and Delgard, M. L.: Long-term trends and resilience of seagrass metabolism: A decadal aquatic eddy covariance study, Limnol Oceanogr, https://doi.org/10.1002/lno.11397, 2020.

Berger, A. C., Berg, P., Mcglathery, K., Reidenbach, M. A., Pace, M. L., and Goodall, J. L.: Long-term aquatic eddy covariance measurements of seagrass metabolism and ecosystem response to warming oceans, 2021.

Bianchi, T. S., Cui, X., Blair, N. E., Burdige, D. J., Eglinton, T. I., and Galy, V.: Centers of organic carbon burial and oxidation at the land-ocean interface, https://doi.org/10.1016/j.orggeochem.2017.09.008, 1 January 2018.

Borges, A. V., Abril, G., and Bouillon, S.: Carbon dynamics and CO2 and CH4 outgassing in the Mekong delta, Biogeosciences, 15, 1093–1114, https://doi.org/10.5194/bg-15-1093-2018, 2018.

Castagno, K. A., Jiménez-Robles, A. M., Donnelly, J. P., Wiberg, P. L., Fenster, M. S., and Fagherazzi, S.: Intense Storms Increase the Stability of Tidal Bays, Geophys Res Lett, 45, 5491–5500, https://doi.org/10.1029/2018GL078208, 2018.

Cole, J. J., Bade, D. L., Pace, M. L., and Van de Bogert, M.: Multiple approaches to estimating air-water gas exchange in small lakes., 2010.

Van Dam, B. R., Edson, J. B., and Tobias, C.: Parameterizing Air-Water Gas Exchange in the Shallow, Microtidal New River Estuary, J Geophys Res Biogeosci, 124, 2351–2363, https://doi.org/10.1029/2018JG004908, 2019.

Van Dam, B., Polsenaere, P., Barreras-Apodaca, A., Lopes, C., Sanchez-Mejia, Z., Tokoro, T., Kuwae, T., Loza, L. G., Rutgersson, A., Fourqurean, J., and Thomas, H.: Global Trends in Air-Water CO2 Exchange Over Seagrass Meadows Revealed by Atmospheric Eddy Covariance, Global Biogeochem Cycles, 35, https://doi.org/10.1029/2020GB006848, 2021.

Dobashi, R. and Ho, D. T.: Air–sea gas exchange in a seagrass ecosystem – results from a 3 He/SF 6 tracer release experiment, Biogeosciences, 20, 1075–1087, https://doi.org/10.5194/bg-20-1075-2023, 2023.

Fagherazzi, S. and Wiberg, P. L.: Importance of wind conditions, fetch, and water levels on wave-generated shear stresses in shallow intertidal basins, J Geophys Res Earth Surf, 114, https://doi.org/10.1029/2008JF001139, 2009.

Fennel, K., Alin, S., Barbero, L., Evans, W., Bourgeois, T., Cooley, S., Dunne, J., Feely, R. A., Martin Hernandez-Ayon, J., Hu, X., Lohrenz, S., Muller-Karger, F., Najjar, R., Robbins, L., Shadwick, E., Siedlecki, S., Steiner, N., Sutton, A., Turk, D., Vlahos, P., and Aleck Wang, Z.: Carbon cycling in the North American coastal ocean: A synthesis, Biogeosciences, 16, 1281–1304, https://doi.org/10.5194/bg-16-1281-2019, 2019.

Frankignoulle, M. and Borges, A. V.: European continental shelf as a significant sink for atmospheric carbon dioxide, Global Biogeochem Cycles, 15, 569–576, https://doi.org/10.1029/2000GB001307, 2001.

Garcia, H. and Gordon, L.: Oxygen Solubility in Seawater: Better Fitting Equations, Limnol Oceanogr, 37, 1307–1312, 1992.

Granville, K. E., Berg, P., and Huettel, M.: A high-resolution submersible oxygen optode system for aquatic eddy covariance, Limnol Oceanogr Methods, 21, 152–163, https://doi.org/10.1002/lom3.10535, 2023.

Ho, D. T., Asher, W. E., Bliven, L. F., Schlosser, P., and Gordan, E. L.: On mechanisms of rain-induced air-water gas exchange, J Geophys Res Oceans, 105, 24045–24057, https://doi.org/10.1029/1999jc000280, 2000.

Ho, D. T., Law, C. S., Smith, M. J., Schlosser, P., Harvey, M., and Hill, P.: Measurements of air-sea gas exchange at high wind speeds in the Southern Ocean: Implications for global parameterizations, Geophys Res Lett, 33, https://doi.org/10.1029/2006GL026817, 2006.

Ho, D. T., Wanninkhof, R., Schlosser, P., Ullman, D. S., Hebert, D., and Sullivan, K. F.: Toward a universal relationship between wind speed and gas exchange: Gas transfer velocities measured with 3He/SF6 during the Southern Ocean Gas Exchange Experiment, J Geophys Res Oceans, 116, https://doi.org/10.1029/2010JC006854, 2011.

Ho, D. T., Coffineau, N., Hickman, B., Chow, N., Koffman, T., and Schlosser, P.: Influence of current velocity and wind speed on air-water gas exchange in a mangrove estuary, Geophys Res Lett, 43, 3813–3821, https://doi.org/10.1002/2016GL068727, 2016.

Ho, D. T., Engel, V. C., Ferrón, S., Hickman, B., Choi, J., and Harvey, J. W.: On Factors Influencing Air-Water Gas Exchange in Emergent Wetlands, J Geophys Res Biogeosci, 123, 178–192, https://doi.org/10.1002/2017JG004299, 2018.

Hsu, S. A.: A Mechanism for the Increase of Wind Stress (Drag) Coefficient with Wind Speed over Water Surfaces: A Parametric Model, J Phys Oceanogr, 16, 144–150, https://doi.org/10.1175/1520-0485(1986)016<0144:AMFTIO>2.0.CO;2, 1986.

Jähne, B., Münnich, K. O., Bösinger, R., Dutzi, A., Huber, W., and Libner, P.: On the parameters influencing air-water gas exchange, J Geophys Res Oceans, 92, 1937–1949, https://doi.org/10.1029/JC092iC02p01937, 1987.

Jeffrey, L. C., Maher, D. T., Santos, I. R., Call, M., Reading, M. J., Holloway, C., and Tait, D. R.: The spatial and temporal drivers of pCO2, pCH4 and gas transfer velocity within a subtropical estuary., Estuar Coast Shelf Sci, 208, 83–95, https://doi.org/10.1016/j.ecss.2018.04.022, 2018.

Kim, S. H., Suonan, Z., Qin, L. Z., Kim, H., Park, J. I., Kim, Y. K., Lee, S., Kim, S. G., Kang, C. K., and Lee, K. S.: Variability in blue carbon storage related to biogeochemical factors in

seagrass meadows off the coast of the Korean peninsula, Science of the Total Environment, 813, https://doi.org/10.1016/j.scitotenv.2021.152680, 2022.

Kulp, S. A. and Strauss, B. H.: New elevation data triple estimates of global vulnerability to sea-level rise and coastal flooding, Nat Commun, 10, https://doi.org/10.1038/s41467-019-12808-z, 2019.

Lawson, S. E., Wiberg, P. L., McGlathery, K. J., and Fugate, D. C.: Wind-driven Sediment Suspension Controls Light Availability in a Shallow Coastal Lagoon, Estuaries and Coasts, 30, 102–112, 2007.

Lin, N., Marsooli, R., and Colle, B. A.: Storm surge return levels induced by mid-to-late-twenty-first-century extratropical cyclones in the Northeastern United States, Clim Change, 154, 143–158, https://doi.org/10.1007/s10584-019-02431-8, 2019.

Long, M. H. and Nicholson, D. P.: Surface gas exchange determined from an aquatic eddy covariance floating platform, Limnol Oceanogr Methods, 16, 145–159, https://doi.org/10.1002/lom3.10233, 2018.

Macreadie, P. I., Costa, M. D. P., Atwood, T. B., Friess, D. A., Kelleway, J. J., Kennedy, H., Lovelock, C. E., Serrano, O., and Duarte, C. M.: Blue carbon as a natural climate solution, Nat Rev Earth Environ, https://doi.org/10.1038/s43017-021-00224-1, 2021.

Mariotti, G., Huang, H., Xue, Z., Li, B., Justic, D., and Zang, Z.: Biased wind measurements in Estuarine waters, J Geophys Res Oceans, 123, 3577–3587, https://doi.org/10.1029/2017JC013748, 2018.

Mcgillis, W. R., Edson, J. B., Ware, J. D., Dacey, J. W. H., Hare, J. E., Fairall, C. W., and Wanninkhof, R.: Carbon dioxide flux techniques performed during GasEx-98, Marine Chemistry, 267–280 pp., 2001.

McGillis, W. R., Edson, J. B., Zappa, C. J., Ware, J. D., McKenna, S. P., Terray, E. A., Hare, J. E., Fairall, C. W., Drennan, W., Donelan, M., DeGrandpre, M. D., Wanninkhof, R., and Feely, R. A.: Air-sea CO2 exchange in the equatorial Pacific, J Geophys Res Oceans, 109, https://doi.org/10.1029/2003JC002256, 2004.

McGlathery, K. J., Reynolds, L. K., Cole, L. W., Orth, R. J., Marion, S. R., and Schwarzschild, A.: Recovery trajectories during state change from bare sediment to eelgrass dominance, Mar Ecol Prog Ser, 448, 209–221, https://doi.org/10.3354/meps09574, 2012.

Mu, L., Stammerjohn, S. E., Lowry, K. E., and Yager, P. L.: Spatial variability of surface pCO2 and air-sea CO2 flux in the Amundsen Sea Polynya, Antarctica, Elementa: Science of the Anthropocene, 2, 000036, https://doi.org/10.12952/journal.elementa.000036, 2014.

Nightingale, P. D., Malin, G., Law, C. S., Watson, A. J., Liss, P. S., Liddicoat, M. I., Boutin, J., and Upstill-Goddard, R. C.: In situ evaluation of air-sea gas exchange parameterizations using novel conservative and volatile tracers, Global Biogeochem Cycles, 14, 373–387, https://doi.org/10.1029/1999GB900091, 2000.

Ollivier, Q. R., Maher, D. T., Pitfield, C., and Macreadie, P. I.: Net Drawdown of Greenhouse Gases (CO2, CH4 and N2O) by a Temperate Australian Seagrass Meadow, Estuaries and Coasts, 45, 2026–2039, https://doi.org/10.1007/s12237-022-01068-8, 2022.

Oreska, M. P. J., McGlathery, K. J., Aoki, L. R., Berger, A. C., Berg, P., and Mullins, L.: The greenhouse gas offset potential from seagrass restoration, Sci Rep, 10, https://doi.org/10.1038/s41598-020-64094-1, 2020.

Orth, R. J., Lefcheck, J. S., Mcglathery, K. S., Aoki, L., Luckenbach, M. W., Moore, K. A., Oreska, M. P. J., Snyder, R., Wilcox, D. J., and Lusk, B.: Restoration of seagrass habitat leads to rapid recovery of coastal ecosystem services, Sci. Adv, 2020.

Prentice, C., Poppe, K. L., Lutz, M., Murray, E., Stephens, T. A., Spooner, A., Hessing-Lewis, M., Sanders-Smith, R., Rybczyk, J. M., Apple, J., Short, F. T., Gaeckle, J., Helms, A., Mattson, C., Raymond, W. W., and Klinger, T.: A Synthesis of Blue Carbon Stocks, Sources, and Accumulation Rates in Eelgrass (Zostera marina) Meadows in the Northeast Pacific, Global Biogeochem Cycles, 34, https://doi.org/10.1029/2019GB006345, 2020.

Reidenbach, M. A. and Thomas, E. L.: Influence of the Seagrass, Zostera marina, on wave attenuation and bed shear stress within a shallow coastal bay, Front Mar Sci, 5, https://doi.org/10.3389/fmars.2018.00397, 2018.

Rheuban, J. E., Berg, P., and McGlathery, K. J.: Multiple timescale processes drive ecosystem metabolism in eelgrass (Zostera marina) meadows, Mar Ecol Prog Ser, 507, 1–13, https://doi.org/10.3354/meps10843, 2014.

Ricart, A. M., York, P. H., Bryant, C. V., Rasheed, M. A., Ierodiaconou, D., and Macreadie, P. I.: High variability of Blue Carbon storage in seagrass meadows at the estuary scale, Sci Rep, 10, https://doi.org/10.1038/s41598-020-62639-y, 2020.

Rosentreter, J. A., Maher, D. T., Ho, D. T., Call, M., Barr, J. G., and Eyre, B. D.: Spatial and temporal variability of CO2 and CH4 gas transfer velocities and quantification of the CH4 microbubble flux in mangrove dominated estuaries, Limnol Oceanogr, 62, 561–578, https://doi.org/10.1002/lno.10444, 2017.

Rosentreter, J. A., Wells, N. S., Ulseth, A. J., and Eyre, B. D.: Divergent Gas Transfer Velocities of CO2, CH4, and N2O Over Spatial and Temporal Gradients in a Subtropical Estuary, J Geophys Res Biogeosci, 126, https://doi.org/10.1029/2021JG006270, 2021.

Saderne, V., Geraldi, N. R., Macreadie, P. I., Maher, D. T., Middelburg, J. J., Serrano, O., Almahasheer, H., Arias-Ortiz, A., Cusack, M., Eyre, B. D., Fourqurean, J. W., Kennedy, H., Krause-Jensen, D., Kuwae, T., Lavery, P. S., Lovelock, C. E., Marba, N., Masqué, P., Mateo, M. A., Mazarrasa, I., McGlathery, K. J., Oreska, M. P. J., Sanders, C. J., Santos, I. R., Smoak, J. M., Tanaya, T., Watanabe, K., and Duarte, C. M.: Role of carbonate burial in Blue Carbon budgets, Nat Commun, 10, https://doi.org/10.1038/s41467-019-08842-6, 2019.

Schwing, F. B. and Blanton, J. O.: The Use of Land and Sea Based Wind Data in a Simple Circulation Model, J Phys Oceanogr, 14, 193–197, https://doi.org/10.1175/1520-0485(1984)014<0193:TUOLAS>2.0.CO;2, 1984.

Vieira Borges, A., Vanderborght, J.-P., Schiettecatte, L.-S., Dé, F., Gazeau, R., Ferro´n, S., Ferro´n-Smith, F., Delille, B., and Frankignoulle, M.: Variability of the Gas Transfer Velocity of CO 2 in a Macrotidal Estuary (the Scheldt), Estuarine Research Federation Estuaries, 593–603 pp., 2004.

Wanninkhof, R.: Relationship between wind speed and gas exchange over the ocean, J Geophys Res, 97, 7373–7382, https://doi.org/10.1029/92JC00188, 1992.

Wanninkhof, R.: Relationship between wind speed and gas exchange over the ocean revisited, Limnol Oceanogr Methods, 12, 351–362, https://doi.org/10.4319/lom.2014.12.351, 2014.

Wanninkhof, R., Doney, S. C., Takahashi, T., and McGillis, W. R.: The effect of using time-averaged winds on regional air-sea CO2 fluxes, in: Gas transfer at water surfaces, vol. 127, Blackwell Publishing Ltd, 351–356, https://doi.org/10.1029/GM127p0351, 2002.

Wanninkhof, R., Asher, W. E., Ho, D. T., Sweeney, C., and McGillis, W. R.: Advances in Quantifying Air-Sea Gas Exchange and Environmental Forcing, Ann Rev Mar Sci, 1, 213–244, https://doi.org/10.1146/annurev.marine.010908.163742, 2009.

Weiss: CO2 solubility, 1974.

Weiss, R. and Price, B.: Nitrous oxide solubility in water and seawater, Mar Chem, 8, 347–359, 1980.

Wiberg, P. L., Carr, J. A., Safak, I., and Anutaliya, A.: Quantifying the distribution and influence of non-uniform bed properties in shallow coastal bays, Limnol Oceanogr Methods, 13, 746–762, https://doi.org/10.1002/lom3.10063, 2015.

Yang, M., Bell, T. G., Brown, I. J., Fishwick, J. R., Kitidis, V., Nightingale, P. D., Rees, A. P., and Smyth, T. J.: Insights from year-long measurements of air-water CH4 and CO2 exchange in a coastal environment, Biogeosciences, 16, 961–978, https://doi.org/10.5194/bg-16-961-2019, 2019.

Zhu, Q. and Wiberg, P. L.: The Importance of Storm Surge for Sediment Delivery to Microtidal Marshes, J Geophys Res Earth Surf, 127, https://doi.org/10.1029/2022JF006612, 2022.

Zhu, Q. and Wiberg, P. L.: Effects of Seasonal Variations in Seagrass Density and Storms on Sediment Retention and Connectivity Between Subtidal Flats and Intertidal Marsh, J Geophys Res Biogeosci, 129, https://doi.org/10.1029/2023JG007785, 2024.

Zhu, Q., Wiberg, P. L., and Reidenbach, M. A.: Quantifying Seasonal Seagrass Effects on Flow and Sediment Dynamics in a Back-Barrier Bay, J Geophys Res Oceans, 126, https://doi.org/10.1029/2020JC016547, 2021.

Chapter 3: Seasonal trends in air-water CO_2, CH_4, and N_2O fluxes over a temperate seagrass meadow

Conducted with support from: Peter Berg and Bongkeun Song.

Abstract

Blue carbon ecosystems such as seagrass meadows are widely regarded as carbon sinks that can help mitigate the effects of climate change. However, the carbon balance in seagrass meadows is complex and can, for example, be affected by emissions of greenhouse gases such as carbon dioxide (CO_2), methane (CH_4), and nitrous oxide (N_2O). Although the importance of measuring these fluxes is widely recognized, there is still a lack of reliable flux data due to internal site variability and low sampling frequencies, especially for temperate seagrass meadows. We addressed these knowledge gaps by measuring air-water CO_2, CH_4, and N_2O fluxes throughout the seagrass growing season over a temperate coastal lagoon with a substrate dominated by a *Zostera marina* meadow (South Bay, Virginia, USA). Here, we report CO_2, CH_4, and N_2O fluxes derived during the early seagrass growing season (April-June), peak seagrass density (July), seagrass senescence (August) and post-senescence (October) across two years. To constrain the variability attributed to the different flux pathways, we measured dissolved CO_2 and CH_4 fluxes continuously with autonomous underwater sensors, and ebullitive and plant-mediated fluxes of CH_4 and N_2O using floating bubble traps. Dissolved N_2O fluxes were estimated from point measurements of water column N_2O concentrations. South Bay was a consistent source of total (dissolved and ebullitive) CH_4 to the atmosphere, but the magnitude varied both seasonally and between emission pathways. We observed distinctly elevated CO_2 and CH_4 emissions during two storm periods. South Bay was a consistent sink of total N_2O throughout the growing season. We observed an overall uptake of CO_2-equivalent gases by South Bay during the early growing season (-0.5 ± 0.03 g CO_2-e m^{-2} d^{-1}, mean ± standard deviation) and outgassing during seagrass senescence (0.9 ± 0.1 g CO_2-e m^{-2} d^{-1}) and post-senescence (0.8 ± 0.04 g CO_2-e m^{-2} d^{-1}). During peak seagrass density, South Bay was in metabolic balance and fluxes were not significantly different from zero (0.002 ± 0.1 g CO_2-e m^{-2} d^{-1}). Summarized over the whole study period (April – October), South Bay is a small source of CO_2-equivalent gases (0.24 ± 0.1 g CO_2-e m^{-2} d^{-1}).

1 Introduction

Carbon dioxide (CO_2), methane (CH_4), and nitrous oxide (N_2O) are greenhouse gases that contribute significantly to atmospheric warming (IPCC 2023). Coastal vegetated ecosystems, which are known to sequester carbon through primary production and store carbon through sediment deposition and organic matter burial, emit or take up these greenhouse gases (Marbà et al. 2015; Serrano et al. 2018; Garcias-Bonet et al. 2019; Rosentreter et al. 2023). Recent studies suggest that coastal vegetated ecosystems are an overall net sink of CO_2-equivalent (CO_2-e) gases (CO_2, CH_4, and N_2O) on the global scale, but that the total CO_2-e uptake is offset by up to 40% by air-water CO_2-e emissions (Al-Haj and Fulweiler 2020; Rosentreter et al. 2021a, 2023). However, local measurements of CO_2, CH_4, and N_2O fluxes are known to vary spatially and temporally, and flux estimates are particularly uncertain in seagrass meadows (Wells et al. 2018; Al-Haj and Fulweiler 2020; Asplund et al. 2022). Increasing evidence shows that seagrass meadows are smaller CH_4 sources that salt marshes and mangroves, and that temperate seagrass meadows may be sinks of N_2O (Al-Haj et al. 2022; Ollivier et al. 2022; Rosentreter et al. 2023).

The dynamics of CH_4 production, consumption, and emissions from seagrass meadows are complex. In anaerobic sediments, the majority of CH_4 is produced through methanogenesis, a form of anaerobic respiration in which oxidized carbon such as CO_2 is used as a terminal electron acceptor. In seagrass meadows, methanogenesis primarily occurs via methylotrophic methanogenesis, a non-competitive form of methanogenesis in which CH_4 is formed from the degradation of methylated compounds such as dimethylamine (DMA), dimethyl sulfide (DMS), and methanol (Schorn et al. 2022; Brodersen et al. 2024). Hydrogenotrophic methanogenesis, in which CO_2 is reduced to CH_4 via H_2, and acetoclastic methanogenesis, can also occur in seagrass meadow sediments when there is enough organic matter to meet the demands of sulfate-reducing bacteria (SRBs), but SRBs routinely outcompete methanogens for hydrogen and acetate substrates (Berghuis et al. 2019; Rosentreter et al. 2021b; Schorn et al. 2022). The CH_4 that is produced may also be removed from the sediments via anaerobic oxidation with sulfate (SO_4^{2-}) or other terminal electron acceptors (Whiticar 2020). The CH_4 that is not removed is usually transported into the water column via diffusion. The role of oxic CH_4 production and consumption in the water column is unclear in coastal environments, but understood to be important (Schubert et al. 2006; Bogard et al. 2014; Tang et al. 2014; Günthel et al. 2020). There

is evidence that CH_4 is produced in the oxic water column by methanogenesis and by processes such as the bacterial degradation of dimethylsulfoniopropionate (DMSP) precursors from phytoplankton metabolism (Tang et al. 2014; Upstill-Goddard and Barnes 2016; Matoušů et al. 2017). (Damm et al. 2010; Whiticar 2020). A fraction of dissolved CH_4 can be removed by methanotrophic bacteria via aerobic oxidation of O_2 (Tang et al. 2014; Upstill-Goddard and Barnes 2016; Matoušů et al. 2017).

CH_4 can also be emitted from the sediment to the water column as bubbles when dissolved CH_4 becomes supersaturated in sediment porewater, when current-induced bottom shear stress increases, or when water pressure increases at low water depths (Joyce and Jewell 2003; McGinnis et al. 2006; Long and Nicholson 2018). This process, known as the ebullitive flux, allows CH_4 to escape the microbial oxidation filter as bubbles rise and exchange gases with the water column before escaping to the atmosphere (Whiticar 2020). The air-water ebullitive flux from the water column over seagrass meadows is highly uncertain, but increasing evidence suggests that the relative contribution of the ebullitive flux is an important component of the total flux (Oreska et al. 2020; Al-Haj et al. 2022; Rosentreter et al. 2023).

Seagrasses may also play a direct role in CH_4 production-consumption dynamics. Plant-mediated transport, in which gases are transported between the sediments and water column through the plant aerenchyma, is an important CH_4 production pathway in other vegetated ecosystems that has not been studied in seagrass meadows (Al-Haj and Fulweiler 2020; Schorn et al. 2022; Vroom et al. 2022). When seagrasses are submerged, plant-mediated transport would likely occur as ebullition from the seagrass blades. Bubble formation on seagrasses has been observed as a result of internal pressurization in the aerenchyma, external pressurization from low water depths, or O_2 supersaturation in the water column (Wilson et al. 2012; Long et al. 2020). Ebullition of O_2 has been measured from these bubbles, and was found to be a significant component of the whole system O_2 flux (Long et al. 2020). Potential CH_4 ebullitive fluxes from the sediment-water and plant-water interfaces are not captured by dissolved gas measurement techniques, and they may have a significant effect on the balance of air-water greenhouse gases over systems such as seagrass meadows.

Plant-mediated transport and ebullition have also been suggested as potentially significant pathways of N_2O exchange in seagrass meadows, but these pathways are under-studied (Al-Haj et al. 2022). N_2O is mainly produced through nitrification and incomplete denitrification, and consumed via complete denitrification when dissolved inorganic nitrogen contents are low (Bange et al. 1996; Murray et al. 2015). Water column O_2 supersaturation can stimulate nitrification, and "hotspots" of denitrification have been observed where seagrass is present (De Wilde and De Bie 2000; Aoki and McGlathery 2018). Additionally, denitrification may be stimulated when methanotrophs consume O_2 during aerobic CH_4 oxidation (Whiticar 2020).

Here, we report air-water CO_2, CH_4, and N_2O fluxes measured over a temperate seagrass meadow during four distinct time periods throughout the seagrass growing season. Hourly dissolved CO_2 and CH_4 fluxes were derived based on *in situ* measurements over multiple diurnal cycles, and point N_2O fluxes were derived from daytime water samples. These fluxes were compared to ebullitive CH_4 and N_2O fluxes derived on daily time scales. Here, the ebullitive flux is considered representative of the sediment-water column ebullitive flux and the potential plant-mediated ebullitive flux.

2 Methods

2.1 Study site

The Virginia Coast Reserve (VCR) is a system of coastal lagoons and barrier islands located between the Delmarva peninsula and the Atlantic Ocean. This study was conducted in South Bay, a shallow coastal lagoon that is bordered by a barrier island (Wreck Island) to the east and is connected to the Atlantic Ocean by two inlets to the north and south of the island (Fig. 1a). South Bay has a mean water depth of 1.0 m below sea level and a tidal range of 1.2 m (Reidenbach and Thomas 2018). Wind-driven waves are the predominant forcing on sediment suspension in South Bay (Lawson et al. 2007). Southerly winds are dominant in the summer and northerly winds occur in the winter (Fagherazzi and Wiberg 2009). The water column is well-mixed with no significant stratification (Berger et al. 2020).

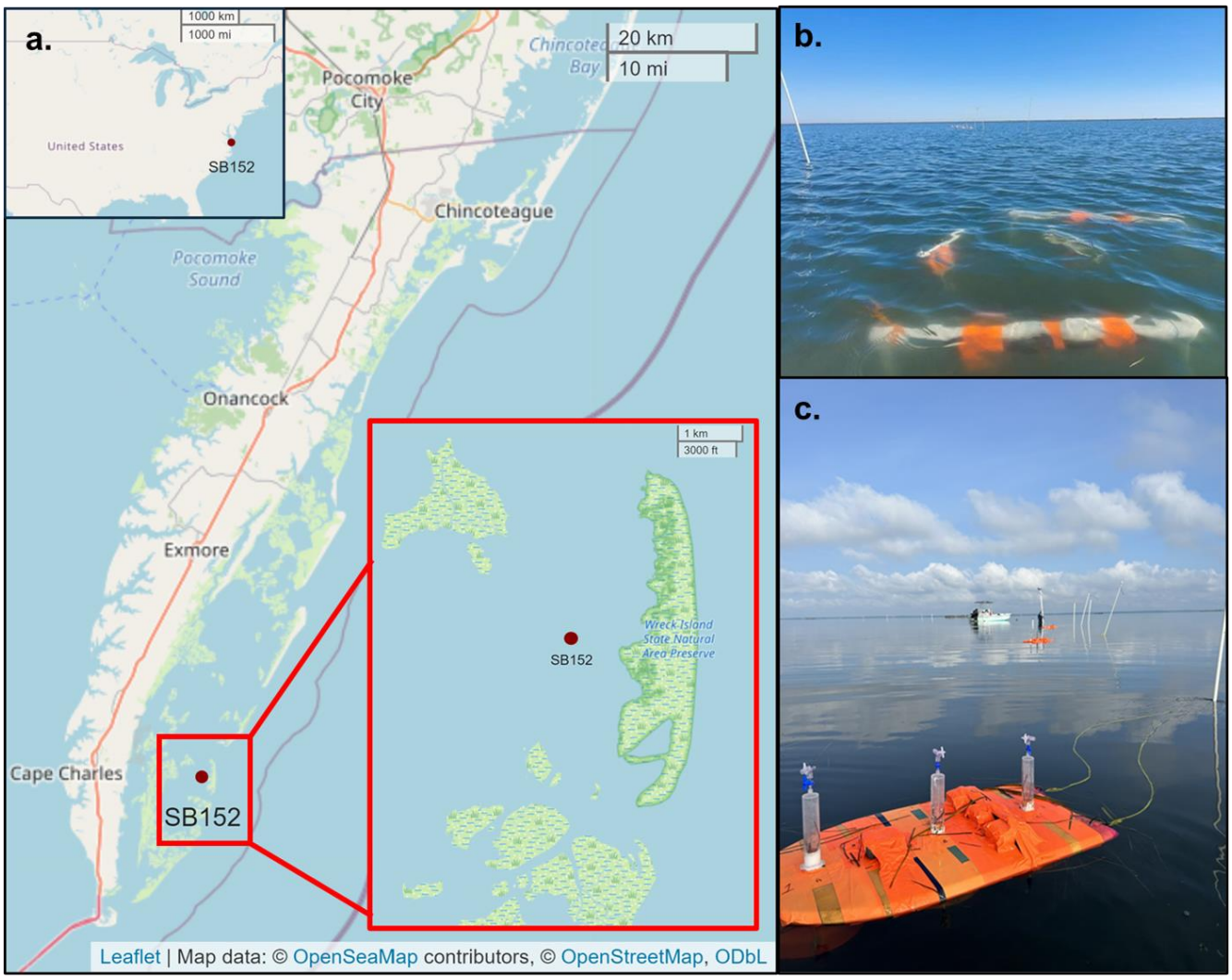

Fig. 1(a). Our study site was located in central South Bay (denoted as "SB152"), a shallow coastal bay in the Virginia Coast Reserve. The Virginia Coast Reserve is located between the Eastern Shore of Virginia and the Atlantic Ocean on the east coast of the United States. **(b)** Autonomous underwater sensors and **(c)** floating bubble traps deployed at the site. Map created with R Studio (v4.3.2, R Core Team, 2023) with the "leaflet" package (Cheng et al. 2024).

The benthic environment is South Bay is dominated by a restored eelgrass (*Zostera marina*) meadow. The South Bay seagrass meadow is in metabolic balance on annual time scales (Berger et al. 2020). The VCR is located at the southern geographical limit of the temperature range for *Z. marina* and as a result the seagrass meadows frequently experience heat stress (Aoki et al. 2020; Berger et al 2020). Seagrass densities increase from late spring to early summer, and peak-summer shoot densities (≥400 shoots m^{-2}) typically occur in June or July (Oreska et al. 2017; Zhu et al. 2021). Senescence, a seasonal loss of seagrass biomass, occurs in August due to high water temperatures (Orth and Moore 1986; Rheuban et al. 2014a). After senescence,

seagrass shoot densities increase slightly before gradually decreasing during the fall and winter to minimum densities of 50-100 shoots m^{-2} (Reidenbach and Thomas 2018; Zhu et al. 2021).

2.2 Sampling design

We conducted four deployments per year. In 2022, the deployments occurred from June 1st-7th, July 6th-11th, August 16th-22nd, and October 6th-12th. In 2023, the deployments occurred April 11th-19th, July 4th-11th, August 9th-14th, and October 5th-11th. Due to instrumentation issues, the fluxes measured during each deployment varied. Continuous dissolved CO_2 fluxes and ebullitive CH_4 fluxes were derived during all deployments except June 2022, while continuous dissolved CH_4 fluxes were derived during all 2023 deployments. Ebullitive N_2O fluxes and point estimates of dissolved N_2O fluxes were derived during all 2022 deployments.

During all deployments, several environmental variables were measured at 1-minute intervals. Water column temperatures and O_2 concentrations were measured at the average seagrass canopy height (30 cm above the sediment surface) with stable O_2 optodes (miniDOT, PME). Photosynthetically active radiation (PAR) at the average seagrass canopy height was measured with a LI-192 underwater quantum sensor (miniPAR, PME). Wind speed and direction were measured with a compact anemometer (WindLog, Rainwise Windlogger) that was mounted on a PVC pole approximately 5 m above the sediment surface. Water depth was measured with a water level data logger (HOBO U20-L, Onset Brands), and used to scale wind speed measurements to 10 m (U_{10}) following methods described in detail in Granville et al. (*in prep*) (Chapter 2). Salinity was measured continuously in June and July of 2022 with a pH sensor (SeapHox V2, Seabird Scientific) (LaRoche et al., *in prep*), and in July, August, and October of 2023 with a salt water conductivity logger (HOBO U24, Onset Brands). Continuous salinity data were not available in August 2022, October 2022, and April 2023, so point salinity measurements were taken with a conductivity meter every 1-2 days (YSI Pro30, Xylem). Hourly barometric pressure data were collected from a station located on a barrier island within the VCR, Hog Island (Porter and Williams 2024). The average seagrass shoot density (shoots m^{-2}) was obtained for each deployment by counting seagrass shoots by hand within 5-10 replicate 0.25 m^2 quadrats thrown randomly within the sampling site (McGlathery et al. 2012; Berger et al. 2020). To increase the robustness of our growing season seagrass density dataset, average

seagrass shoot density counts obtained by the same methodology from May 27th, 2021, to August 8th, 2021 were included in our analysis.

2.3 Storm periods

Storm periods that occurred during each deployment period were identified using wind speed and water level thresholds. Previous work at the VCR has identified major storm surge events as periods when wind speeds were >11 m s^{-1} and when the difference between measured and predicted water levels was > 0.2 m (Castagno et al., 2018; Zhu and Wiberg, 2022). We used a more conservative wind speed threshold, U_{10} > 8.0 m s^{-1}, which was determined by evaluating wind speeds before, during, and after two known storms that occurred at the site that are discussed below (see Section 3.2). This lower threshold seeks to account for smaller storm events that have been shown to have an impact on flux magnitudes (Granville et al. *in prep*) (Chapter 2). We collected astronomical tide predictions and hourly measured water levels from the NOAA NDBC station at Wachapreague for all deployments. Time periods when wind speeds were > 8.0 m s^{-1} and the difference between measured and predicted water levels was > 0.2 m were classified as storm periods. Time periods where one or both variables were below the respective threshold were classified as "fair-weather" periods.

To determine the likelihood of storms affecting air-water gas fluxes throughout the year, we assessed the amount of time this threshold was crossed in 2022 and 2023 using tide and water level data from Wachapreague and wind speed data from the NOAA NDBC station Rappahannock, which was shown to be representative of wind speeds measured over South Bay (Granville et al. *in prep*) (Chapter 2). The likelihood of storms was determined for each month during the deployment, and the percentage of storm periods and fair-weather periods per month was used to scale our total monthly flux estimates so that the storm periods were not overrepresented in the total dataset.

2.4 Dissolved gas fluxes

Continuous dissolved CO_2 and CH_4 fluxes were derived following methods described in detail in Granville et al. (*in prep*) (Chapter 2, Section 2.5). Briefly, standard mass transfer equations were used to estimate 1-minute dissolved CO_2 fluxes (Chapter 2, Eqn. 5) and CH_4

fluxes (Chapter 2, Eqn. 1). Continuous water column pCO_2 and pCH_4 were measured with autonomous underwater sensors (miniCO_2 and miniCH_4, Pro Oceanus Systems Inc.). Atmospheric pCO_2 was derived from atmospheric xCO_2 mole fractions collected by NOAA CarbonTracker Near-Real Time (CT-NRT.v2023-5, Jacobson et al. 2023) and barometric pressure collected by the VCR-LTER (Porter and Williams 2024). CarbonTracker Near-Real Time data were unavailable for all CH_4 deployments and for the July, August, and October 2023 CO_2 deployments. For these deployments, monthly marine surface averages of xCO_2 and xCH_4 mole fractions were used (NOAA GML). The gas transfer velocity was derived from *in situ* U_{10} using Nightingale et al. (2000), an empirical relationship where wind speed is the primary driver that was determined to be a best fit at our site (Chapter 2), and scaled to CO_2 and CH_4 using the Schmidt numbers of each gas (Wanninkhof 2014). Dissolved CO_2 and CH_4 fluxes were summarized to hourly values for analysis. Dissolved N_2O fluxes were not measured continuously because, to our knowledge, a sensor that could continuously measure the low levels of pN_2O at our site was not available.

In June, July, August, and October of 2022, water column CH_4 and N_2O concentrations were assessed via the headspace equilibration technique to obtain point estimates of air-water CH_4 and N_2O fluxes (Hudson 2004; Helton et al. 2014; Borges et al. 2018). Briefly, we collected 80-100 ml of water in 120-ml glass serum bottles that had previously been crimp-capped, weighed, and evacuated of air (Helton et al. 2014). The serum bottles were held approximately 1-5 cm below the water surface and a 20 g needle was inserted through the septum to collect the water samples (Helton et al. 2014). Samples were poisoned with mercuric chloride ($HgCl_2$) to prevent microbial activity and stored septum-side-down, underwater, and on ice until analysis. At the time of analysis, the serum bottles were injected with a known volume of helium and shaken vigorously before a sample volume of gas was extracted. The gas samples were analyzed for CH_4 on a gas chromatograph fitted with a flame ionization detector (GC-FID) that used ultra-high purity He as the carrier gas (7890A GC, Agilent), and for N_2O on a gas chromatograph fitted with an electron capture detector (GC-ECD) that used a P5 mixture as the make-up gas (GC-8A Series, Shimadzu Corporation). The limit of detection (LOD) for CH_4 and N_2O was determined daily from known standards and gas concentrations were determined from the known standards compared to the peak areas of the samples. Samples were run in triplicate and averaged. When the relative percent difference of the samples was greater than 5%, we assessed the triplicates

and removed outliers, assuming a sampling error associated with a syringe or serum bottle leak. The CH_4 samples were consistently below the LOD, so they were not analyzed further. For the N_2O samples, water column N_2O concentrations were derived following Henry's law, which assumes that the gas components in the serum bottle headspace and liquid phase are in equilibrium (Hudson 2004; Helton et al. 2014). N_2O fluxes were derived following the standard procedure for CO_2 and N_2O (Chapter 2) (Weiss 1974; Weiss and Price 1980; Mu et al. 2014).

2.5 Bubble traps

We designed floating bubble traps to measure ebullitive CH_4 and N_2O emissions at the air-water interface (Fig. 1c). For this study, we defined ebullitive emissions as emissions of bubbles occurring at both the sediment-water and plant-water interfaces. Nine bubble traps were deployed across three floating foam boards. On each board, three 24-cm diameter funnels were inserted into pre-drilled holes and fitted with a 100 ml syringe with a luer lock tip. The connection between the funnel, board, and syringe was sealed with 3M 5200 marine adhesive sealant and reinforced with strings that connected the funnel and the syringe to the board. The floating boards were deployed in an east-west transect 15 m apart. Each floating board was weighed down with three 5 lb dive weights to keep the boards steady at the air-water interface, and anchored to a 10-m-tall PVC pole with floating polypropylene line. This allowed the bubble traps to rise and fall with changes in water depth.

Multiple bubble trap deployments that were 24-72 h in length occurred during each deployment. At the start of each bubble trap deployment, each bubble trap was fitted with two stopcocks with luer connections to prevent leakage. The air was evacuated from each trap via a syringe connected to the uppermost stopcock. At the end of each bubble trap deployment, the gas volume in the syringes was recorded and a 12 ml gas sample was extracted. The gas samples were injected into 12 ml Exetainers (Labco) that had previously been flushed for 5 minutes with inert He gas (Sturm et al. 2015). The bubble trap samples were analyzed for CH_4 on the GC-FID and for N_2O on the GC-ECD following the procedure described in the dissolved gas fluxes section. CH_4 fluxes were calculated following the equation:

$$FCH_{4Bubble} = \frac{[CH_4]*V}{A* t_d} \qquad \text{Eqn.}$$

where $FCH_{4Bubble}$ is the combined ebullitive and plant-mediated CH_4 flux (μmol m^{-2} d^{-1}), $[CH_4]$ is the CH_4 concentration in the trap (μmol m^{-2}), V is the gas volume in the bubble trap (m^3), A is the surface area of the funnel (m^2), and t_d is the deployment time in days (Barbosa et al. 2021).

2.6 Data analysis

All analyses were conducted in R Studio version 4.3.2, primarily with the 'tidyverse' package (R Core Team 2023). Simple linear regressions were conducted to determine correlations between dissolved CO_2, CH_4, and N_2O fluxes and their potential environmental drivers. Bubble-mediated fluxes were grouped by bubble trap deployment and then by month. Pairwise Wilcoxon rank-sum tests with a Benjamin-Hochberg correction were conducted to determine significant differences in bubble-mediated CH_4 fluxes between months. CO_2-equivalent fluxes of dissolved and bubble-mediated CH_4 and N_2O were derived by converting CH_4 and N_2O fluxes on the 100-year time horizon. We used global warming potentials reported by IPCC AR6 and used the non-fossil origin potential for CH_4. On the 100-year time horizon, CH_4 and N2O fluxes have a global warming potential equivalent to 27.2 kg CO_2 and 273 kg CO_2, respectively (IPCC 2023). For reference, on the 20-year time horizon, CH_4 fluxes have a global warming potential equivalent to 80.3 kg CO_2 and the global warming potential of N_2O fluxes remains equivalent to 273 kg CO_2 (IPCC 2023).

3 Results

3.1 Environmental variables

The average wind speeds, dissolved O_2 concentrations, and atmospheric pressures varied significantly between deployments and no clear trends were observed on the monthly scale (Table 1). Water column temperature varied significantly between all deployments, except for October 2022 and April 2023 (Table 1). Seagrass shoot densities varied inter-annually and throughout the growing season, peaking annually in early July (Fig. 2). Seagrass shoot densities significantly increased with increasing water temperatures ($R^2 = 0.91$, $p = 0.0015$).

Table 1. Each deployment was assigned a period: growing season (GS), peak seagrass density (PD), senescence (SC), or post-senescence (PS). Average values (mean ± standard deviation) are reported each deployment for wind speed scaled to a height of 10 m (U_{10}, m s^{-1}), depth (m), photosynthetically active radiation (PAR, µmol m^{-2} s^{-1}), water column temperature (°C), salinity (ppt), seagrass shoot density (shoots, shoots m^{-2}) and atmospheric pressure (P_{atm}, mbar).

	Period	*U_{10}*	*Depth*	*PAR*	*O_2*	*Temperature*	*Salinity*	*Shoots*	*P_{atm}*
June 2022	GS	5.36 ± 2.2	1.32 ± 0.3	224.3 ± 260.8	245.7 ± 50.4	25.6 ± 1.8	31.3 ± 0.3	315 ± 17.3	1012.0 ± 3.9
July 2022	PD	5.85 ± 2.2	1.16 ± 0.4	176.3 ± 257.0	239.7 ± 70.7	26.1 ± 2.7	30.3 ± 2.0	410 ± 70.6	1013.9 ± 1.5
Aug. 2022	SC	4.58 ± 2.2	1.22 ± 0.4	196.3 ± 232.2	227.5 ± 64.3	25.7 ± 1.7	31.9 ± 1.3	241 ± 63.8	1016.4 ± 2.5
Oct. 2022	PS	4.06 ± 2.5	1.03 ± 0.5	209.3 ± 328.6	260.1 ± 30.5	18.1 ± 1.4	31.5 ± 0.4	97.6 ± 26.6	1020.3 ± 3.4
April 2023	GS	5.09 ± 1.5	1.00 ± 0.4	281.1 ± 374.9	286.2 ± 46.7	17.7 ± 2.2	31.7 ± 0.3	172 ± 24.8	1012.5 ± 5.0
July 2023	PD	4.04 ± 1.6	1.40 ± 0.5	129.9 ± 164.7	266.4 ± 80.6	28.6 ± 0.9	28.9 ± 2.2	491 ± 61.4	1010.3 ± 2.4
Aug. 2023	SC	4.86 ± 1.8	1.25 ± 0.4	192.1 ± 283.8	255.4 ± 119.2	28.0 ± 1.7	29.7 ± 0.8	425 ± 43.4	1010.4 ± 2.6
Oct. 2023	PS	5.28 ± 2.5	1.44 ± 0.3	70.0 ± 142.7	251.6 ± 72.7	20.0 ± 2.3	30.5 ± 0.8	116 ± 8.29	1010.7 ± 3.4

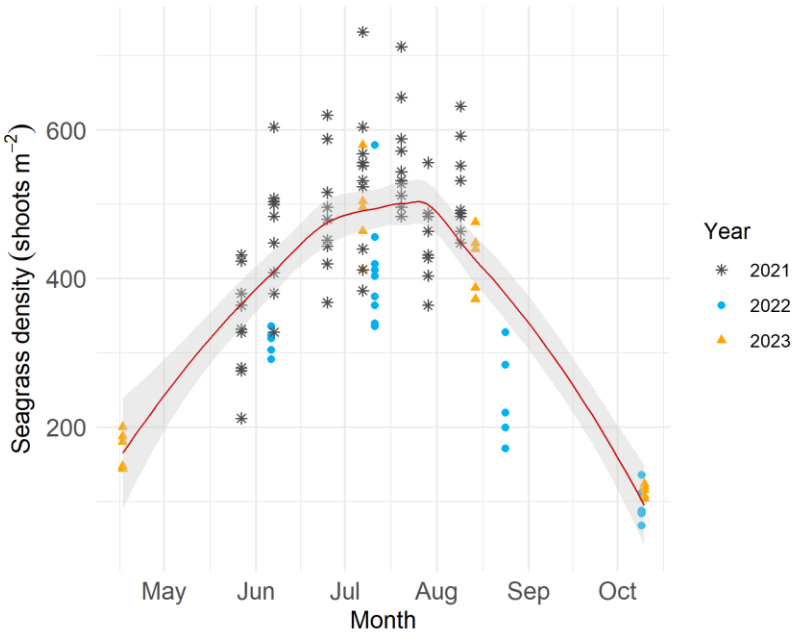

Fig. 2. Seagrass shoot densities measured throughout the growing season were plotted by the month and the day of data collection. Shoot densities were counted biweekly from late May – early August of 2021 and during each deployment in 2022 and 2023.

We defined four time periods throughout the seagrass growing season from existing estimates of *Z. marina* biomass changes and measured seagrass shoot density counts and water temperatures (Fig. 1) (Rheuban et al. 2014b; Reidenbach and Thomas 2018). The early growing season (GS) occurred from April to the end of June. The peak seagrass density period (PS) occurred in early July. The senescence period (SC) occurred from late July through August and represented the annual die-back and sloughing-off of seagrass leaves. The post-senescence period (PS) occurred from September to the end of October (Table 1, Fig. 2). Each deployment was then grouped into one of these time periods (Table 1).

3.2 Storm periods

The field site was primarily affected by two storms during this study. In July 2022, a consecutive storm period occurred from July 9th, 2022, at 17:00 EDT to July 10th, 2022, at 08:00 EDT (Chapter 2). The storm threshold (U_{10} > 8 m s^{-1} and storm surge > 0.2 m) was also crossed from 13:00-14:00 on July 9th, from 11:00-14:00 on July 10th, and during the 16:00 hour on July 10th. CO_2 fluxes and ebullitive CH_4 fluxes were measured during this storm. In October 2023, remnants of post-tropical cyclone Phillipe passed over the study site from October 7th, 2023, at 10:00 EDT to October 8th, 2023, at 03:00 EDT. During the October deployment, the storm threshold was also crossed at 09:00, 10:00, and 19:00 on October 8th. The storm period threshold was further validated by other *in situ* conditions. The maximum wind speed during the October 2023 storm period was U_{10} = 12.5 m s^{-1}, which was significantly higher than the October 2023 deployment average of U_{10} = 5.28 ± 2.5 m s^{-1} (Table 1). The wind direction shifted from predominantly north/northwest (20-30°) to predominantly west/northwest (290-300°), suggesting that winds were blowing in the anticlockwise direction. Anticlockwise winds are expected for low pressure systems that form in the northern hemisphere. Barometric pressure gradually decreased from 1022.1 mbar at the start of the deployment to 1006.2 mbar during the storm period, indicating the approaching low pressure center of the system. Barometric pressure stabilized around the deployment average (1010.7 ± 3.4 mbar, Table 1) by midnight on October 8th. In addition to the two major storms, the deployment periods were above the storm threshold for eleven hours in August 2022, five hours in April 2023, and two hours in July 2023, but these

hours were not always consecutive. The analysis of annual Rappahannock wind speeds and water levels and tide predictions at Wachapreague showed that storm periods occurred for 13.2 % of the total year in 2022 and 16.0 % of the total year in 2023.

3.3 Dissolved CO_2 and CH_4 fluxes

South Bay was a consistent sink of atmospheric CO_2 in the early growing season (April) on an hourly scale (Table 2, Fig. 3a). During the peak seagrass density period (July), South Bay was a minor CO_2 sink that was not significantly different from zero (Table 2, Fig. 3a). South Bay was an overall source of CO_2 to the atmosphere during senescence (August) and post-senescence (October) (Table 2, Fig. 3a). During all deployments, the maximum negative CO_2 flux occurred in the afternoon (Fig. 3a). July and August demonstrated a pattern of the maximum positive CO_2 flux occurring around dawn (Fig. 3a). Dawn also corresponded with the minimum negative CO_2 flux in April (Fig. 3a).

Dissolved CH_4 fluxes were always positive, indicating that South Bay was a consistent source of dissolved CH_4 to the atmosphere throughout the growing season. The daily dissolved CH_4 flux decreased significantly from April to July (Table 2, Fig. 2b). Dissolved CH_4 fluxes then increased significantly from July to August, and again from August to October (Table 2, Fig. 2b). Unlike CO_2, dissolved CH_4 fluxes did not exhibit a clear diurnal pattern (Fig. 2). Simple linear regressions revealed that water column pCO_2 and pCH_4 were strongly negatively correlated during and after seagrass senescence (August $R^2 = -0.95$, October $R^2 = -0.95$, $p < 0.05$). pCH_4 was also strongly positively correlated with water column temperatures during these periods (August $R^2 = 0.95$, October $R^2 = 0.97$, $p < 0.05$), but was not correlated with temperature during the early growing season or during peak density.

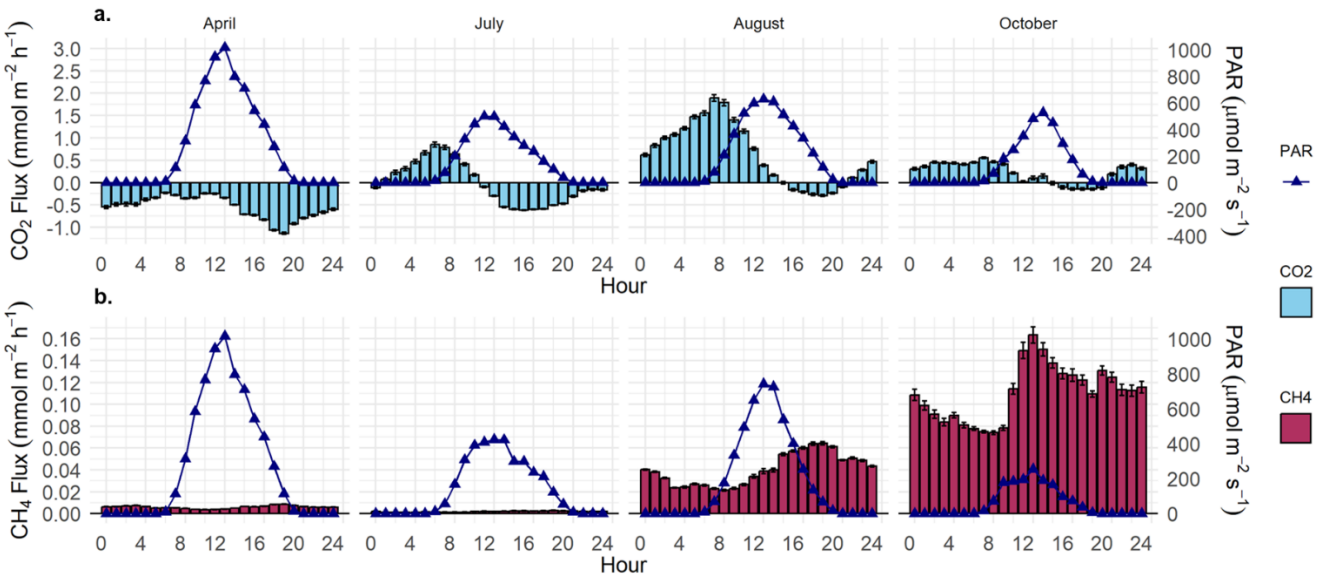

Fig 3. (a) Full dataset of mean dissolved CO_2 and **(b)** mean dissolved CH_4 fluxes measured in April, July, August, and October deployments in 2023. Fluxes are represented as the hourly average flux per hour of the day (0-24). Note the different scales for CO_2 and CH_4. Positive fluxes represent a source to the atmosphere and negative fluxes represent uptake from the atmosphere. Error bars depict standard error.

Table 2. The daily mean ± standard deviation of the dissolved CO_2 fluxes, dissolved CH_4 fluxes, bubble mediated CH_4 fluxes, total CH_4 fluxes (dissolved + bubble mediated) are shown for each full deployment and for the fair-weather dataset which excludes the storm periods (mmol m^{-2} d^{-1}). Total CH_4 fluxes are expressed as CO_2-equivalent fluxes on a 100-year time horizon (CH_4 CO_2-e), as well as the combined CO_2 and CH_4 fluxes (Total CO_2-e) in units of g CO_2 m^{-2} d^{-1}. "July: fair-weather" and "October: fair-weather" depict the July and October datasets when the storm periods were removed in units of mmol m^{-2} d^{-1}.

Period	Dissolved CO_2	Dissolved CH_4	Bubble-mediated CH_4	Total CH_4	CH_4 CO_2-e	Total CO_2-e
Full dataset						
April	-11.8 ± 6.2	0.1 ± 0.05	0.2 ± 0.1	0.3 ± 0.03	0.1 ± 0.01	-0.5 ± 0.1
July	-0.4 ± 12.9	0.04 ± 0.02	0.3 ± 0.2	0.3 ± 0.03	0.2 ± 0.01	0.1 ± 0.2
August	12.7 ± 14.4	0.8 ± 0.3	0.2 ± 0.2	1.04 ± 0.1	0.5 ± 0.06	1.0 ± 0.3
October	4.5 ± 9.9	2.3 ± 1.6	0.06 ± 0.05	2.4 ± 0.6	1.02 ± 0.3	1.2 ± 0.2
Fair-weather dataset						
July: fair weather	-4.5 ± 5.7	0.038 ± 0.02	0.2 ± 0.07	0.21 ± 0.01	0.1 ± 0.004	-0.1 ± 0.03
October: fair weather	0.9 ± 5.4	1.5 ± 0.8	0.03 ± 0.02	1.5 ± 0.4	0.7 ± 0.2	0.7 ± 0.04

3.4 Ebullitive CH_4 and N_2O fluxes

Daily ebullitive CH_4 fluxes were variable across months and years, and were most variable during the summer months (Fig. 4a). In both 2022 and 2023, ebullitive CH_4 fluxes were smallest in October (Fig. 4a). When the 2022 and 2023 fluxes were averaged, July CH_4 fluxes were not significantly different from August fluxes ($p = 0.092$) (Fig 4b), but were significantly greater than April ($p = 0.00047$) and October ($p = 1.0 * 10^{-7}$).

Daily ebullitive N_2O fluxes were significantly smaller than ebullitive CH_4 fluxes in all months and exhibited less variability (Fig. 4b). The majority of the variability in the ebullitive N_2O fluxes occurred in April. Ebullitive N_2O fluxes were smallest in October (Fig. 4b).

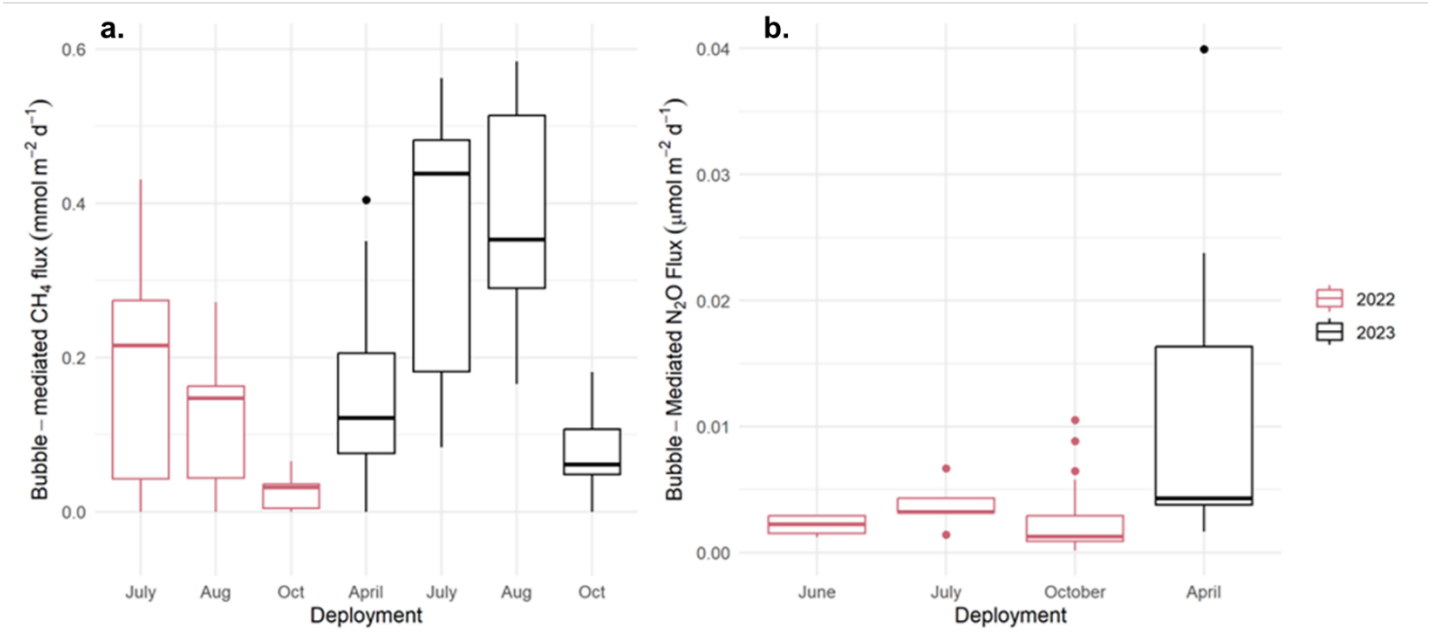

Fig. 4 (a) Bubble-mediated CH_4 and **(b)** N_2O fluxes were averaged by day within each deployment month in 2022 and 2023. Here, the bubble-mediated flux includes the ebullitive fluxes across the sediment-water and plant-water interface. Note that CH_4 fluxes are shown here in units of mmol m^{-2} d^{-1} and N_2O fluxes are shown in units of µmol m^{-2} d^{-1}.

3.5 Total CH_4 fluxes

The daily dissolved and bubble-mediated CH_4 fluxes were binned by month to produce the daily total CH_4 flux (Fig. 5). The bubble-mediated flux was 54% of the total CH_4 flux in April, 89% in July, 22% in August, and 2.5% in October (Fig. 5). Total CH_4 fluxes were not

significantly different in April and July, even though the ratio of dissolved to bubble-mediated fluxes changed between months (Fig. 5).

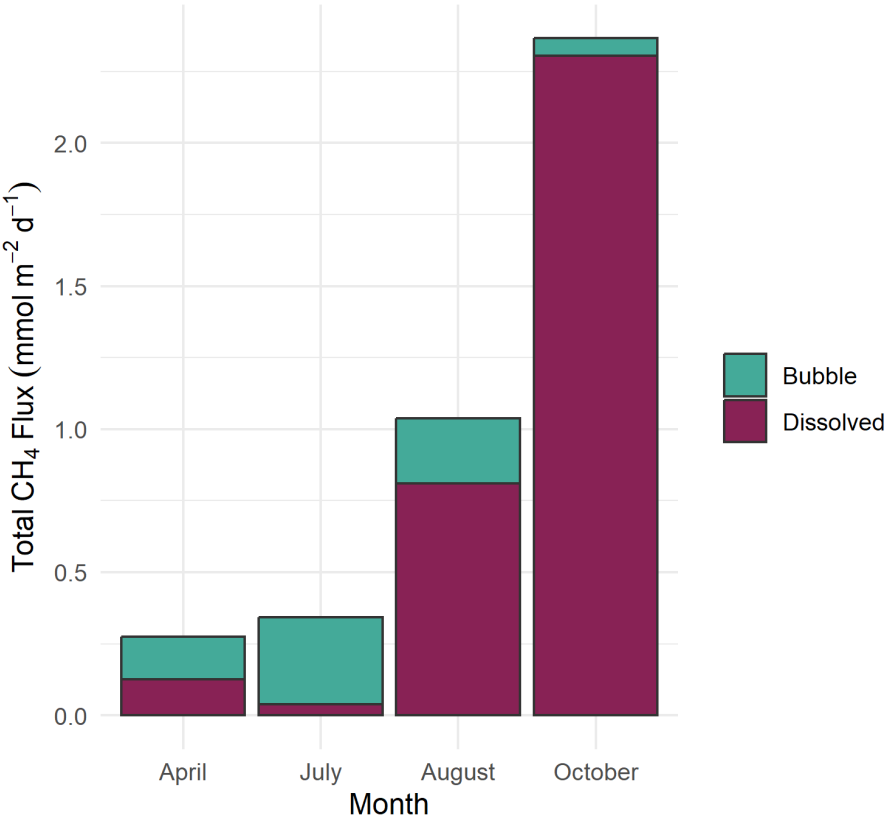

Fig. 5. The total daily CH_4 flux was averaged by month. The total CH_4 flux is the sum of the bubble-mediated CH_4 flux and the dissolved CH_4 flux.

3.6 N_2O flux estimates

Water column N_2O concentrations were below the detection limit of the gas chromatograph (0.1 ppm N_2O) in all deployments. Atmospheric N_2O concentrations over South Bay were consistently above the detection limit. To estimate maximum possible air-water N_2O fluxes for South Bay, we assigned all water column N_2O concentrations to the detection limit and derived the flux. The estimated dissolved N_2O flux was negative in all months. N_2O fluxes were not significantly different in July and August (-0.005 ± 0.002 mmol m^{-2} d^{-1}, mean ± standard deviation) (Fig. 6, Table 3). N_2O fluxes were greatest in June (-0.01 ± 0.002 mmol m^{-2} d^{-1}) (Fig. 6, Table 3). Ebullitive N_2O fluxes were negligible in comparison to the dissolved fluxes and comprised < 1% of the total N_2O flux in every deployment (Fig. 4b).

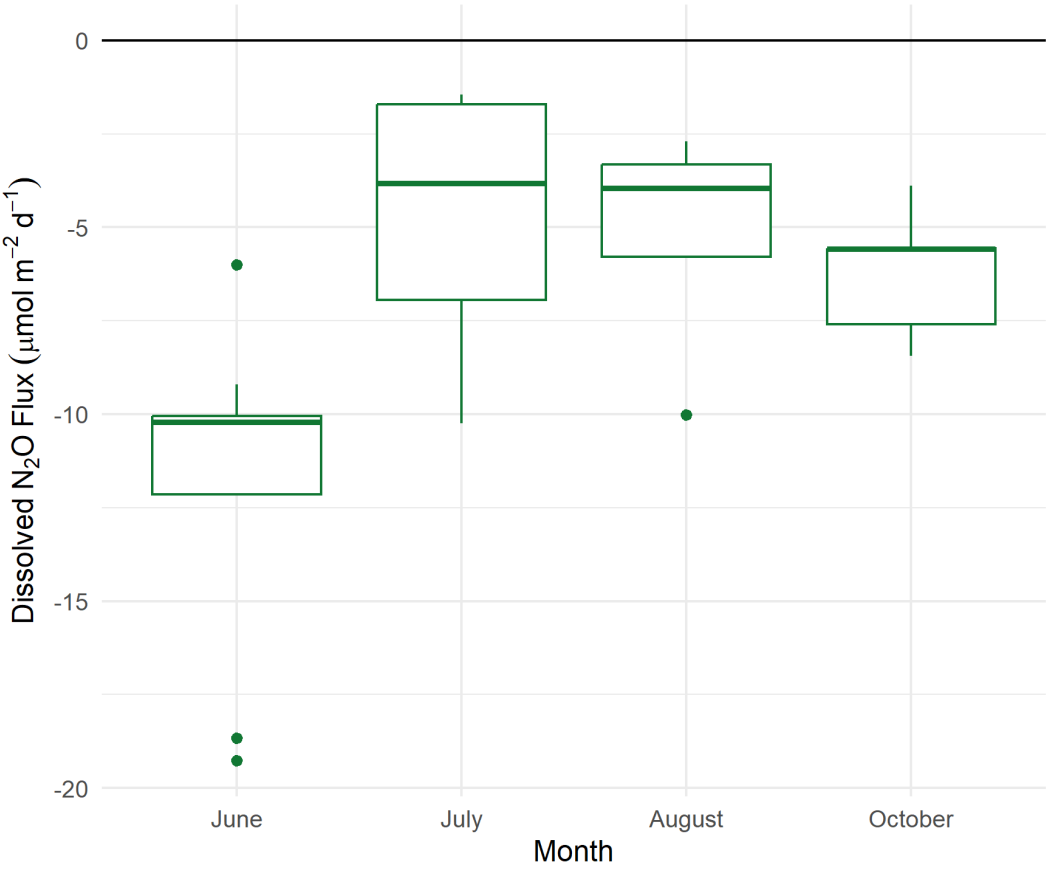

Fig 6. Estimates of the maximum possible dissolved N_2O flux from point samples in June (n = 9), July (n = 6), August (n = 4), and October (n = 9) 2022. A negative flux indicates uptake by the water column. b). Dissolved N_2O concentrations increase with increasing water temperatures.

Table 3. The total (dissolved + ebullitive) N_2O flux is given for each month in mmol m^{-2} d^{-1} (mean ± standard deviation). Each month was also categorized into one of the growing season periods. N_2O fluxes were converted into CO_2-e (g m^{-2} d^{-1}) for comparison. Finally, the N_2O CO_2-e fluxes were combined with the CO_2 and CH_4 CO_2-e fluxes from Table 2 by period.

Month	Period	N_2O flux	N_2O CO_2-e N_2O	Total CO_2-e by period
June	GS	-0.01 ± 0.002	-0.1 ± 0.02	-0.5 ± 0.03
July	PD	-0.005 ± 0.002	-0.06 ± 0.03	0.89± 0.1
August	SC	-0.005 ± 0.002	-0.06 ± 0.02	0.07 ± 0.1
October	PS	-0.007 ± 0.0005	-0.09 ± 0.006	1.1 ± 0.04

3.6 Growing season estimates

Our existing data were used to interpolate average daily fluxes for the entire growing season (April – October). To estimate each gas flux for months during the growing season that were not included in this analysis, a standard linear interpolation was conducted between each existing data point with the function "approx" in the "stats" package. On average, the interpolated flux estimates suggest that South Bay is a modest CO_2 sink (-0.34 ± 8.2 mmol CO_2 m^{-2} d^{-1}), a source of ebullitive CH_4 (0.19 ± 0.08 mmol CH_4 m^{-2} d^{-1}), a source of dissolved CH_4 (0.59 ± 0.7 mmol CH_4 m^{-2} d^{-1}), and a small sink of N_2O (-0.007 ± 0.002 mmol N_2O m^{-2} d^{-1}). In CO_2-equivalents, this amounts to 0.24 g CO_2-e m^{-2} d^{-1}.

3.7 Fair-weather fluxes

The "fair-weather" dataset, comprised of time points where wind speeds and storm surges did not meet the threshold to qualify as storm periods, was compared to the full dataset (Fig. 7, Table 2). In the fair-weather dataset, the magnitude of the CO_2 sink increased in July and the magnitude of the CO_2 source decreased in October (Table 2). The variability in the flux was reduced for both months (Table 2). The magnitude of the dissolved CH_4 flux also decreased in the fair-weather dataset, but the decrease was not significant (Table 2). Bubble-mediated CH_4 fluxes significantly decreased during the July 2022 storm period ($p = 0.004$) and during the October 2023 storm period ($p = 0.015$), and ebullitive fluxes were greater in the fair-weather dataset as a result (Table 2).

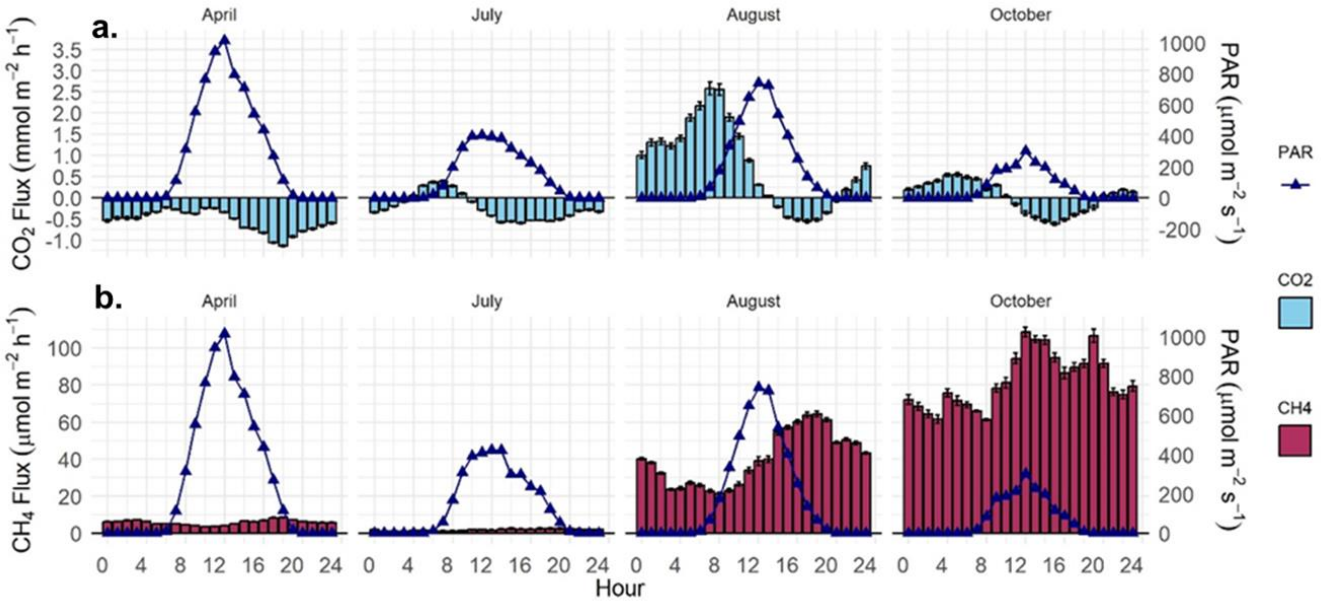

Fig. 7. (a) Fair-weather dataset of mean dissolved CO_2 and **(b)** mean dissolved CH_4 fluxes measured in April, July, August, and October deployments in 2023. Positive fluxes represent a source to the atmosphere and negative fluxes represent uptake from the atmosphere. Error bars depict standard error.

4 Discussion

4.1 Overview of *in situ* fluxes

Air-water gas fluxes varied seasonally over a temperate seagrass meadow located in a shallow lagoonal estuary (South Bay). South Bay was a source of CO_2-equivalent gases (CO_2-e) during and after seagrass senescence, and was a sink of CO_2-e gases in the early growing season. During the peak seagrass density period in July, CO_2-e gas fluxes were not significantly different from zero, despite high variations in the flux magnitudes throughout the day (Fig. 3). This gradual shift from a sink to a source of CO_2-e gases over time shows the importance of measuring fluxes throughout the seagrass growing season before scaling fluxes up for global accounting projects (Rosentreter et al., 2021b; Saunois et al., 2020). Other temperate seagrass meadows have been reported to be either net sinks or negligible sources of CO_2-e gases (Al-Haj et al. 2022; Ollivier et al. 2022). On average, South Bay was a minor source of CO_2-equivalent gases during our study period (0.24 g CO_2-e m^{-2} d^{-1}); however, our study included nighttime and

storm period fluxes that were more representative of overall conditions at our site. Similarly to studies conducted in other coastal vegetated systems, our study did not encompass the wintertime period, in which fluxes are likely to be reduced compared to the growing season (Rosentreter et al., 2023). On the coastal shelf, CO_2 uptake increases during the winter (Dai et al., 2022).

In this study, we defined a storm threshold using established protocols and *in situ* conditions during two storm periods, one in July 2022 and the other in October 2023. We found that dissolved air-water CO_2 and CH_4 fluxes increased significantly during the storm periods due to increases in wind speed and water column gas concentrations, and decreases in temperatures, while ebullitive CH_4 fluxes decreased significantly during storm periods (Fig. 7). These altered water column gas concentrations are likely partially driven by increased sediment resuspension from wind-waves during the storm period, which can facilitate the transport of dissolved gases from the sediment to the water column (Zhu and Wiberg, 2024, 2022). Whitecapping, rainfall, and bubble entrainment likely enhance gas exchange as well during storms (Wanninkhof et al., 2009; Ho et al., 2006). South Bay was above the storm threshold for 13.2 % of the year in 2022 and 16.0 % of the year in 2023, which demonstrates the importance of evaluating fluxes during all potential weather conditions.

4.2 Dissolved CO_2 fluxes

South Bay was a consistent sink of air-water CO_2 fluxes during the early growing season in April (Fig. 3). During the peak seagrass density period in July, we found that South Bay was in metabolic balance and CO_2 fluxes were not significantly different from zero. South Bay shifted to an overall CO_2 source in August during senescence, likely due to increased water column temperatures that have been shown to increase CO_2 outgassing in other seagrass meadows by reducing CO_2 solubility (Fig. 3) (Burkholz et al., 2020; Weiss, 1974). South Bay remained a CO_2 source after senescence, but the magnitude of the source decreased, likely due to decreases in water temperatures, air temperatures, and seagrass biomass (Rheuban et al., 2014b; Reidenbach and Thomas, 2018). Respiration and gross primary production in seagrass meadows peak with seagrass densities, so this result suggests that the air-water CO_2 flux is primarily driven by ecosystem metabolism of the benthos and the water column during this time of year (Berger et al., 2020; Oreska et al., 2018). Additionally, we observed a decrease in PAR in October, which

could be attributed to increased sediment resuspension from the reduced seagrass biomass (Nardin et al., 2018; Zhu et al., 2021).

Our continuous flux methodology may explain why South Bay is a modest CO_2 sink compared to other studies where measurements were only collected during the day (Banerjee et al., 2019; Burkholz et al., 2020). Importantly, South Bay was primarily a CO_2 source during the nighttime hours and primarily a sink CO_2 during the afternoon hours, which suggests that exclusively measuring daytime CO_2 fluxes, especially in the afternoon, will lead to an overestimation of the magnitude of the CO_2 sink (Rosentreter et al., 2023). These results are in agreement with a study conducted over a temperate seagrass meadow in Australia, where a diurnal time series flux was -0.46 ± 0.18 mmol CO_2 m^{-2} d^{-1} and it was determined that daytime spatial sampling overestimated the sink capacity of their meadow by 96% (Ollivier et al., 2022).

4.3 Total CH_4 fluxes

The dissolved and ebullitive CH_4 fluxes exhibited different patterns throughout the growing season (Fig. 5, Fig. 6). In contrast to CO_2, dissolved CH_4 fluxes were low in April and July, increased significantly during senescence, and then peaked during the post-senescence period (Fig. 3). Ebullitive CH_4 flux patterns varied slightly by year, but generally increased throughout the growing season from April to July and then decreased during and after senescence in August and October (Fig. 4a, Fig. 5). Other studies that measured benthic ebullitive CH_4 emissions also found that CH_4 emissions were highest when biomass was greatest (Oreska et al., 2020; Bahlmann et al., 2015). Total CH_4 fluxes increased throughout the growing season, which aligns with the findings of a study that measured fluxes across the air-water interface with cavity ring-down spectrometry and found that CH_4 emissions were highest when biomass was lowest (Fig. 5) (Ollivier et al., 2022). Our mean total CH_4 flux (0.78 mmol CH_4 m^{-2} d^{-1}) is within the range of the mean air-water fluxes reported by other studies in seagrass meadows and a recent global synthesis (0.104 ± 0.039 mmol CH_4 m^{-2} d^{-1}, mean ± SE) (Eyre et al., 2023; Burkholz et al., 2020). Our total flux was approximately five times greater than the average CH_4 flux measured at our site with benthic chambers (0.137 mmol CH_4 m^{-2} d^{-1}), but our ebullitive flux was similar (0.19 ± 0.08 mmol CH_4 m^{-2} d^{-1}, mean ± standard deviation) (Oreska et al., 2020).

We observed the highest CH_4 emissions during and after seagrass senescence, when seagrasses can often experience heat stress from high temperatures (Berger et al., 2020; Aoki et al., 2021). This stress likely causes seagrasses and other organisms to produce increased amounts of methylated compounds, which then increases the amount of substrate available for methylotrophic methanogenesis to proceed (Schorn et al., 2022; Berghuis et al., 2019). Increased substrate for methylotrophic methanogenesis is likely one reason why dissolved CH_4 fluxes significantly increased from July to August. After senescence, O_2 produced by seagrass photosynthesis is reduced (Berger et al., 2020), in turn reducing the potential for CH_4 to be removed via oxidation in the seagrass rhizospheres or the water column (Ollivier et al., 2022; Rosentreter et al., 2021a; Brodersen et al., 2024). Additionally, methylotrophic methanogenesis can occur in living or dead seagrass tissues, so supply of biodegradable substrate for methanogenesis persists throughout the fall and autumn and leads to increased fluxes during this time (Schorn et al., 2022; Vroom et al., 2022). We did not identify a significant diel pattern in the dissolved CH_4 fluxes, but we observed moderately heightened CH_4 fluxes overnight in April, July, and August. This may occur because CH_4 consumption by methanotrophs living on submerged plants increases during the day, which would reduce available CH_4 concentrations in the water column (Fig. 3b) (Vroom et al., 2022).

The diel and seasonal dynamics of methanogenesis and methanotrophy may indirectly influence CO_2 fluxes. pCO_2 and pCH_4 were strongly negatively correlated in August and October. This phenomenon indicates that aerobic CH_4 oxidation to CO_2 is occurring in the water column above the seagrass meadow, resulting in a removal of some CH_4 from the system and potentially increasing CO_2 concentrations during and after senescence (Whiticar, 2020). Thus, the enhanced CO_2 flux shown in August and October may be a result of reduced CH_4 concentrations from CH_4 oxidation.

4.4 CH_4 ebullition

We found that ebullition was a significant component of the total CH_4 flux, contributing 54% of total emissions in April, 89% in July, and 22% during senescence (Fig. 6). Ebullition was a minor component of the total CH_4 emissions (2.5%) in October, after senescence. Similarly to lakes, a major percentage of sediment-water column ebullition may occur in the summer because

ebullition increases with increasing temperatures and sedimentation rates (DelSontro et al., 2016; Praetzel et al., 2021). The decrease in the ebullitive flux during and after seagrass senescence also suggests that plant-mediated transport is also an important ebullitive transport pathway (Fig. 6) (Schorn et al., 2022). In lakes, pressure gradients are established in the lacunar system of submerged plants with high photosynthetic activity, such as *Potamogeton amplifolius*, due to O_2 accumulation from photosynthesis (Vroom et al., 2022; Whiticar, 2020). This gradient causes a pressurized flow of CH_4 from the roots to the shoots that follows a diel pattern with photosynthesis and contributes 19-29 % of the total daytime emission of CH_4 from the benthic system (Vroom et al., 2022). Plant-mediated transport of CH_4 has not been explicitly studied in seagrass meadows, but the pathway has been suggested as a potential mechanism for CH_4 emissions by recent studies (Al-Haj et al., 2022; Schorn et al., 2022). Plant-mediated transport of photosynthetic O_2 is known to occur in seagrass meadows because the ebullition of O_2 from *Z. marina* has been observed, primarily during daytime low tides when the pressure differences between the water column and the gases in the seagrass aerenchyma would be greatest (Long et al., 2020). O_2 comprised < 40% of the total gas in the observed bubbles, which suggests that ebullition of other gases, such as CH_4, is occurring in *Z. marina* meadows (Long et al., 2020). Overall, measuring diffusion, sediment-water column ebullition, and plant-mediated ebullition is important for constraining the total CH_4 flux in seagrass meadows.

4.5 N_2O fluxes

Similarly to other seagrass meadows, South Bay is a net sink of N_2O across the air-water interface (Al-Haj et al. 2022; Ollivier et al. 2022). The concept of seagrass meadows as sinks of N_2O on the global scale is relatively new and is contrary to mangroves and salt marshes, which are sources of N_2O (Rosentreter et al., 2021b; Eyre et al., 2023). Previous studies have shown that the benthos in South Bay emits N_2O, as sediment-water column N_2O fluxes measured with benthic chambers were 3.65 μmol m^{-2} d^{-1} (Oreska et al., 2020). Average air-water N_2O fluxes measured by this study were -7.0 ± 2.0 μmol m^{-2} d^{-1}, which is about five times larger than the global average for *Z. marina* reported by a recent synthesis (Fig. 4b, Fig. 6, Table 3) (Eyre et al., 2023). It is likely that the N_2O produced by the benthic environment is removed from the system through burial, retention in biomass, and denitrification (Aoki et al., 2020). In other oligotrophic seagrass meadows and mangrove forests, N_2O consumption in the water column has been

observed when NO_3^- concentrations are below 5 µmol L^{-1} (Murray et al., 2020; Wells et al., 2018). We identified air-water ebullitive N_2O emissions in this study, but they were consistently small (approximately 5.0 * 10^{-3} µmol m^{-2} d^{-1}) and had a negligible effect on the total N_2O uptake (Fig. 5) (Al-Haj et al., 2022).

The negative N_2O fluxes observed here are an important consideration for greenhouse gas accounting. Although the N_2O flux data in this study were limited by available methodologies, N_2O uptake offset CH_4 emissions by 100% in the early growing season, 40% during peak seagrass density, 18% during seagrass senescence, and 13% during post-senescence (Table 3). Our dissolved N_2O flux measurements were obtained from point samples collected during the day and as a result, do not capture potential diel variations in the dissolved N_2O flux. However, the N_2O percent saturation in the water column was lower overnight compared to the day in a similar system, suggesting that the magnitude of the negative N_2O flux may increase overnight in South Bay, and that our daytime fluxes may be an underestimate of the total negative flux (Ollivier et al., 2022). In the future, more measurements of nighttime and wintertime dissolved N_2O fluxes would help establish a clearer picture of the potential for N_2O uptake to offset CH_4 emissions in temperate seagrass meadows.

5 Conclusions

Overall, our results show the importance of evaluating local-scale, in situ fluxes of CO_2, CH_4, and N_2O on diurnal and seasonal scales. South Bay was primarily a source of dissolved CO_2 overnight in all months except April, and dissolved CH_4 fluxes were highest overnight in all months except October (Fig. 3). Thus, measuring daytime fluxes exclusively would have under-estimated the emission of CO_2-equivalent gases from our site. Throughout the growing season, CH_4 was a consistent source to the atmosphere and N_2O was a consistent sink, while CO_2 shifted from a sink to a source throughout the growing season (Fig. 3, Fig. 5, Fig. 6). In April, negative CO_2 and N_2O fluxes were greater than CH_4 emissions and South Bay was a net CO_2-e sink. In July, South Bay was in metabolic balance and net CO_2-e was not significantly different from zero. During seagrass senescence and post-senescence, South Bay was a source of CO_2-e gases that was partially offset by negative N_2O fluxes. These shifts in the overall CO_2-e flux throughout the growing season are critical to consider when scaling fluxes for global estimations.

6 Literature Cited

Al-Haj, A. N. and Fulweiler, R. W.: A synthesis of methane emissions from shallow vegetated coastal ecosystems, https://doi.org/10.1111/gcb.15046, 1 May 2020.

Al-Haj, A. N., Chidsey, T., and Fulweiler, R. W.: Two temperate seagrass meadows are negligible sources of methane and nitrous oxide, Limnol Oceanogr, https://doi.org/10.1002/lno.12250, 2022.

Aoki, L. R. and McGlathery, K. J.: Restoration enhances denitrification and DNRA in subsurface sediments of Zostera marina seagrass meadows, Mar Ecol Prog Ser, 602, 87–102, https://doi.org/10.3354/meps12678, 2018.

Aoki, L. R., McGlathery, K. J., and Oreska, M. P. J.: Seagrass restoration reestablishes the coastal nitrogen filter through enhanced burial, Limnol Oceanogr, 65, 1–12, https://doi.org/10.1002/lno.11241, 2020.

Aoki, L. R., McGlathery, K. J., Wiberg, P. L., Oreska, M. P. J., Berger, A. C., Berg, P., and Orth, R. J.: Seagrass Recovery Following Marine Heat Wave Influences Sediment Carbon Stocks, Front Mar Sci, 7, https://doi.org/10.3389/fmars.2020.576784, 2021.

Asplund, M. E., Bonaglia, S., Boström, C., Dahl, M., Deyanova, D., Gagnon, K., Gullström, M., Holmer, M., and Björk, M.: Methane Emissions From Nordic Seagrass Meadow Sediments, Front Mar Sci, 8, https://doi.org/10.3389/fmars.2021.811533, 2022.

Bahlmann, E., Weinberg, I., Lavrič, J. V., Eckhardt, T., Michaelis, W., Santos, R., and Seifert, R.: Tidal controls on trace gas dynamics in a seagrass meadow of the Ria Formosa lagoon (southern Portugal), Biogeosciences, 12, 1683–1696, https://doi.org/10.5194/bg-12-1683-2015, 2015.

Banerjee, K., Paneerselvam, A., Ramachandran, P., Ganguly, D., Singh, G., and Ramesh, R.: Seagrass and macrophyte mediated CO2 and CH4 dynamics in shallow coastal waters, PLoS One, 13, https://doi.org/10.1371/journal.pone.0203922, 2019.

Bange, H. W., Rapsomanik, S., and Andreae, M. O.: Nitrous oxide in coastal waters, Global Biogeochem Cycles, 10, 197–207, https://doi.org/10.1029/95GB03834, 1996.

Barbosa, P. M., Melack, J. M., Amaral, J. H. F., Linkhorst, A., and Forsberg, B. R.: Large Seasonal and Habitat Differences in Methane Ebullition on the Amazon Floodplain, J Geophys Res Biogeosci, 126, https://doi.org/10.1029/2020JG005911, 2021.

Berger, A. C., Berg, P., McGlathery, K. J., and Delgard, M. L.: Long-term trends and resilience of seagrass metabolism: A decadal aquatic eddy covariance study, Limnol Oceanogr, https://doi.org/10.1002/lno.11397, 2020.

Berghuis, B. A., Yu, F. B., Schulz, F., Blainey, P. C., Woyke, T., and Quake, S. R.: Hydrogenotrophic methanogenesis in archaeal phylum Verstraetearchaeota reveals the shared ancestry of all methanogens, Proc Natl Acad Sci U S A, 116, 5037–5044, https://doi.org/10.1073/pnas.1815631116, 2019.

Bogard, M. J., Del Giorgio, P. A., Boutet, L., Chaves, M. C. G., Prairie, Y. T., Merante, A., and Derry, A. M.: Oxic water column methanogenesis as a major component of aquatic CH4 fluxes, Nat Commun, 5, https://doi.org/10.1038/ncomms6350, 2014.

Borges, A. V., Abril, G., and Bouillon, S.: Carbon dynamics and CO2 and CH4 outgassing in the Mekong delta, Biogeosciences, 15, 1093–1114, https://doi.org/10.5194/bg-15-1093-2018, 2018.

Brodersen, K. E., Mosshammer, M., Bittner, M. J., Hallstrøm, S., Santner, J., Riemann, L., and Kühl, M.: Seagrass-mediated rhizosphere redox gradients are linked with ammonium accumulation driven by diazotrophs, Microbiol Spectr, https://doi.org/10.1128/spectrum.03335-23, 2024.

Burkholz, C., Garcias-Bonet, N., and Duarte, C. M.: Warming enhances carbon dioxide and methane fluxes from Red Sea seagrass (Halophila stipulacea) sediments, Biogeosciences, 17, 1717–1730, https://doi.org/10.5194/bg-17-1717-2020, 2020.

Castagno, K. A., Jiménez-Robles, A. M., Donnelly, J. P., Wiberg, P. L., Fenster, M. S., and Fagherazzi, S.: Intense Storms Increase the Stability of Tidal Bays, Geophys Res Lett, 45, 5491–5500, https://doi.org/10.1029/2018GL078208, 2018.

Cheng, J., Schloerke B, Karambelkar B, and Xie Y: Leaflet: Create Interactive Web Maps with the JavaScript “Leaflet” Library., 2024.

Dai, M., Su, J., Zhao, Y., Hofmann, E. E., Cao, Z., Cai, W.-J., Gan, J., Lacroix, F., Laruelle, G. G., Meng, F., Müller, J. D., Regnier, P. A. G., Wang, G., and Wang, Z.: Carbon Fluxes in the Coastal Ocean: Synthesis, Boundary Processes, and Future Trends, https://doi.org/10.1146/annurev-earth-032320, 2022.

Damm, E., Helmke, E., Thoms, S., Schauer, U., Nöthig, E., Bakker, K., and Kiene, R. P.: Methane production in aerobic oligotrophic surface water in the central Arctic Ocean, Biogeosciences, 7, 1099–1108, https://doi.org/10.5194/bg-7-1099-2010, 2010.

DelSontro, T., Boutet, L., St-Pierre, A., del Giorgio, P. A., and Prairie, Y. T.: Methane ebullition and diffusion from northern ponds and lakes regulated by the interaction between temperature and system productivity, Limnol Oceanogr, 61, S62–S77, https://doi.org/10.1002/lno.10335, 2016.

Eyre, B. D., Camillini, N., Glud, R. N., and Rosentreter, J. A.: The climate benefit of seagrass blue carbon is reduced by methane fluxes and enhanced by nitrous oxide fluxes, Commun Earth Environ, 4, https://doi.org/10.1038/s43247-023-01022-x, 2023.

Fagherazzi, S. and Wiberg, P. L.: Importance of wind conditions, fetch, and water levels on wave-generated shear stresses in shallow intertidal basins, J Geophys Res Earth Surf, 114, https://doi.org/10.1029/2008JF001139, 2009.

Garcias-Bonet, N., Delgado-Huertas, A., Carrillo-de-Albornoz, P., Anton, A., Almahasheer, H., Marbà, N., Hendriks, I. E., Krause-Jensen, D., and Duarte, C. M.: Carbon and Nitrogen Concentrations, Stocks, and Isotopic Compositions in Red Sea Seagrass and Mangrove Sediments, Front Mar Sci, 6, https://doi.org/10.3389/fmars.2019.00267, 2019.

Günthel, M., Klawonn, I., Woodhouse, J., Bižić, M., Ionescu, D., Ganzert, L., Kümmel, S., Nijenhuis, I., Zoccarato, L., Grossart, H., and Tang, K. W.: Photosynthesis-driven methane production in oxic lake water as an important contributor to methane emission, Limnol Oceanogr, lno.11557, https://doi.org/10.1002/lno.11557, 2020.

Helton, A. M., Bernhardt, E. S., and Fedders, A.: Biogeochemical regime shifts in coastal landscapes: The contrasting effects of saltwater incursion and agricultural pollution on greenhouse gas emissions from a freshwater wetland, Biogeochemistry, 120, 133–147, https://doi.org/10.1007/s10533-014-9986-x, 2014.

Ho, D. T., Law, C. S., Smith, M. J., Schlosser, P., Harvey, M., and Hill, P.: Measurements of air-sea gas exchange at high wind speeds in the Southern Ocean: Implications for global parameterizations, Geophys Res Lett, 33, https://doi.org/10.1029/2006GL026817, 2006.

Hudson, F.: STANDARD OPERATING PROCEDURE Sample Preparation and Calculations for Dissolved Gas Analysis in Water Samples Using a GC Headspace Equilibration Technique, 2004.

IPCC: Climate Change 2023: Synthesis Report. Contribution of Working Groups I, II and III to the Sixth Assessment Report of the Intergovernmental Panel on Climate Change [Core Writing Team, H. Lee and J. Romero (eds.)], Geneva, Switzerland, 35–115 pp., https://doi.org/10.59327/IPCC/AR6-9789291691647, 2023.

Joyce, J. and Jewell, P. W.: Physical Controls on Methane Ebullition from Reservoirs and Lakes, Environmental & Engineering Geoscience, 4, 167–178, 2003.

Lawson, S. E., Wiberg, P. L., McGlathery, K. J., and Fugate, D. C.: Wind-driven Sediment Suspension Controls Light Availability in a Shallow Coastal Lagoon, Estuaries and Coasts, 30, 102–112, 2007.

Long, M. H. and Nicholson, D. P.: Surface gas exchange determined from an aquatic eddy covariance floating platform, Limnol Oceanogr Methods, 16, 145–159, https://doi.org/10.1002/lom3.10233, 2018.

Long, M. H., Sutherland, K., Wankel, S. D., Burdige, D. J., and Zimmerman, R. C.: Ebullition of oxygen from seagrasses under supersaturated conditions, Limnol Oceanogr, 65, 314–324, https://doi.org/10.1002/lno.11299, 2020.

Marbà, N., Arias-Ortiz, A., Masqué, P., Kendrick, G. A., Mazarrasa, I., Bastyan, G. R., Garcia-Orellana, J., and Duarte, C. M.: Impact of seagrass loss and subsequent revegetation on carbon sequestration and stocks, Journal of Ecology, 103, 296–302, https://doi.org/10.1111/1365-2745.12370, 2015.

Matoušů, A., Osudar, R., Šimek, K., and Bussmann, I.: Methane distribution and methane oxidation in the water column of the Elbe estuary, Germany, Aquat Sci, 79, 443–458, https://doi.org/10.1007/s00027-016-0509-9, 2017.

McGinnis, D. F., Greinert, J., Artemov, Y., Beaubien, S. E., and Wüest, A.: Fate of rising methane bubbles in stratified waters: How much methane reaches the atmosphere?, J Geophys Res Oceans, 111, https://doi.org/10.1029/2005JC003183, 2006.

McGlathery, K. J., Reynolds, L. K., Cole, L. W., Orth, R. J., Marion, S. R., and Schwarzschild, A.: Recovery trajectories during state change from bare sediment to eelgrass dominance, Mar Ecol Prog Ser, 448, 209–221, https://doi.org/10.3354/meps09574, 2012.

Mu, L., Stammerjohn, S. E., Lowry, K. E., and Yager, P. L.: Spatial variability of surface pCO2 and air-sea CO2 flux in the Amundsen Sea Polynya, Antarctica, Elementa: Science of the Anthropocene, 2, 000036, https://doi.org/10.12952/journal.elementa.000036, 2014.

Murray, R., Erler, D. V., Rosentreter, J., Wells, N. S., and Eyre, B. D.: Seasonal and spatial controls on N2O concentrations and emissions in low-nitrogen estuaries: Evidence from three tropical systems, Mar Chem, 221, https://doi.org/10.1016/j.marchem.2020.103779, 2020.

Murray, R. H., Erler, D. V., and Eyre, B. D.: Nitrous oxide fluxes in estuarine environments: Response to global change, https://doi.org/10.1111/gcb.12923, 1 September 2015.

Nardin, W., Larsen, L., Fagherazzi, S., and Wiberg, P.: Tradeoffs among hydrodynamics, sediment fluxes and vegetation community in the Virginia Coast Reserve, USA, Estuar Coast Shelf Sci, 210, 98–108, https://doi.org/10.1016/j.ecss.2018.06.009, 2018.

Ollivier, Q. R., Maher, D. T., Pitfield, C., and Macreadie, P. I.: Net Drawdown of Greenhouse Gases (CO2, CH4 and N2O) by a Temperate Australian Seagrass Meadow, Estuaries and Coasts, 45, 2026–2039, https://doi.org/10.1007/s12237-022-01068-8, 2022.

Oreska, M. P. J., McGlathery, K. J., and Porter, J. H.: Seagrass blue carbon spatial patterns at the meadow-scale, PLoS One, 12, https://doi.org/10.1371/journal.pone.0176630, 2017.

Oreska, M. P. J., Wilkinson, G. M., McGlathery, K. J., Bost, M., and McKee, B. A.: Non-seagrass carbon contributions to seagrass sediment blue carbon, Limnol Oceanogr, 63, S3–S18, https://doi.org/10.1002/lno.10718, 2018.

Oreska, M. P. J., McGlathery, K. J., Aoki, L. R., Berger, A. C., Berg, P., and Mullins, L.: The greenhouse gas offset potential from seagrass restoration, Sci Rep, 10, https://doi.org/10.1038/s41598-020-64094-1, 2020.

Orth, R. J. and Moore, K. A.: SEASONAL AND YEAR-TO-YEAR VARIATIONS IN THE GROWTH OF ZOSTERA MARINA L. (EELGRASS) IN THE LOWER CHESAPEAKE BAY, Aquat Bot, 24, 335–341, 1986.

Porter, J. H. and Williams, T.: Atmospheric pressure on Hog Island, Phillips Creek Marsh and Oyster, VA 2012-2023, Virginia Coast Reserve Long-Term Ecological Research Project Data Publication knb-lter-vcr.307.6, https://doi.org/doi:10.6073/pasta/32e5275136fcd2c29ed53fcf6afcf1ef, 2024.

Praetzel, L. S. E., Schmiedeskamp, M., and Knorr, K. H.: Temperature and sediment properties drive spatiotemporal variability of methane ebullition in a small and shallow temperate lake, Limnol Oceanogr, 66, 2598–2610, https://doi.org/10.1002/lno.11775, 2021.

R Core Team: R: A Language and Environment for Statistical Computing, 2023.

Reidenbach, M. A. and Thomas, E. L.: Influence of the Seagrass, Zostera marina, on wave attenuation and bed shear stress within a shallow coastal bay, Front Mar Sci, 5, https://doi.org/10.3389/fmars.2018.00397, 2018.

Rheuban, J. E., Berg, P., and McGlathery, K. J.: Ecosystem metabolism along a colonization gradient of eelgrass (Zostera marina) measured by eddy correlation, Limnol Oceanogr, 59, 1376–1387, https://doi.org/10.4319/lo.2014.59.4.1376, 2014a.

Rheuban, J. E., Berg, P., and McGlathery, K. J.: Multiple timescale processes drive ecosystem metabolism in eelgrass (Zostera marina) meadows, Mar Ecol Prog Ser, 507, 1–13, https://doi.org/10.3354/meps10843, 2014b.

Rosentreter, J. A., Borges, A. V., Deemer, B. R., Holgerson, M. A., Liu, S., Song, C., Melack, J., Raymond, P. A., Duarte, C. M., Allen, G. H., Olefeldt, D., Poulter, B., Battin, T. I., and Eyre, B. D.: Half of global methane emissions come from highly variable aquatic ecosystem sources, Nat Geosci, 14, 225–230, https://doi.org/10.1038/s41561-021-00715-2, 2021a.

Rosentreter, J. A., Al-Haj, A. N., Fulweiler, R. W., and Williamson, P.: Methane and nitrous oxide emissions complicate coastal blue carbon assessments, Global Biogeochem Cycles, https://doi.org/10.1029/2020gb006858, 2021b.

Rosentreter, J. A., Laruelle, G. G., Bange, H. W., Bianchi, T. S., Busecke, J. J. M., Cai, W. J., Eyre, B. D., Forbrich, I., Kwon, E. Y., Maavara, T., Moosdorf, N., Najjar, R. G., Sarma, V. V. S. S., Van Dam, B., and Regnier, P.: Coastal vegetation and estuaries are collectively a greenhouse gas sink, Nat Clim Chang, 13, 579–587, https://doi.org/10.1038/s41558-023-01682-9, 2023.

Saunois, M., Stavert, A. R., Poulter, B., Bousquet, P., Canadell, J. G., Jackson, R. B., Raymond, P. A., Dlugokencky, E. J., Houweling, S., Patra, P. K., Ciais, P., Arora, V. K., Bastviken, D., Bergamaschi, P., Blake, D. R., Brailsford, G., Bruhwiler, L., Carlson, K. M., Carrol, M., Castaldi, S., Chandra, N., Crevoisier, C., Crill, P. M., Covey, K., Curry, C. L., Etiope, G., Frankenberg, C., Gedney, N., Hegglin, M. I., Höglund-Isaksson, L., Hugelius, G., Ishizawa, M., Ito, A., Janssens-Maenhout, G., Jensen, K. M., Joos, F., Kleinen, T., Krummel, P. B., Langenfelds, R. L., Laruelle, G. G., Liu, L., Machida, T., Maksyutov, S., McDonald, K. C., McNorton, J., Miller, P. A., Melton, J. R., Morino, I., Müller, J., Murguia-Flores, F., Naik, V., Niwa, Y., Noce, S., O'Doherty, S., Parker, R. J., Peng, C., Peng, S., Peters, G. P., Prigent, C., Prinn, R., Ramonet, M., Regnier, P., Riley, W. J., Rosentreter, J. A., Segers, A., Simpson, I. J., Shi, H., Smith, S. J., Steele, L. P., Thornton, B. F., Tian, H., Tohjima, Y., Tubiello, F. N., Tsuruta, A., Viovy, N., Voulgarakis, A., Weber, T. S., van Weele, M., van der Werf, G. R., Weiss, R. F., Worthy, D., Wunch, D., Yin, Y., Yoshida, Y., Zhang, W., Zhang, Z., Zhao, Y., Zheng, B., Zhu, Q., Zhu, Q., and Zhuang, Q.: The Global Methane Budget 2000–2017, Earth Syst Sci Data, 12, 1561–1623, https://doi.org/10.5194/essd-12-1561-2020, 2020.

Schorn, S., Ahmerkamp, S., Bullock, E., Weber, M., Lott, C., Liebeke, M., Lavik, G., Kuypers, M. M. M., Graf, J. S., and Milucka, J.: Diverse methylotrophic methanogenic archaea cause high methane emissions from seagrass meadows, PNAS, 119, https://doi.org/10.1073/pnas.2106628119/-/DCSupplemental, 2022.

Schubert, C. J., Coolen, M. J. L., Neretin, L. N., Schippers, A., Abbas, B., Durisch-Kaiser, E., Wehrli, B., Hopmans, E. C., Damsté, J. S. S., Wakeham, S., and Kuypers, M. M. M.: Aerobic and anaerobic methanotrophs in the Black Sea water column, Environ Microbiol, 8, 1844–1856, https://doi.org/10.1111/j.1462-2920.2006.01079.x, 2006.

Serrano, O., Almahasheer, H., Duarte, C. M., and Irigoien, X.: Carbon stocks and accumulation rates in Red Sea seagrass meadows, Sci Rep, 8, https://doi.org/10.1038/s41598-018-33182-8, 2018.

Sturm, K., Keller-Lehmann, B., Werner, U., Raj Sharma, K., Grinham, A. R., and Yuan, Z.: Sampling considerations and assessment of Exetainer usage for measuring dissolved and gaseous methane and nitrous oxide in aquatic systems, Limnol Oceanogr Methods, 13, 375–390, https://doi.org/10.1002/lom3.10031, 2015.

Tang, K. W., McGinnis, D. F., Frindte, K., Brüchert, V., and Grossart, H. P.: Paradox reconsidered: Methane oversaturation in well-oxygenated lake waters, Limnol Oceanogr, 59, 275–284, https://doi.org/10.4319/lo.2014.59.1.0275, 2014.

Upstill-Goddard, R. C. and Barnes, J.: Methane emissions from UK estuaries: Re-evaluating the estuarine source of tropospheric methane from Europe, Mar Chem, https://doi.org/10.1016/j.marchem.2016.01.010, 2016.

Vroom, R. J. E., van den Berg, M., Pangala, S. R., van der Scheer, O. E., and Sorrell, B. K.: Physiological processes affecting methane transport by wetland vegetation – A review, Aquat Bot, 182, 103547, https://doi.org/10.1016/J.AQUABOT.2022.103547, 2022.

Wanninkhof, R.: Relationship between wind speed and gas exchange over the ocean revisited, Limnol Oceanogr Methods, 12, 351–362, https://doi.org/10.4319/lom.2014.12.351, 2014.

Wanninkhof, R., Asher, W. E., Ho, D. T., Sweeney, C., and McGillis, W. R.: Advances in Quantifying Air-Sea Gas Exchange and Environmental Forcing, Ann Rev Mar Sci, 1, 213–244, https://doi.org/10.1146/annurev.marine.010908.163742, 2009.

Weiss: CO2 solubility, 1974.

Weiss, R. and Price, B.: Nitrous oxide solubility in water and seawater, Mar Chem, 8, 347–359, 1980.

Wells, N. S., Maher, D. T., Erler, D. V., Hipsey, M., Rosentreter, J. A., and Eyre, B. D.: Estuaries as Sources and Sinks of N2O Across a Land Use Gradient in Subtropical Australia, Global Biogeochem Cycles, 32, 877–894, https://doi.org/10.1029/2017GB005826, 2018.

Whiticar, M. J.: The Biogeochemical Methane Cycle, in: Hydrocarbons, Oils and Lipids: Diversity, Origin, Chemistry and Fate, Springer International Publishing, 669–746, https://doi.org/10.1007/978-3-319-90569-3_5, 2020.

De Wilde, H. P. J. and De Bie, M. J. M.: Nitrous oxide in the Schelde estuary: Production by nitrification and emission to the atmosphere, Mar Chem, https://doi.org/10.1016/S0304-4203(99)00106-1, 2000.

Wilson, C. J., Wilson, P. S., and Dunton, K. H.: An acoustic investigation of seagrass photosynthesis, Mar Biol, 159, 2311–2322, https://doi.org/10.1007/s00227-012-2016-4, 2012.

Zhu, Q. and Wiberg, P. L.: The Importance of Storm Surge for Sediment Delivery to Microtidal Marshes, J Geophys Res Earth Surf, 127, https://doi.org/10.1029/2022JF006612, 2022.

Zhu, Q. and Wiberg, P. L.: Effects of Seasonal Variations in Seagrass Density and Storms on Sediment Retention and Connectivity Between Subtidal Flats and Intertidal Marsh, J Geophys Res Biogeosci, 129, https://doi.org/10.1029/2023JG007785, 2024.

Zhu, Q., Wiberg, P. L., and Reidenbach, M. A.: Quantifying Seasonal Seagrass Effects on Flow and Sediment Dynamics in a Back-Barrier Bay, J Geophys Res Oceans, 126, https://doi.org/10.1029/2020JC016547, 2021.

Chapter 4: At the intersection of science and education: The process of scientists and educators co-developing authentic learning experiences for K-16 students

This chapter was published in Limnology and Oceanography: Bulletin, a magazine-style journal, after receiving an invitation to contribute from the journal editors.

Adapted from: Granville, K.E., C. Baird, C. Carlson, and P. Berg. 2024. At the Intersection of Science and Education: The Process of Scientists and Educators Co-developing Authentic Learning Experiences for K-16 Students. Limnology and Oceanography: Bulletin. https://doi.org/10.1002/lob.10627

Abstract

Students lose interest in science as they progress from elementary to high school. There is a need for authentic, place-based science learning experiences that can increase students' interest in science. Scientists have unique skillsets that can complement the work of educators to create exciting experiences that are grounded in pedagogy and science practices. As scientists and educators, we co-developed a lesson plan for high school students on the Eastern Shore of Virginia, a historically-underserved coastal area, that demonstrated realistic scientific practices in students' local estuaries. After implementation of the lesson plan, we observed that students had a deeper understanding of ecosystem processes compared to their peers who had not been involved, were enthusiastic about sharing their experiences, and had a more well-rounded ability to think like a scientist than before the lesson plan. We share our experiences and five best practices that can serve as a framework for scientists and educators who are motivated to do similar work. Through collaboration, scientists and educators have the potential to bolster student science identities and increase student participation in future scientific endeavors.

1 Student views of science

Picture a scientist. Who do you see? From the time students enter kindergarten around age five to the time they graduate from twelfth grade around age eighteen, these students, hereafter referred to as K-12 students, are unlikely to identify themselves as people who can, or should, be scientists (Kang et al. 2019). This lack of "science identity" may be because classroom science experiences represent science as a difficult subject focused on memorizing complex facts and deep knowledge (Wade-Jaimes et al. 2023). Classroom experiences often do

not relate science to the skills that scientists typically consider most important, such as developing questions through logical thinking and curiosity, learning about and finding solutions to problems, and collaborating with others (Wade-Jaimes et al. 2023). This disconnect likely contributes not only to a lack of student science identity, but also to the decrease in science identity as students' progress from primary to secondary school (Miller et al. 2018; Wade-Jaimes et al. 2023). This lack of student science identity was analyzed by a meta-analysis of the Draw-A-Scientist studies, in which K-12 students in the U.S. were asked to draw a picture of a scientist (Miller et al. 2018). Older students tended to draw scientists indoors with laboratory coats and eyeglasses, which was likely due to the stereotypical conceptions of scientists that students learned in and out of the classroom. Further, these studies demonstrated that a strong science identity was particularly difficult for girls and students of color to develop and maintain. 79% of all students drew a Caucasian scientist (Miller et al. 2018). The percentage of girls who drew male scientists increased from 30% at the age of six to 75% at the age of sixteen, whereas the percentage of boys who drew male scientists increased from 83% to 98% over the same age range (Miller et al. 2018).

Students who were able to develop and maintain a strong science identity were more likely to identify with science, technology, engineering, and math (STEM) careers (Kang et al. 2019). A lack of strong science identity, especially in girls and students of color, may contribute to the broader lack of diversity and representation in STEM fields in the U.S, including marine and coastal sciences (Fry et al. 2021; Wade-Jaimes et al. 2023). From 1973-2016, less than 8% of ocean science Ph.D. degrees in the U.S. were awarded to students who identified as American Indian or Alaska Native, Black or African American, and Hispanic or Latino (Bernard and Cooperdock 2018). From 2010-2019, the combined number of undergraduate and graduate degrees in marine sciences awarded to Black or African American and Hispanic students in the U.S. was less than 1% of the total marine science degrees awarded (Harris et al. 2022).

Representation in the STEM educational system is correlated with diversity of the U.S. STEM workforce (Fry et al. 2021). Black or African American and Hispanic workers remain underrepresented in STEM fields when compared to their percentages in the total U.S. population, while the representation of women varies by field (Fry et al. 2021). According to the UNESCO Institute for Statistics (UIS), although women now earn a majority of both

undergraduate and advanced degrees, they make up less than 30% of the research and development workforce worldwide (https://uis.unesco.org/en/topic/women-science, last accessed Nov. 30, 2023). Increasing diversity and representation in STEM fields is important for continued scientific advancement, but the path to doing so is long, complex, and requires multiple approaches (Bernard and Cooperdock 2018; Fry et al. 2021). Providing support for students to develop and maintain science identities during both their K-12 and undergraduate educations (grades 13-16, hereafter referred to together as K-16) may help increase participation in science fields (Kang et al. 2019; Fry et al. 2021).

Scientists can contribute to this work. While authentic science activities done in classrooms can facilitate a positive change in student attitudes towards science, many teachers are not trained to develop these activities (Wade-Jaimes et al. 2023). As scientists, we have unique skills that can be leveraged to support student science identity and increase their environmental literacy. As environmental scientists, we also tend to have a deep understanding of our focal research areas and research sites that can be shared to benefit the local community. When we work together with educators, we can co-develop authentic science learning experiences for students that accurately reflect the experiences and identities of scientists. This is an emerging field of research, but there is evidence to suggest that experiences such as these can positively impact student science identities and within and beyond the classroom (Kang et al. 2019; Wade-Jaimes et al. 2023).

We - a high school ocean sciences teacher, a marine science graduate student, and our collaborators - co-developed a lesson plan for high school students based on the coastal ecosystems of Virginia (VA). Our goals were to: 1) demonstrate the process scientists follow during research projects from start to finish, 2) deepen students' scientific understanding of local ecosystems, 3) increase students' science identity in a historically-underserved area, and 4) increase data literacy by guiding students through the use of publicly-available data and resources. Our resulting lesson plan was implemented in a high school classroom in 2022 and can be accessed online (https://doi.org/10.6084/m9.figshare.24738627.v1, last accessed Dec. 5, 2023). Here, we share insights from our collaboration to offer our view on best practices for others venturing into the co-production of authentic science learning experiences for K-16 students (Fig. 1).

2 Responding to local community needs

Coastal and shoreline communities in the U.S. tend to be more diverse in their ethnic and racial identities than non-coastal areas, and are also more likely to be described as socially vulnerable, overburdened, and underserved (Harris et al. 2022). Our team works and does research on the Eastern Shore of Virginia (ESVA), a coastal community located on the Delmarva peninsula and separated from mainland VA by the Chesapeake Bay. To the east of the ESVA are the shallow lagoons that comprise the longest stretch of coastal wilderness on the east coast of the U.S, hereafter referred to as the Virginia Coast Reserve (VCR). When compared to the state of VA, the ESVA has a higher percentage of persons in poverty, a lower median household income, and a smaller percentage of high school and college graduates (https://www.census.gov/quickfacts/, last accessed Oct. 30, 2023). In 2022, the ESVA had one of the lowest environmental justice scores across the Chesapeake Bay watershed, indicating a high social vulnerability, environmental burden, and health vulnerability (UMCES 2023).

ESVA locals have a unique cultural heritage and relationship to both the Chesapeake Bay and the VCR, locally known as the 'seaside'. Watermen, waterwomen, fishers, and aquacultural farmers have worked on the ESVA for generations. As scientists working on the ESVA, we wanted to develop a learning experience that expanded on this knowledge in a scientific context, while prioritizing the needs of students on the ESVA.

3 Best practices for developing authentic science learning experiences

Developing an authentic science learning experience for students can seem daunting. Fortunately, there are many tools and structures available to support this endeavor. Here, we share five best practices that helped us navigate and simplify the process, as well as several examples from our own work (Fig. 1).

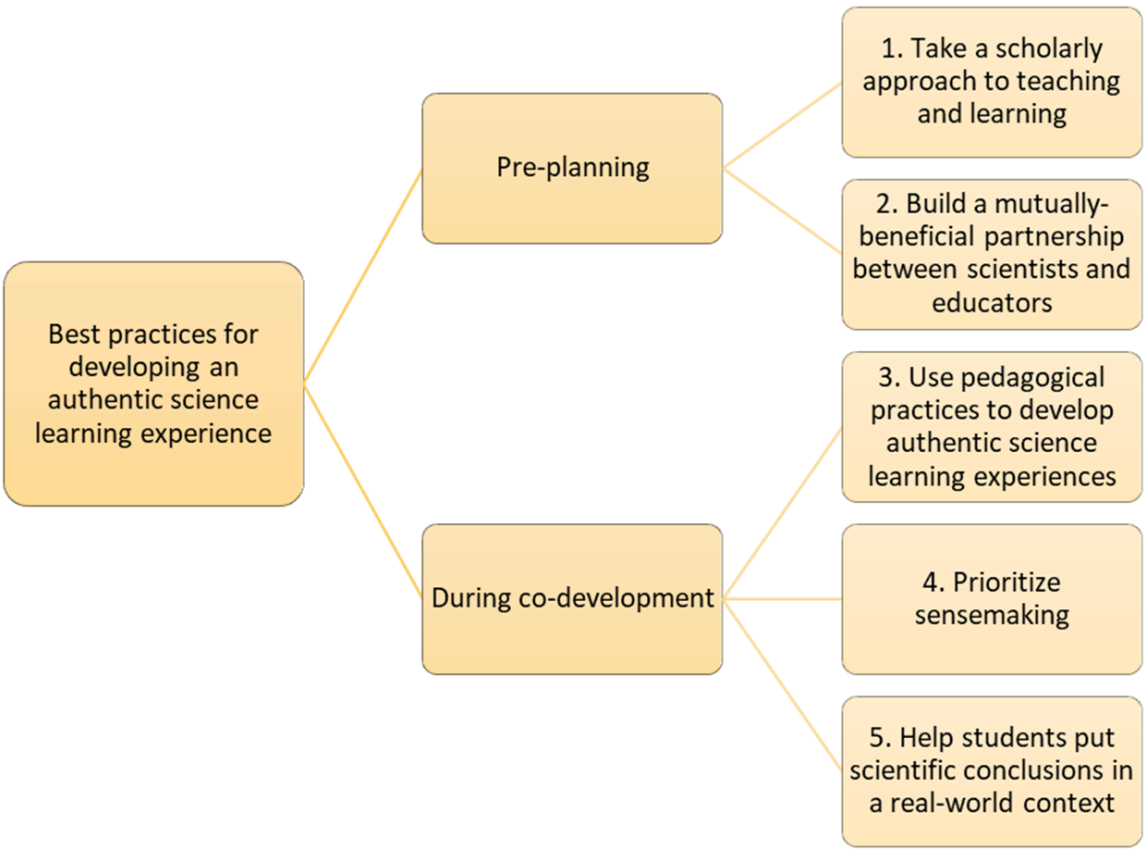

Fig 1. We identified five best practices for scientists and educators to use to co-develop authentic science learning experiences for K-16 students. Here, they are divided between the pre-planning and co-development stages of our work.

3.1 Take a scholarly approach to teaching and learning

Before reaching out to a teacher, the scientists reviewed the scholarly literature on student science identity and on pedagogy, or the theory and practice of teaching. This practice added nuance to our understanding of student learning, and provided context for how evidence-based educational practices can be used to teach authentic and impactful science (Alegado and Lewis 2018; Fick and Arias 2019; Kang et al. 2019; Wade-Jaimes et al. 2023). We also sought other available resources, including a short course developed by the University of Virginia School of Education and the Coastal Research Center designed to help scientists improve their mentoring skills by introducing the fundamentals of learning. A similar course is available online for free through the Center for the Integration of Research, Teaching, and Learning (https://www.stemteachingcourse.org/, last accessed Nov. 20, 2023). This initial effort helped us identify the pedagogical practices and support structures that we used to develop the lesson plan,

which are described below as a part of the third best practice. Even scientists without plans to incorporate formal teaching into their careers can benefit from these foundations, as they are relevant to the mentorship and informal learning scenarios that often arise throughout the scientific endeavor.

To identify curriculum concepts relevant to our work, we also reviewed the Virginia K-12 Standards of Learning (SOLs), which are publicly available online and provide standardized expectations for student learning concepts and curriculum framework (https://www.doe.virginia.gov/teaching-learning-assessment/instruction, last accessed Apr. 18, 2022). The science SOLs reflected a transition in classroom science from a focus on the scientific method to a focus on science practices. There were several authentic science practices in the SOLs that we believed scientists could uniquely support: supporting students throughout the scientific process, providing students with opportunities to explore science-related careers and interests, and helping students develop their scientific curiosity, creativity, and collaboration skills. These skills are critical for future generations of scientists and are generally not adequately supported in classroom science (Wade-Jaimes et al. 2023).

Doing this preparation allowed us to create a lesson plan pitch that was tailored specifically towards student and teacher needs on the ESVA. Our understanding of pedagogical practices helped convey a willingness to think about the tools and challenges of teaching science in the classroom, which is becoming increasingly relevant to teachers. Throughout the process of developing the lesson plan, we were able to share a vocabulary and a way of thinking with the teacher we worked with.

3.2 Build a mutually-beneficial partnership between scientists and educators

After we reviewed the scholarly literature and curriculum standards, we reached out to a high school teacher on the ESVA with a lesson plan pitch and an invitation to collaborate. We discussed ways to make the collaboration beneficial to both scientists and educators. As scientists who work at the Virginia Coast Reserve Long-Term Ecological Research site (VCR-LTER), we wanted to communicate our scientific work to students on the ESVA in a way that would support their development both as scientists and as stewards to their local estuaries. As an educator at Broadwater Academy, a private school on the ESVA, the teacher was also interested in providing more hands-on field and data analysis experiences for high school students who were close to

graduation. For these reasons and because high school students typically have diminished science identities, we decided that an upper-level high school class would benefit the most from our efforts (Miller et al. 2018).

The teacher had been teaching an environmental sciences course for high school students in grades 11 and 12 that was dual-enrollment with a nearby college. The dual-enrollment status increased the rigor of the class compared to other high school classes. In previous years, part of this rigor had come from a field experience that required travel and an overnight stay. However, overnight travel had been cancelled due to COVID-19 restrictions. The teacher had a specific need for a replacement activity that would be equally rigorous. As a group, we modified the original pitch from the scientists to meet this need. Our resulting lesson plan had two classroom sessions and a field experience. For the field experience, the class used established scientific methods and existing equipment from the VCR-LTER and Broadwater Academy to collect data at sites in both the Chesapeake Bay and the VCR.

Although our priority was to provide an authentic learning experience for this classroom, we were also interested in making our work accessible for other students on the ESVA and beyond. The lesson plan has been shared online and can be implemented by other scientists and educators or used as a guide for developing similar work (https://doi.org/10.6084/m9.figshare.24738627.v1, last accessed Dec. 5, 2023). Because the lesson plan was developed for a high school class on the cusp of the college level, it can easily be scaled up or down for other high school and college classrooms. The structure of the lesson plan can also be used as a guide to develop a similar local learning experience with two other estuaries or bodies of water. We found that developing a high-quality, local learning experience had the potential to be more inclusive for students who may have experienced cost barriers or other obstacles for trips that required extensive travel. Support from scientific institutions can also make these experiences possible for classrooms and schools who lack the specific materials to conduct such work independently.

A cornerstone in our collaboration was to establish a foundation of trust and recognize our shared and individual areas of interest and expertise. As scientists, our background research on pedagogy and curriculum standards helped us understand student needs, while our own expertise helped us translate the scientific processes outlined in the SOLs into practices. The

teacher had an established relationship with the VCR-LTER and some experience in biology and environmental sciences that enabled him to scale our work for high school students. As a private school educator, he had the capacity and resources to work on this learning experience. Two of our team members were ESVA locals and the others had spent extensive periods of time on the ESVA, which helped us incorporate local perspectives into our work. Working with an experienced teacher with the skills and capacity for lesson design helped make co-development and sharing feasible.

3.3 Use pedagogical practices to develop authentic science learning experiences

Our research into pedagogy helped us identify useful structures for developing authentic science learning experiences. Here, we share two pedagogical practices that were essential to our work: 'backward design' and 'scaffolding'.

'Backward design' is a method for building learning experiences that support focal learning outcomes (Michael and Libarkin 2016). In backward design, the learning experience is shaped to provide students with the necessary knowledge, experience, and data to reach an understanding of a topic. After a discussion of potential scientific concepts and practices, the teacher determined that a focal outcome of understanding the drivers of coastal ecosystem health would be best for his class. This framework simultaneously tied our lesson plan to other concepts that students were learning and expanded the class syllabus. Following backward design, we first outlined the claims, or outcomes, about ecosystem health that we wanted students to be able to make at the end of the lesson plan. We then determined the investigative questions and student learning goals using our expected claims, science learning priorities, and the VA SOL priorities.

Once the questions, goals, and outcomes of the lesson plan were established, we continued with this 'backward design' approach and worked together to determine the topics that would lead students to our expected claims. We familiarized ourselves with relevant work on ecosystem health in the area by reviewing the Chesapeake Bay Ecosystem Health Report Card, a freely available, annual report that uses publicly-available data to translate economic, ecological, and societal indicators into letter grades (https://ecoreportcard.org/report-cards/chesapeake-bay/, last accessed Nov. 30, 2023). We then reviewed the publicly-available VCR-LTER data catalog to identify variables that overlapped with the report card and that would be reasonable for students to measure (https://www.vcrlter.virginia.edu/cgi-bin/browseData.cgi, last accessed Nov.

30, 2023). Whenever possible, we aligned the environmental variables discussed in the lesson plan with both the report card and the VCR-LTER long-term datasets. Backward design was a useful way to determine what content would help students understand ecosystem health in the Chesapeake Bay and VCR and what content needed to be removed as extraneous or too high-level.

Scaffolding is a classroom teaching technique in which instructors add support for students to enhance their learning. These supports systematically build on prior experiences and knowledge students gain as they learn (Fick and Arias 2019). Less and less support is given over time as students master new concepts or material. The scaffold essentially fades away as the learner becomes skilled enough to no longer need the guidance. Using this technique is a way to ensure the educational content can support students who may be at different learning levels. Throughout the lesson plan development, the teacher provided critical insight into areas where high school students would need additional support through scaffolding to understand specific concepts and ideas.

The lesson plan's introduction to ecosystem health is an example of how we used scaffolding to model the beginning of the scientific process. First, the students were given a prompt: "What are some ways we might be able to tell if a coastal ecosystem is healthy or not?" After the students individually answered the prompt, the class discussed their answers and the teacher guided the discussion towards measurable variables. In addition to helping the teacher understand individual students' background knowledge, the practice of sharing out allowed the class to establish a common knowledge baseline. Next, the teacher connected elements of the class discussion to definitions of ecosystem health and environmental drivers. Here, we used the anecdote of a car as a scaffold to explain how environmental variables could drive ecosystem health. In the anecdote, the person driving the car was an analogy for an environmental variable, and the car itself was an analogy for ecosystem health. Just like the driver of the car would determine where the car was going, the environmental variable would determine the health of the ecosystem. The students were already familiar with the role of drivers in cars, so this scaffold was an effective way to explain that measuring environmental drivers was necessary for understanding ecosystem health.

We felt that the learning experience would be more authentic if we guided the students through the process of selecting the environmental drivers that they wanted to measure to evaluate ecosystem health in the Chesapeake Bay and the VCR instead of telling them. To simulate this experience, we grouped the variables we had chosen for the field experience into four driver categories: physical, biogeochemical, biodiversity, and human impacts (Fig. 2a). The purpose of grouping the drivers was to demonstrate that different variables were inter-connected. For the category titles, we had intentionally chosen words that either matched vocabulary the students were familiar with from previous classroom activities or that could be easily explained using the students' background knowledge. During the lesson plan, the teacher wrote the four categories on the board (Fig. 2b). The class used the introductory exercise and the categories as scaffolds to brainstorm environmental drivers (Fig. 2b). After the brainstorm, the teacher showed the list of variables that the students would actually measure (Fig. 2a). The class talked about what the students had missed, as well as additional variables the students had mentioned that the class would not measure. We used this as an opportunity to discuss how equipment availability could influence a scientists' methods. These exercises gave students a better opportunity to think critically about their study objective and take ownership of their research methods. More detailed explanations of the exercises outlined here can be found in the lesson plan (https://doi.org/10.6084/m9.figshare.24738627.v1, last accessed Dec. 5, 2023).

Fig. 2. The scaffolding technique was used to guide students through the process of deciding what variables should be measured to assess ecosystem health. **(a)** The variables the students would measure during the field experience were pre-determined and grouped into four categories. **(b)** The teacher wrote the four categories from (a) on the board. The class brainstormed environmental drivers that they thought were important to measure using the categories as a scaffold. After the brainstorming session, the class compared their drivers to the list of variables shown in (a).

3.4 Prioritize sensemaking

If you've ever heard a student summarize a science class as 'we looked at water today' or 'we used lasers in science class', then you've likely experienced the outcome of a science experience that did not focus enough on sensemaking. Sensemaking, or the process of interpreting and synthesizing the results, fitting them into a real-world context, and discussing them with classmates, is often not prioritized in traditional science classrooms and labs. Instead, time is spent following protocols to do an experiment. The lack of sensemaking can leave students feeling frustrated with or disconnected from their experience (Wade-Jaimes et al. 2023). Prioritizing sensemaking takes a lot of work and careful support, but when done well, it can cultivate student science identity by helping students understand and remember the 'findings' of their investigation. Much of our planning involved adapting scientific practices of data analysis and presentation into activities that were authentic but suitable for high school students. Two of our activities are described below.

In advance of the lesson plan, we created time series plots of publicly-available VCR-LTER water quality data, including water temperature, salinity, nitrate, and dissolved oxygen

(https://www.vcrlter.virginia.educgi-bin/showDataset.cgi?docid=knb-lter-vcr.247.17, last accessed May 1, 2022). During the field experience, students used VCR-LTER water quality sampling protocols to measure these variables, among others. After the field experience, students drew their datapoints on top of the plots we had made, which allowed us to use the plots as a scaffold for understanding the students' water quality data in the context of the broader water quality patterns in the VCR. Our water temperature plot from this activity is shown as an example (Fig. 3a). This exercise served as a way for students to put their data in a real-world context and learn about local water quality trends.

We also used the students' data to demonstrate that qualitative data can be valuable and that science can be communicated in multiple ways. In the field, students had circled adjectives that described inner and outer leaves on seagrass shoots to evaluate how the leaves changed visually over time. We entered all words circled by each student into a free online word cloud generator and generated word clouds for the inner and outer seagrass leaves (Fig. 3b, 3c). Essentially, the students were able to see a summary of what adjectives the class agreed and disagreed on. They were given a chance to discuss and explain their individual reasoning, which allowed them to practice collaboration with their peers and apply appropriate vocabulary. This activity is an example of how an accessible visual representation of data can support student sensemaking.

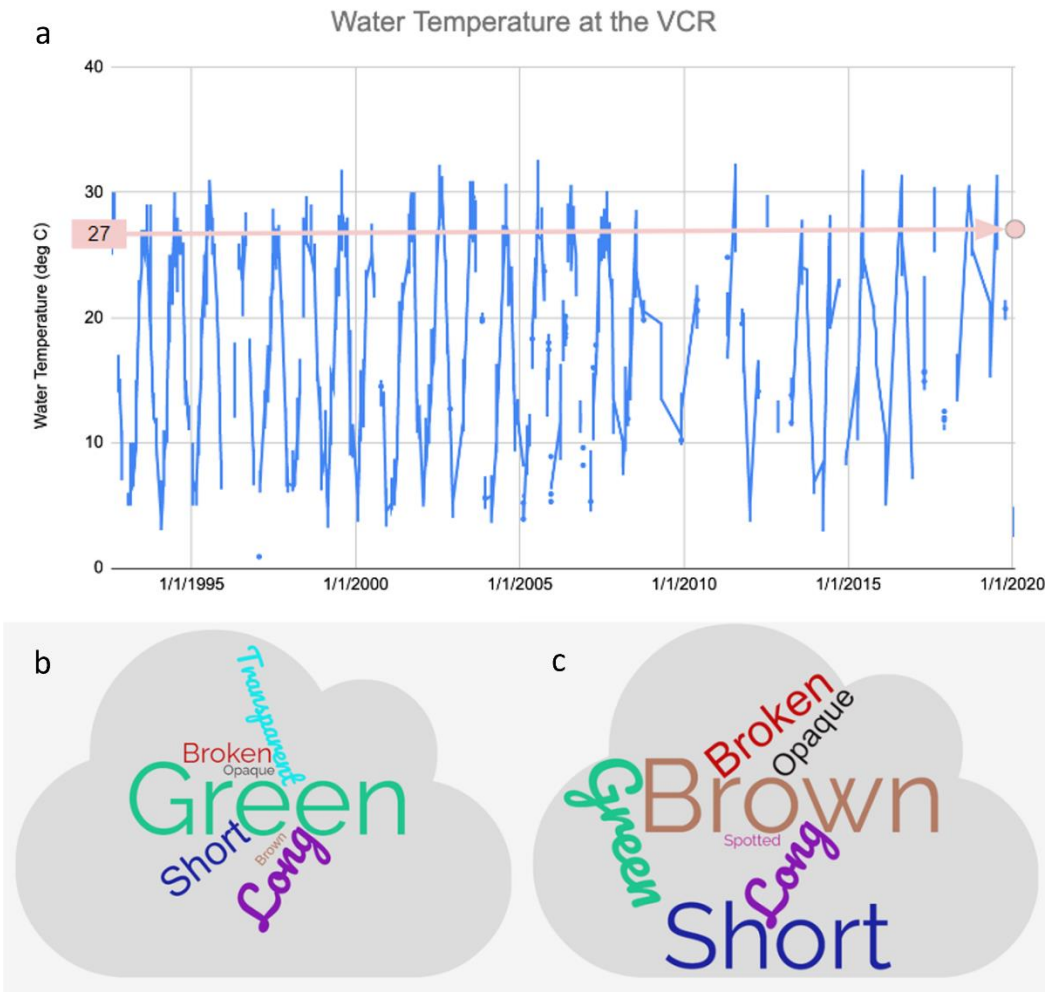

Fig. 3. Examples of the data analysis done in the sensemaking portion of the lesson plan. **(a)** Before the lesson plan, the teacher plotted a time series of measured water temperature at the students' field site in the VCR in blue. During the lesson plan, students plotted their measured water temperature datapoint from the VCR on top of the plot for comparison, which is represented here by a horizontal line at 27 °C. Long-term data were provided by a publicly-available VCR-LTER dataset. In a separate activity, the adjectives used to describe the characteristics of **(b)** inner and **(c)** outer seagrass leaves by individual students were summarized with word clouds. Word clouds, or diagrams of words, where the size of each word is positively correlated to the number of times the word is entered into the generator, are a visual tool that students are generally familiar with.

3.5 Help students put scientific conclusions into a real-world context

Like sensemaking, the practice of drawing meaningful conclusions is generally not prioritized in classroom settings. We dedicated intentional time for students to relate their field experiences and results back to real-world science and outreach efforts by asking them to explore the online Chesapeake Bay Ecosystem Health Report Card outreach tool

(https://ecoreportcard.org/report-cards/chesapeake-bay/, last accessed Nov. 30, 2023). The 2022 report card gave both the Chesapeake Bay and the Chesapeake Bay Watershed a 'C' for overall ecosystem health (UMCES 2023). We learned that the report card was an excellent way to challenge student perceptions of ecosystem health across spatial scales. Many students were used to seeing more pristine areas of the Chesapeake Bay, and were surprised that the letter grades were so low. The report card structure was an ideal scaffold, because K-16 students could easily conceptualize the differences between letter grades. The intentional overlap between the variables in their data and the report card helped students relate their data to the report's conclusions. Since this type of report card does not exist for the VCR, this exercise was also a scaffold that encouraged students to think about what a VCR report card would look like. Overall, this exercise had the additional broader impact of demonstrating how data can be communicated with the public.

To conclude the lesson plan, we asked students to make evidence-based claims about 1) whether the Chesapeake Bay or the VCR was healthier and 2) which driver was the most important indicator of ecosystem health. Students followed the Claim, Evidence, Reasoning, and Rebuttal framework, where they backed up their claims with evidence from their dataset, explained why the evidence fit their claim, and then challenged their claims by providing counter-evidence and counter-reasoning (Alegado and Lewis 2018). We expected students' claims to match the ones we had identified during our backward design planning. Instead, the students' claims were more nuanced and showed a deeper understanding of the scientific concepts than we had anticipated. Several students challenged the investigative questions and used their data to argue either that one variable was not enough to determine ecosystem health in a whole estuary, or that ecosystem health was likely variable inside both estuaries. We were positively surprised and impressed by the complexity and maturity of their claims. Ultimately, their claims showed that the lesson plan helped the students practice authentic science while increasing their scientific understanding of the local estuaries – the major goal of our work.

4 Outcomes

Through collaborative work, we co-developed a lesson plan that gave students a far better understanding and appreciation of their local ecosystems. Students were able to practice the scientific process, interact with real scientists, and learn how to use publicly-available data and

resources. Although this work could be further developed through repetitive use and formal evaluations of how student sentiments about science and science identity changed over time, our observations of the participating class suggest that this lesson plan met our goals.

This learning experience likely strengthened students' science identities and deepened their connections to their local environment (Kang et al. 2019; Wade-Jaimes et al. 2023). After completing the lesson plan, the teacher observed that students had a deeper understanding of the scientific process. Their confidence of ecosystem processes in the Chesapeake Bay and the VCR was demonstrated by their nuanced claims about how ecosystem health should be evaluated. Beyond their local estuaries, the students in this class also seemed to have a firmer grasp of scientific concepts and practices compared to their peers. Specifically, the students were able to better explain how multiple fields – biology, chemistry, ecology, and physics – were connected and influenced one another in the natural world. This may be because our lesson plan was structured to follow the scientific process instead of focusing on the scientific method that is historically taught in classrooms (Wade-Jaimes et al. 2023). The teacher observed that these students had a more well-rounded ability to think like a scientist compared to students who were just given a dataset to analyze. Later, some students in this class placed third in a regional competition of the National Sciences Bowl (the Blue Crab Bowl), which the teacher partially attributed to their ability to connect to the ecosystem on a deeper level after this lesson plan. Overall, the teacher believed that the lesson plan experience and the ownership of a dataset empowered students' science identity, regardless of whether or not students pursued a career in STEM.

Working with scientists during the field experience may have helped students deconstruct some of the common stereotypes about scientists (Miller et al. 2018; Wade-Jaimes et al. 2023). Many students had been unaware that the University of Virginia and other research centers maintained field stations on the ESVA. It was valuable for them to see that a university was a part of their community, and that university scientists were interested in contributing to student learning. After the lesson plan, students were passionate about sharing their findings and experiences with other peers outside of class, which helped foster a collaborative and enriching learning environment.

Teachers and scientists can co-produce authentic science learning experiences that are strongly needed in today's classrooms. When we collaborate, our combined skill sets and perspectives can positively impact student science identities and potentially shape the next generation of scientists. Our lesson plan can be modified to fit other local ecosystems and can be scaled for high school and college classrooms (https://doi.org/10.6084/m9.figshare.24738627.v1, last accessed Dec. 5, 2023). The best practices outlined here can also serve as a guide to help scientists meet teachers where they are and work with them to translate our science in a way that is meaningful for everyone.

5 Literature cited

Alegado, K., and A. Lewis. 2018. The four elements of the Claim, Evidence, Reasoning, and Rebuttal (CERR) Framework. Sci. Scope **41**: 72–78.

Bernard, R. E., and E. H. G. Cooperdock. 2018. No progress on diversity in 40 years. Nat. Geosci. **11**: 292–295. doi:10.1038/s41561-018-0116-6

Fick, S. J., and A. M. Arias. 2019. Scaffolding Beginning Teaching Practices: An Analysis of Roles Played by Tools Provided to Preservice Elementary Teachers, *In* E.A. Davis, C. Zembal-Saul, and S.M. Kademian [eds.], Sensemaking in Elementary Science: Supporting Teacher Learning. Routledge.

Fry, R., B. Kennedy, and C. Funk. 2021. STEM Jobs See Uneven Progress in Increasing Gender, Racial, and Ethnic Diversity.

Harris, L. A., T. Grayson, H. A. Neckles, and others. 2022. A Socio-ecological Imperative for Broadening Participation in Coastal and Estuarine Research and Management. Estuaries and Coasts **45**: 38–48. doi:10.1007/s12237-021-00944-z/Published

Kang, H., A. Calabrese Barton, E. Tan, S. D. Simpkins, H. yon Rhee, and C. Turner. 2019. How do middle school girls of color develop STEM identities? Middle school girls' participation in science activities and identification with STEM careers. Sci. Educ. **103**: 418–439. doi:10.1002/sce.21492

Michael, N. A., and J. C. Libarkin. 2016. PERSPECTIVES Understanding by Design: Mentored Implementation of Backward Design Methodology at the University Level.

Miller, D. I., K. M. Nolla, A. H. Eagly, and D. H. Uttal. 2018. The Development of Children's Gender-Science Stereotypes: A Meta-analysis of 5 Decades of U.S. Draw-A-Scientist Studies. Child Dev. **89**: 1943–1955. doi:10.1111/cdev.13039

UMCES. 2023. 2022 Chesapeake Bay & Watershed Report Card.

Wade-Jaimes, K., K. Ayers, and R. A. Pennella. 2023. Identity across the STEM ecosystem: Perspectives of youth, informal educators, and classroom teachers. J. Res. Sci. Teach. **60**: 885–914. doi:10.1002/tea.21820

Conclusions

Blue carbon ecosystems such as seagrass meadows play a significant role in global carbon cycling and the mitigation of greenhouse gases, but the dynamics of these fluxes are poorly understood on diurnal, tidal, and seasonal scales (Al-Haj & Fulweiler, 2020; Rosentreter et al., 2023). This dissertation evaluates tools used to measure fluxes across the air-water interface, provides a thorough accounting of air-water greenhouse gas flux magnitudes and pathways in a temperate seagrass meadow, and outlines best practices for communicating complex scientific concepts to students. Throughout this work, we show the importance of collecting high-quality and high-frequency *in situ* data when constraining gas fluxes. The majority of the work in this dissertation was conducted in South Bay, a shallow coastal bay located in the Virginia Coast Reserve (VCR) that has a benthic environment dominated by a *Zostera marina* meadow. This dissertation builds on the work of previous scientists who constrained ecosystem metabolism and gas fluxes *in situ* in South Bay (Berg et al., 2019; Berger et al., 2020; Oreska et al., 2020).

There is a growing body of literature that describes the aquatic eddy covariance technique and applies it to various ecosystems to estimate ecosystem metabolism and carbon flows (Berg et al., 2003, 2022; Berger et al., 2020). As the use of this technique becomes more widespread, the evaluation of new potential O_2 sensing systems is critical to ensure accurate flux estimates (Berg et al., 2016; Chipman et al., 2012). This dissertation builds on previous work that tests new sensors by evaluating a new O_2 optode system (meter and fiber-optic sensor) for aquatic eddy covariance in various conditions that represent common field environments (Chapter 1) (Granville et al., 2023). The rigorous evaluation protocol identified here can serve as a guideline for tests of future systems. We found that the new O_2 sensing system had a fast response time that was well within the range of sensors currently used for aquatic eddy covariance. In the field, O_2 fluxes measured using the new system were in agreement with fluxes measured at our site using established systems. The data were less noisy compared to other systems and no sensors broke or were fouled during our deployments. Overall, we found that the O_2 sensing system is suitable for aquatic eddy covariance. However, it is not an ideal choice for upside-down aquatic eddy covariance. O_2 concentrations measured by O_2 sensors are inherently sensitive to temperature changes, and the distance between the O_2 sensor and the temperature sensor, located on the meter, indicates the potential for heat fluxes to bias the O_2 concentration readings at the

air-water interface, where heat fluxes are greater than at the benthic interface (Berg & Pace, 2017). At the air-water interface, a more suitable system is the dual O_2-temperature planar optode, in which the O_2 and temperature sensors are both located at the tip of the sensor.

Gas exchange across the air-water interface is poorly constrained in temperate seagrass meadows due to a lack of high-frequency *in situ* measurements and uncertainties in flux methodologies (Al-Haj & Fulweiler, 2020; Rosentreter et al., 2021). In this dissertation, we built on established flux measurement techniques to constrain air-water CO_2 exchange over diurnal and tidal cycles (Chapter 2) (Berg et al., 2020; Wanninkhof, 2014). We compared measured and modeled gas transfer velocities (k) because k is the primary source of uncertainty in the flux equation, and we evaluated local wind speeds, which are recognized as a primary driver of k (Ho et al., 2006; Wanninkhof et al., 2009). Wind speeds that were measured at a station in the Chesapeake Bay with no proximity to land were representative of wind speeds over South Bay, while stations located in the VCR in proximity to land under-estimated wind speeds over South Bay. We derived *in situ* k values using the upside-down aquatic eddy covariance technique and compared them to modeled values derived from multiple empirical parameterizations based on wind speed, current velocity, and water depth. From this comparison, we identified four best fitting models that were most appropriate to use at our site when *in situ* data were not available. The best fitting models were wind-based models with an intercept of zero that were originally derived over the open ocean. This result varies from other vegetated ecosystems, which shows the importance of evaluating gas transfer velocity on a site-specific basis (Dobashi & Ho, 2023; Ho et al., 2016). Using a best-fitting model, appropriate wind speed measurements, and high-frequency autonomous underwater sensors, we derived hourly air-water CO_2 fluxes over South Bay for multiple days in July of 2021, 2022, and 2023, when the seagrass meadow was at peak seagrass density. CO_2 fluxes varied by year and by hour of the day, with the maximum positive CO_2 fluxes, which represent outgassing to the atmosphere, occurring at dawn, and the maximum negative CO_2 fluxes, which represent uptake by the water column, occurring in the afternoon (Fig. 7, Chapter 2). During a thunderstorm, CO_2 outgassing significantly increased, indicating the importance of evaluating fluxes over multiple weather conditions. On average, South Bay was in metabolic balance in July.

The seasonality of air-water CO_2, CH_4, and N_2O fluxes is poorly understood in seagrass meadows, especially on local scales (Al-Haj et al., 2022; Oreska et al., 2020). This dissertation provides an accounting of air-water CO_2, CH_4, and N_2O fluxes over a temperate seagrass meadow from April to October by expanding on the methods of Chapter 2 and measuring fluxes throughout the seagrass growing season and during storm periods. We found that CO_2 and CH_4 fluxes South Bay were strongly influenced by the seagrass growing season. South Bay was an overall sink of CO_2 during the early growing season and shifted to an overall source of CO_2 during seagrass die-off in August. In July, during the peak seagrass density period, South Bay was in metabolic balance, as CO_2 fluxes were not significantly different from zero. Similarly to other seagrass meadows, South Bay was an overall source of CH_4 (Eyre et al., 2023; Rosentreter et al., 2023). We evaluated both dissolved and ebullitive CH_4 fluxes and found that ebullition, which includes plant-mediated transport and sediment-water column ebullition, was a significant component of the total air-water CH_4 flux (Schorn et al., 2022; Vroom et al., 2022). Overall, total CH_4 fluxes increased throughout the growing season, although the proportion of dissolved to ebullitive fluxes changed over time. South Bay was a sink of total and dissolved N_2O (Rosentreter et al., 2023). Unlike CH_4, we found that N_2O ebullition was negligible and was fully offset by the dissolved N_2O fluxes. Overall, South Bay was a minor source of CO_2-equivalent gases during this period, and CO_2 and N_2O fluxes partially offset the total CH_4 emissions.

Communicating complex scientific topics such as gas exchange to the public is a difficult but critical task, especially in coastal areas that are at a high risk of potential harm from environmental hazards (Harris et al., 2022). Increasing scientific literacy in students, who generally lose the ability to identify with scientists and science as they progress through their K-12 education, is one way to make this task easier (Miller et al., 2018). The observed lack of science identity in students partially attributed to a lack of authentic science learning experiences in classrooms (Wade-Jaimes et al., 2021, 2023). Environmental scientists have a unique skill set that can be leveraged alongside teachers to develop authentic science learning experiences that connect students to their local environment. In this dissertation, we co-developed an authentic science learning experience for students on the Eastern Shore of Virginia and outlined a series of best practices that were important for our work for scientists and educators who want to do similar work (Chapter 4) (Granville et al., 2024). The best practices are 1) take a scholarly approach to teaching and learning, 2) build a mutually-beneficial partnership between scientists

and educators, 3) use pedagogical practices to develop authentic science learning experiences, 4) prioritize sensemaking, and 5) help students put scientific conclusions into a real-world context. We observed several positive impacts on the students after the science learning experience, including an improved ability to connect complex scientific concepts across fields and a deeper understanding of the organisms and processes in their local environment. This work can be used as a guideline for other scientists who want to connect with their communities in similar ways.

Literature cited

Al-Haj, A. N., Chidsey, T., & Fulweiler, R. W. (2022). Two temperate seagrass meadows are negligible sources of methane and nitrous oxide. *Limnology and Oceanography*. https://doi.org/10.1002/lno.12250

Al-Haj, A. N., & Fulweiler, R. W. (2020). A synthesis of methane emissions from shallow vegetated coastal ecosystems. In *Global Change Biology* (Vol. 26, Issue 5, pp. 2988–3005). Blackwell Publishing Ltd. https://doi.org/10.1111/gcb.15046

Berg, P., Delgard, M. L., Polsenaere, P., McGlathery, K. J., Doney, S. C., & Berger, A. C. (2019). Dynamics of benthic metabolism, O 2 , and pCO 2 in a temperate seagrass meadow . *Limnology and Oceanography*. https://doi.org/10.1002/lno.11236

Berg, P., Huettel, M., Glud, R. N., Reimers, C. E., & Attard, K. M. (2022). Aquatic Eddy Covariance: The Method and Its Contributions to Defining Oxygen and Carbon Fluxes in Marine Environments. *Annual Review of Marine Science*, *14*(1), 431–455. https://doi.org/10.1146/annurev-marine-042121-012329

Berg, P., Koopmans, D. J., Huettel, M., Li, H., Mori, K., & Wüest, A. (2016). A new robust oxygen-temperature sensor for aquatic eddy covariance measurements. *Limnology and Oceanography: Methods*, *14*(3), 151–167. https://doi.org/10.1002/lom3.10071

Berg, P., & Pace, M. L. (2017). Continuous measurement of air-water gas exchange by underwater eddy covariance. *Biogeosciences*, *14*(23), 5595–5606. https://doi.org/10.5194/bg-14-5595-2017

Berg, P., Pace, M. L., & Buelo, C. D. (2020). Air–water gas exchange in lakes and reservoirs measured from a moving platform by underwater eddy covariance. *Limnology and Oceanography: Methods*, lom3.10373. https://doi.org/10.1002/lom3.10373

Berg, P., Roy, H., Janssen, F., Meyer, V., Jorgensen, B. B., Huettel, M., & de Beer, D. (2003). Oxygen uptake by aquatic sediments measured with a novel non-invasive eddy-correlation technique. *Marine Ecology Progress Series*, *261*, 75–83.

Berger, A. C., Berg, P., McGlathery, K. J., & Delgard, M. L. (2020). Long-term trends and resilience of seagrass metabolism: A decadal aquatic eddy covariance study. *Limnology and Oceanography*. https://doi.org/10.1002/lno.11397

Chipman, L., Huettel, M., Berg, P., Meyer, V., Klimant, I., Glud, R., & Wenzhoefer, F. (2012). Oxygen optodes as fast sensors for eddy correlation measurements in aquatic systems.

Limnology and Oceanography: Methods, *10*(5), 304–316. https://doi.org/10.4319/lom.2012.10.304

Dobashi, R., & Ho, D. T. (2023). Air–sea gas exchange in a seagrass ecosystem – results from a $^{3}He/SF_{6}$ tracer release experiment. *Biogeosciences*, *20*(6), 1075–1087. https://doi.org/10.5194/bg-20-1075-2023

Eyre, B. D., Camillini, N., Glud, R. N., & Rosentreter, J. A. (2023). The climate benefit of seagrass blue carbon is reduced by methane fluxes and enhanced by nitrous oxide fluxes. *Communications Earth and Environment*, *4*(1). https://doi.org/10.1038/s43247-023-01022-x

Granville, K. E., Baird, C., Carlson, C., & Berg, P. (2024). At the Intersection of Science and Education: The Process of Scientists and Educators Co-developing Authentic Learning Experiences for K-16 Students. *Limnology and Oceanography Bulletin*. https://doi.org/10.1002/lob.10627

Granville, K. E., Berg, P., & Huettel, M. (2023). A high-resolution submersible oxygen optode system for aquatic eddy covariance. *Limnology and Oceanography: Methods*, *21*(3), 152–163. https://doi.org/10.1002/lom3.10535

Harris, L. A., Grayson, T., Neckles, H. A., Emrich, & C. T., Lewis, K. A., Grimes, K. W., Williamson, S., Garza, C., Whitcraft, C. R., Pollack, & J. B., Talley, & D. M., Fertig, & B., Palinkas, C. M., Park, & S., Vaudrey, J. M. P., Fitzgerald, & A. M., & Quispe, J. (2022). A Socio-ecological Imperative for Broadening Participation in Coastal and Estuarine Research and Management. *Estuaries and Coasts*, *45*, 38–48. https://doi.org/10.1007/s12237-021-00944-z/Published

Ho, D. T., Coffineau, N., Hickman, B., Chow, N., Koffman, T., & Schlosser, P. (2016). Influence of current velocity and wind speed on air-water gas exchange in a mangrove estuary. *Geophysical Research Letters*, *43*(8), 3813–3821. https://doi.org/10.1002/2016GL068727

Ho, D. T., Law, C. S., Smith, M. J., Schlosser, P., Harvey, M., & Hill, P. (2006). Measurements of air-sea gas exchange at high wind speeds in the Southern Ocean: Implications for global parameterizations. *Geophysical Research Letters*, *33*(16). https://doi.org/10.1029/2006GL026817

Miller, D. I., Nolla, K. M., Eagly, A. H., & Uttal, D. H. (2018). The Development of Children's Gender-Science Stereotypes: A Meta-analysis of 5 Decades of U.S. Draw-A-Scientist Studies. *Child Development*, *89*(6), 1943–1955. https://doi.org/10.1111/cdev.13039

Oreska, M. P. J., McGlathery, K. J., Aoki, L. R., Berger, A. C., Berg, P., & Mullins, L. (2020). The greenhouse gas offset potential from seagrass restoration. *Scientific Reports*, *10*(1). https://doi.org/10.1038/s41598-020-64094-1

Rosentreter, J. A., Borges, A. V., Deemer, B. R., Holgerson, M. A., Liu, S., Song, C., Melack, J., Raymond, P. A., Duarte, C. M., Allen, G. H., Olefeldt, D., Poulter, B., Battin, T. I., & Eyre, B. D. (2021). Half of global methane emissions come from highly variable aquatic ecosystem sources. *Nature Geoscience*, *14*(4), 225–230. https://doi.org/10.1038/s41561-021-00715-2

Rosentreter, J. A., Laruelle, G. G., Bange, H. W., Bianchi, T. S., Busecke, J. J. M., Cai, W. J., Eyre, B. D., Forbrich, I., Kwon, E. Y., Maavara, T., Moosdorf, N., Najjar, R. G., Sarma, V. V. S. S., Van Dam, B., & Regnier, P. (2023). Coastal vegetation and estuaries are collectively a greenhouse gas sink. *Nature Climate Change*, *13*(6), 579–587. https://doi.org/10.1038/s41558-023-01682-9

Schorn, S., Ahmerkamp, S., Bullock, E., Weber, M., Lott, C., Liebeke, M., Lavik, G., Kuypers, M. M. M., Graf, J. S., & Milucka, J. (2022). Diverse methylotrophic methanogenic archaea cause high methane emissions from seagrass meadows. *PNAS*, *119*(9). https://doi.org/10.1073/pnas.2106628119/-/DCSupplemental

Vroom, R. J. E., van den Berg, M., Pangala, S. R., van der Scheer, O. E., & Sorrell, B. K. (2022). Physiological processes affecting methane transport by wetland vegetation – A review. *Aquatic Botany*, *182*, 103547. https://doi.org/10.1016/J.AQUABOT.2022.103547

Wade-Jaimes, K., Ayers, K., & Pennella, R. A. (2023). Identity across the STEM ecosystem: Perspectives of youth, informal educators, and classroom teachers. *Journal of Research in Science Teaching*, *60*(4), 885–914. https://doi.org/10.1002/tea.21820

Wade-Jaimes, K., King, N. S., & Schwartz, R. (2021). "You could like science and not be a science person": Black girls' negotiation of space and identity in science. *Science Education*, *105*(5), 855–879. https://doi.org/10.1002/sce.21664

Wanninkhof, R. (2014). Relationship between wind speed and gas exchange over the ocean revisited. *Limnology and Oceanography: Methods*, *12*(JUN), 351–362. https://doi.org/10.4319/lom.2014.12.351

Wanninkhof, R., Asher, W. E., Ho, D. T., Sweeney, C., & McGillis, W. R. (2009). Advances in Quantifying Air-Sea Gas Exchange and Environmental Forcing. *Annual Review of Marine Science*, *1*(1), 213–244. https://doi.org/10.1146/annurev.marine.010908.163742

Funding acknowledgement

Kayleigh E. Granville was supported by a Virginia Sea Grant Graduate Research Fellowship, a Jefferson Scholars Foundation Dissertation Year Fellowship, and research and teaching assistantships from the Department of Environmental Sciences at the University of Virginia. This work was also funded by the National Science Foundation (NSF) through grants to the Virginia Coast Reserve Long-Term Ecological Research Program (DEB-1832221) and through grants awarded to Peter Berg (OCE-1851424, OCE-1824144, and OCE-2223204).